Universidade Nova de Lisboa
OMNIS CIVITAS CONTRA SE DIVISA NON STABIT
Faculdade de Ciências e Tecnologia

Dissertação de Doutoramento

Molybdenum-containing proteins from Sulphate Reducing Bacteria:

studying proteins with novel cofactors and revealing new features of old enzymes.

Maria Gabriela Rivas

Lisboa, 2006

Maria Gabriela Rivas

Molybdenum-containing proteins from Sulphate Reducing Bacteria: *studying proteins with novel cofactors and revealing new features of old enzymes.*

Dissertação apresentada para a obtenção do Grau de Doutor em Bioquímica, especialidade de Bioquímica-Física pela Universidade Nova de Lisboa, Faculdade de Ciências e Tectologia.

Lisboa, 2006

-Nº de arquivo

-"Copyright"

...to Pablo...

ACKNOWLEDGMENTS

A minha orientadora, Prof. Isabel Moura, quero agradecer ter-me aceite (ainda sem me conhecer) no seu grupo de investigação e por ter depositado toda a sua confianza no meu trabalho. A sua energia e entusiasmo têm sido um incentivo permanente na realizacão desta tese. Quero ainda acrescentar a minha grande admiração pelo seu domínio na área teórica e experimental tanto na purificação como caracterização de proteínas.

Ao Prof. José Moura pelo seu dinamismo e orientação científica alêm da simpatía e da boa disposição demonstrada em todo momento.

Al Dr. Carlos Brondino quiero agradecerle muy especialmente por todo el conocimiento transmitido a lo largo de estos años, por la paciencia y la incansable disposición a la hora de trabajar, analizar y discutir los resultados. El gran interés demostrado en todos los temas discutidos en esta tesis es de gran admiración. Su simpatía y buen humor fueron una importantísima contribución para que la propuesta de cruzar la frontera y empezar nuevos desafíos tenga un balance muy positivo.

Quiero agradecer al Dr. Jose Calvete del Instituto de Biomedicina de Valencia por la colaboración en la secuenciación de la *Blue protein* de *D. aminophilus*. Ha sido un gran placer conocer a una excelente persona tanto desde el punto de vista profesional como humano. La estadía en su laboratorio así como las tapas, la visita al mercado central de Valencia, la paella y el asado serán inolvidables. Agradezco también a todo su grupo de investigación, especialmente a Libia, por el compañerismo demostrado haciendo todavía más placenteras las horas de trabajo en el instituto.

Ao Prof. Dr. Graham N. Jorge e a Dra. Gosia Korbas (*University of Saskatchewan, Canada*) pela adquicição e análises dos resultados de espectroscopía absorção de raios-X.

Ao Lic. Cristiano Mota, quem levou a cabo a sequenciação do operão da Fdh e da *Blue protein* de *D. alaskensis* sob a minha orientação, agradeço a boa dispocição, a calma, a persistência e o excelente espírito de trabalho que o caracterizam.

Agradeço ao Prof. Jorge Lampreia pela disponibilização do sequenciador de proteínas e especialmente Dra. Marta Santos por a grande ajuda e o interesse demonstrados na sequenciação das subunidades da *Dd* Fdh e da *Blue protein* de *D. alaskensis*. Quero ainda agradecer ao Prof. Jorge Caldeira pela disponibilização das colunas de fase reversa utilizadas na separação de péptidos.

Quero agradecer à Dra. Raquel Rial-Otero e à Lic. Luz Fernadez pelos análises por espectrometria de massas da *Blue protein* de *Desulfovibrio alaskensis* (FCT-UNL, Caparica, Portugal).

Gostaría ainda de agradecer aos meus colegas de laboratório incluindo ao Grupos Bion e X-tal. Particularmente agradeço ao Dr. Sergey Bursakov pela ajuda na primeira purificação da *Dd* Fdh e a Prof. Alice Pereira pela ajuda prestada na sequenciação de DNA da *Blue protein* de *D. aminophilus*.

À Prof. Maria João Romão pela simpatía com que sempre me tratou e pelas discussões científica relativas à Fdh.

Quero expressar o meu agradecimento à Eng. Lúcia, à Dra. Isabel Rodrigues, à Dra. Maria José Carapinha e Dra. Fátima por todo o apoio na parte burocrática, mas principalmente pela simpatia e a paciência que sempre demonstraram.

Ao *pessoal da salinha* quero agradecer as animadas conversas ao almoço e durante o café.

À Casimira por fazer que cada dia de trabalho tenha um final feliz.

A toda la gente del Departamento de Física de la Facultad de Bioquímica y Ciencias Biológicas de la Universidad Nacional del Litoral por la simpatía y el excelente ambiente de trabajo con el que me acogieron en el último mes de escritura de esta tesis. Especialmente a Aberto Rizzi.

A mis amigas en Argentina (mis grandes amigas): Marianela, Mariana, Noelia y Verónica. Les agradezco el cariño y la compañía (aun a *larga distancia*).

A Ana e a Roeland por los momentos lindos que pasamos juntos.

A Laura por su amistad, por las charlas sobre todo y más y por hacerme ver la Costa con otros ojos.

A Carlos y José Luis quiero agradecerles el cariño y la compañía que me ofrecieron desde la llegada a Portugal. Los momentos compartidos (incluyendo días de playa, cenas, almuerzos, bodas, caminatas, viajes por lugares inhóspitos y superpoblados) así como los consejos recibidos han hecho que sean considerados como nuestra familia en Portugal. GRACIAS!

Quero agradecer aos meus amigos em Portugal: Sofia, Ana Teresa, Inês, Marta, Pedro, Jorginho, Teresinha, Stef & Cathy (mais Prisca e Tom!), Jorge, Simone, Fancesca, Joana e Fançoise pelo carinho, pelas palavras certas e por fazer que tenha tantas saudades de Portugal quando estou longe. Um reconhecimento especial à Sofia pelo exemplo dado no dia e pela inmensa quantidade de coisas que aprendi (e continuo a aprender) com ela, pelas correcções ao meu *portunhol*. À Marta ainda quero agradecer a leitura crítica de alguns capítulos desta tese.

A mi familia (papá, mamá, Pao, Cande, Vale, Walter, Lara, Mica y nonos) les agradezco el apoyo, la paciencia y el haber estado siempre a mi lado. A mi familia González (incluyendo a Sarita) por el apoyo y la preocupación constante.

A Pablo, mi marido, compañero y amigo, le agradezco el haberme incentivado siempre y la ayuda en todo. Tu compañía, paciencia y buen humor me ayudan a sobrepasar todas las dificultades. GRACIAS

Agradeço a SECYT (Argentina) e GRICES (Portugal) pelo apoio económico dado no marco do acordo de Cooperação Científica e Tecnológica Portugal - Argentina.

Agradeço ao governo de Portugal por permitir a formação avanzada tanto de cidadãos portugueses como estrangeiros, particularmente o apoio financiero que a Fundação para a Ciência e a Tecnologia me concedeu através da bolsa de doutoramento.

RESUMO

O trabalho apresentado nesta tese corresponde ao estudo de duas classes distintas de proteínas isoladas de bactérias redutoras de sulfato. A proteína descrita na primeira parte é a enzima mononuclear de molibdénio desidrogenase do formato de *D. desulfuricans* ATCC 27774 (*Dd* Fdh). As Fdhs são enzimas que catalisam a oxidação do formato a dióxido de carbono, reacção que envolve a transferência de dois electrões. Estudos preliminares de EPR e EXAFS realizados na *Dd* Fdh demonstraram que esta enzima pertence à familia da reductase do dimetilsulfóxido de metilo e que está relacionada com outras Fdhs de bactérias reductoras de sulfato e de *E. coli*. A estrutura cristalina de três Fdhs que pertencem a esta família encontram-se resolvidas: a Fdh-H e a Fdh-N de *E. coli* e a W-Fdh de *D. gigas*. A subunidade catalítica destas três enzimas apresenta um folding idêntico e contém, além do centro activo, um centro [4Fe-4S]. O sítio activo inclui um ião [Mo/W(VI)] coordenado a quatro enxofres provenientes de duas pterinas, um átomo de selénio de uma selenocisteína e um ligando cuja origem é controversa. Nas Fdhs de *E. coli* e *Dd* o sexto ligando foi identificado como sendo um átomo de oxigénio. No entanto, dados obtidos da estrutura de Raios X da W-Fdh de *D. gigas* sugerem um átomo de enxofre na posição deste ligando. O mecanismo de reacção destas enzimas é baseado nos resultados obtidos de estudos de EPR e Raios X da desidrogenase do formato H de *E. coli*. A função fisiológica destas enzimas é variável facto que poderá dever-se à sua variável localização celular, aos parceiros fisiológicos, à composição de subunidades e ao conteúdo de cofactores.

O trabalho descrito na primeira parte desta tese tem por objetivo a compreensão da organização dos genes que codificam para a Fdh e as propriedades cinéticas e de EPR desta enzima. Os genes que codificam para a Fdh (*fdhABEC*) estão organizados de forma similar ao operão que codifica para a Fdh-3 de *D. vulgaris* Hildenborough. É de salientar a

presença de duas sequências de DNA a montante e a jusante do gene *fdhE* sem homologia relativamente a outras proteínas conhecidas.

Estudos cinéticos nos quais deuteroformato foi usado como substrato alternativo demonstraram um efeito isotópico primário o que indica que a ruptura da ligação C-H é o passo limitante da oxidação do formato. Estudos de inibição demonstraram que o nitrato é um inibidor competitivo e a azida e o cianeto são inibidores mistos da enzima. O espectro de EPR da Fdh reduzida com formato é diferente do observado quando a enzima é reduzida com ditionito. Este sinal é rómbico e apresenta desdobramentos hiperfinos atribuíveis à presença de dois núcleos com I=1/2. Um dos dois núcleos é não permutável com o solvente e poderá corresponder ao protão que se encontra sobre o carbono do β-metileno da selenocisteína coordenada ao Mo. O segundo núcleo é, pelo contrário, permutável com o solvente e poderá pertencer a protões unidos a uma molécula de solvente coordenada ao Mo. Estudos de EPR em condições de inibição detectaram a presença de um sinal conhecido como *2.094* e que fora proposto como pertencendo a um intermediário na oxidação do formato. Assim, neste trabalho é ainda apresentada uma análise da relevância destas duas espécies paramagnéticas na catalise e a origem do sexto ligando.

A segunda parte desta dissertação inclui o estudo de duas proteínas que parecem ser membros de uma nova família de metaloproteínas e que são conhecidas com o nome genérico de *Blue proteins*. Estas proteínas foram isoladas de diferentes bactérias do género *Desulfovibrio* e a sua função é ainda desconhecida. Nos anos 1978 e 1986 foi descrito pela primeira vez o isolamento de proteínas contendo Mo-Fe de *Desulfovibrio africanus* e *Desulfovibrio salexigens*. Mais tarde, uma proteína homóloga que contém no seu centro metálico Mo, Fe e Cu foi isolada de *D. gigas*. O trabalho realizado nesta parte compreende a caracterização primária de duas *Blue proteins* isoladas de *D. aminophilus* e de *Desulfovibrio alaskensis*. Todas estas proteínas apresentam-se como agregados multiméricos com baixa homologia relativamente à sequência primária. As sequências de

nucleótidos das *Blue proteins* destes dois organismos foram obtidas e a sequência traduzida de aminoácidos sugere uma localização periplásmica para ambas. O valor de pI calculado a partir da sequências de aminoácidos derivadas da sequência do DNA está de acordo com o comportamento das proteínas nas colunas de troca aniónica. A analise de metais detectou a presença de Mo e Fe na *Blue protein* de *D. alaskensis* e de Cu e Fe na poteína isolada de *D. aminophilus*. No que se refere aos centros metálicos, datos de espectroscopía de absorção de raios-X sugerem agregados heterometálicos com diferenças na coordenação dos ligandos em torno do ião metálico.

ABSTRACT

The work presented in this thesis was oriented to the study of two different types of proteins isolated from sulphate reducing bacteria. One of them is the mononuclear molybdenum containing enzyme Formate dehydrogenase from *D. desulfuricans* ATCC 27774 (*Dd* Fdh). Formate dehydrogenases are enzymes that catalyze the two-electron oxidation of formate to carbon dioxide. *Dd* Fdh belongs to the dimethylsulphoxide reductase family and is closely related to other Fdhs isolated from both sulphate reducing organisms and *E. coli*. The crystal structures of three Fdhs belonging to this family have been reported to date: the Mo-containing Fdh-H and Fdh-N from *E coli*, and the W-containing Fdh from *D. gigas*. The catalytic subunit of these three proteins contains the active site and one [4Fe-4S] cluster, and presents an identical fold. The oxidized active site comprises a [Mo/W(VI)] ion coordinated to four sulphurs from two pterins, a Se atom provided by the Seleno-Cysteine, and a sixth ligand whose nature is still controversial. This ligand has been identified as a hydroxyl group in *Dd* and *E. coli* Fdhs. However, the X-ray data obtained from the *D. gigas* enzyme suggest a sulphur atom. Despite all these enzymes catalyze a unique reaction, their physiological roles are variable, which could arise from their different cellular localization, physiological partners, and subunit and cofactor composition.

The work performed was oriented to understand the gene organization, and the kinetic and EPR properties of *Dd* Fdh. The genes codifying the Fdh enzyme are organized as a *fdhABEC* cluster similar to the *D. vulgaris* Hildenborough Fdh-3 operon. Two gaps containing ORFs without homology with any annotated sequences were identified upstream and downstream from *fdhE*. Kinetic studies using deuteroformate as substrate revealed a primary isotope effect indicating that the break of the C-H bond is the rate limiting-step in the formate oxidation. Inhibition studies showed that nitrate is a competitive inhibitor whereas azide and cyanide are mixed inhibitors. The reduction of *Dd* Fdh with

sodium formate yields a different signal from the dithionite reduced enzyme. The EPR signal obtained on formate reduction is a rhombic signal and is split by two interacting I=1/2 nuclei. One of them is not solvent exchangeable and according to the proposed structure for the Mo site is located on the β-methylene carbon of the Se-Cysteine. In contrast, the second interacting nucleus is exchangeable with solvent and could be produced by protons of a solvent molecule bound to the Mo. EPR studies in inhibiting conditions yields a signal called *2.094* which was proposed to be produced by an intermediate of the catalytic reaction in the *E coli* enzyme. The relevance of these paramagnetic species in catalysis as well as the nature of the six ligand of the Mo site is discussed.

The second type of proteins corresponds to two proteins belonging to a new family of metalloproteins that receives the generic name of *Blue* proteins. These proteins were isolated from several bacteria of the *Desulfovibrio* genus and their function in the cell is still unknown. There are few reports on these proteins. The first ones, which date from 1978 and 1986, describe the isolation of two novel Mo-Fe containing proteins from *D. africanus* and *D. salexigens*, respectively. More recently, a homologous protein, containing Mo, Fe and Cu, was isolated from *D. gigas*. In this work, the *Blue* proteins isolated from *Desulfovibrio aminophilus* and *Desulfovibrio alaskensis* are reported. The function of both proteins is also unknown and the work was oriented to perform their primary characterization. These *Blue* proteins are multimeric proteins sharing low aminoacid sequence homology. The sequencing of the open reading frame showed to contain a signal peptide which suggests a periplasmic location. The high pI calculated from the deduced amino acid sequences is in agreement with the behaviour showed through anionic chromatographic columns. Metal analysis detected Mo and Fe for *D. alaskensis* and Cu and Fe for the *D. aminophilus*. X-ray adsorption spectroscopy studies suggest multinuclear clusters with potential differences in the coordination around metal ions, and which has not been observed in Mo-containing proteins.

Abbreviations

ATCC	**A**merican **T**ype **C**ulture **C**ollection
Blast	**B**asic **L**ocal **A**lignment **S**earch **T**ool
D.	*Desulfovibrio*
Dd	*Desulfovibrio desulfuricans*
DEAE	**D**i**E**thyl**A**mino**E**thyl
DLP	**D**irect **L**inear **P**lot
DMSOR	**D**imethyl**S**ulfoxide **R**eductase
DNA	**D**eoxyribo**N**ucleic **A**cid
DvH	*D esulfovibrio v ulgaris* Hildenborough
E coli	*E scherichia coli*
Ec	*E scherichia c oli*
EPR	**E**lectron **P**aramagnetic **R**esonance
EXAFS	**E**xtended **X**-ray **A**bsorption **F**ine **S**tructure
Fdh	**F**ormate **d**e**h**ydrogenase
FeMo	**I**ron-**M**olybdenum
FHL	**F**ormate **H**ydrogen **L**yase
HPLC	**H**igh **P**erformance **L**iquid **C**hromatography
HTP	Hydroxyapatite
LB	**L**uria **B**ertani
MALDI-TOF	**M**atrix-**A**ssisted **L**aser **D**esorption/**I**onisation-**T**ime **O**f **F**light
MCD	**M**olybdopterin **C**ytosine **D**inucleotide
MGD	**M**olybdopterin **G**uanine **D**inucleotide
NCBI	**N**ational **C**enter for **B**iotechnology **I**nformation
ORF	**O**pen **R**eading **F**rame
PCR	**P**olymerase **C**hain **R**eaction
PFL	**P**yruvate **F**ormate-**L**yase
pI	**I**soelectric **p**oint
RBS	**R**ibosome **B**inding **S**ite
SDS-PAGE	**S**odium **D**odecyl **S**ulphate **P**olyacrylamide **G**el **E**lectrophoresis
SECIS	**Se**lenocysteine **I**nsertion **S**equence
SeCys	**S**elenO**C**ysteine
SO	**S**ulfite **O**xidase
SRB	**S**ulphate **R**educing **B**acteria
Tat	**T**win **a**rginine **t**ransport
Tm	annealing temperature
XAS	**X**-ray **A**bsorption **S**pectroscopy
XO	**X**anthine **O**xidase

INDEX

FIGURE INDEX

TABLE INDEX

I. General Introduction

Molybdenum is found in biological systems in a mononuclear form or forming part of multinuclear metal clusters in the active site of a diverse group of enzymes that generally catalyze electron-transfer reactions [1, 2]. These enzymes are ubiquitous and participate in several biological processes occurring in nature, such as denitrification, the greenhouse effect, and pollution of the soil water [3-5].

The best characterized example of an enzyme containing a multinuclear active site is perhaps the enzyme nitrogenase. This enzyme catalyzes the following reaction:

$$N_2 + 8e^- + 8\,H^+ + 16\,MgATP \leftrightarrow 2\,NH_3 + H_2 + 16\,MgADP + 16\,Pi$$

The site of substrate activation and reduction has been localized to a complex cofactor (Figure I.1), called FeMo cofactor. Until now the complexity of the system has denied information concerning exactly where and how substrates interact with the metal-sulphur framework of the active site.

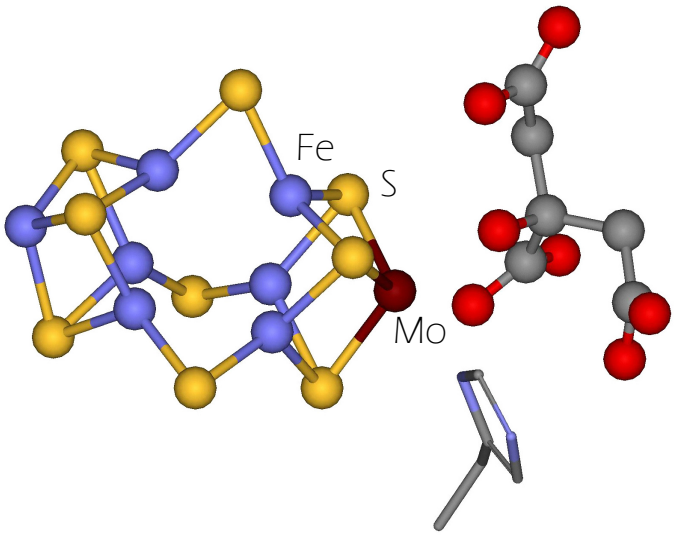

Figure I.1 Catalytic active site of MoFe nitrogenase from *Azotobacter vinelandii* [6].

Another example is the heterodimer containing Cu and Mo present in the enzyme CO dehydrogenase (Figure I.2). This enzyme catalyzes the oxidation of CO according to the following reaction:

$$CO + H_2O \rightarrow CO_2 + 2e^- + 2H^+$$

The oxidized cluster contains the Mo ion in the +VI oxidation state which upon incubation with CO or sodium dithionite is reduced to Mo(IV). The Cu ion permanently remains in the +1 oxidation state.

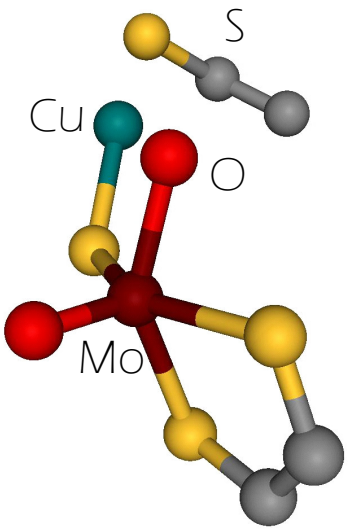

Figure I.2 Catalytic active site of Cu,Mo-CO Dehydrogenase from *Oligotropha carboxidovorans* [7].

Molybdenum is also present in a mononuclear form in the active site of distinct types of enzymes that are classified under the general name of Mononuclear molybdenum enzymes. These enzymes have been divided into three groups called the xanthine oxidase (XO), dimethyl sulfoxide reductase (DMSOR), and sulfite oxidase (SO) families [1, 8]. These three families include not only the enzymes that give the name to the different groups but also diverse enzymes such as aldehyde oxidoreductases, nitrate reductases, and formate dehydrogenases among others. The active site of these enzymes (Figure I.3a) includes the metal atom coordinated to one or two pyranopterin molecules and to a variable number

of ligands such as oxygen (oxo, hydroxo, water, serine, and aspartic acid), sulphur (cysteines), and selenium (selenocysteines) atoms. The pyranopterin molecule is an organic ligand that can be either in the monophosphate form or have a nucleotide molecule attached by a pyrophosphate link (Figure I.3b)[9]. In addition, these proteins may also have other redox cofactors such as iron-sulphur (FeS) centres, hemes, and flavin groups, which are involved in intra- and intermolecular electron-transfer processes [10].

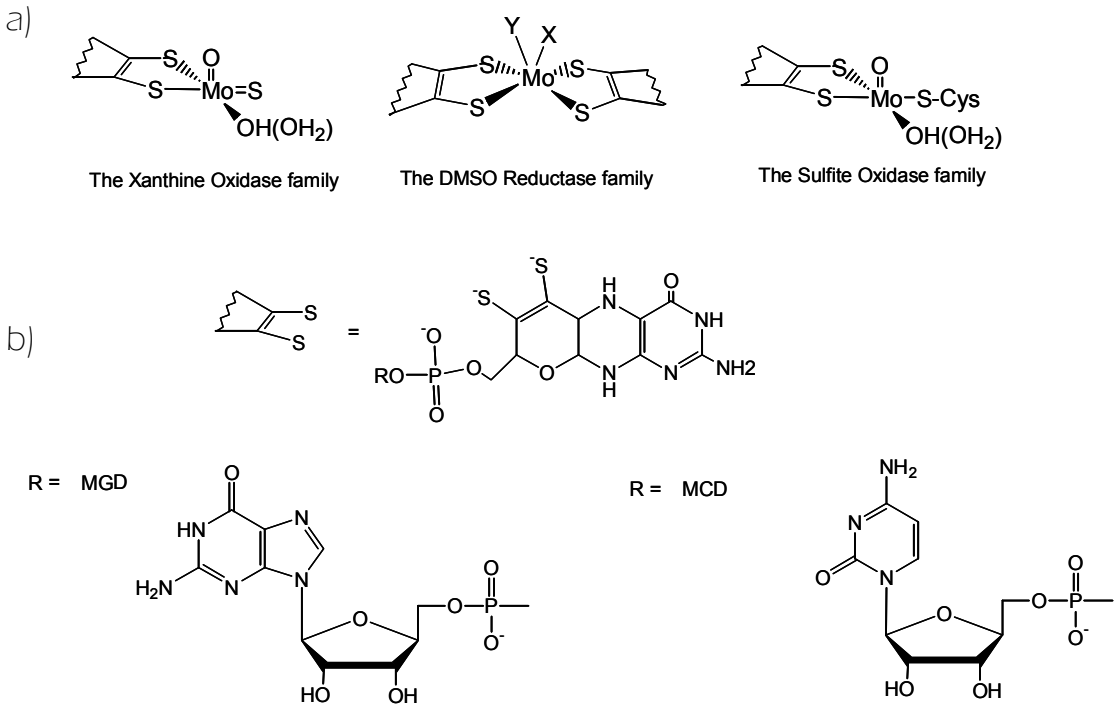

Figure I.3 *(a) Active-site structure of the three families of mononuclear molybdenum- and tungsten-containing enzymes. X and Y represent ligands such as oxygen (oxo, hydroxo, water, serine, and aspartic acid), sulphur (cysteine), and selenium (selenocysteine) atoms. (b) Structure of the pyranopterin molecule.*

With a few exceptions, these enzymes catalyze the transfer of an oxygen atom from water to the product (or vice versa) in reactions that imply a net exchange of two electrons between the enzyme and substrate and in which the metal ion cycles between the redox states IV and VI. Figure I.4 shows two representative examples of half-reactions catalyzed by mononuclear molybdenum enzymes. The members of the XO family catalyze the oxidative hydroxylation of a diverse range of aldehydes (Figure I.4a) and aromatic heterocycles in

reactions that involve the cleavage of a C-H and the formation of a C-O bond [11]. In contrast, the members of the DMSOR and SO families catalyze the transfer of an oxygen atom to or from a lone electron pair of the substrate (e.g., the reduction of nitrate to nitrite, Figure I.4b). The only exception are the formate dehydrogenases, which catalyze the conversion of formate to CO_2 without oxygen incorporation [10, 11].

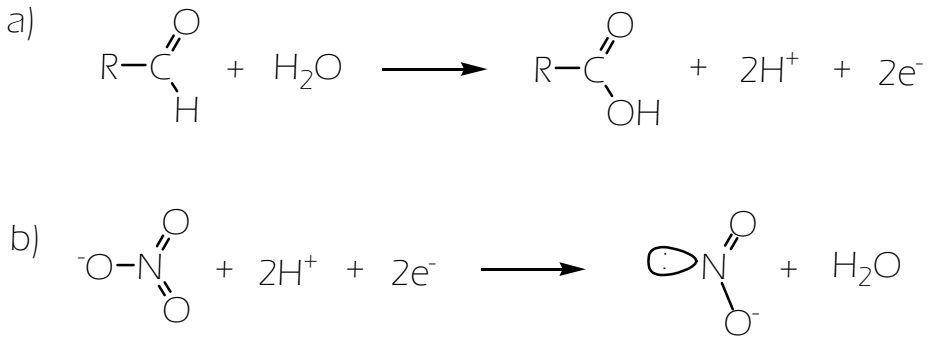

Figure I.4 (a) Half-reaction catalyzed by the enzyme aldehyde oxidoreductase of the XO family. (b) Half-reaction catalyzed by the enzyme nitrate reductase, which, depending upon the source can belong to either the DMSOR or SO family.

The accepted general mechanism of the reactions catalyzed by these enzymes is shown in Figure I.5. The substrate reacts with the molybdenum centre, which is reduced from Mo(VI) to Mo(IV) in those reactions that involve the substrate oxidation or oxidized from Mo(IV) to Mo(VI) in those reactions occurring in the opposite direction. The two reducing equivalents generated in the course of oxidative reactions are then transferred to an external electron acceptor by means of an electron-transfer process mediated by other redox cofactors present in the structure of these proteins. In contrast, two reducing equivalents given by an external electron donor are consumed by the substrate in reductive reactions, and the electron flow occurs in the opposite direction.

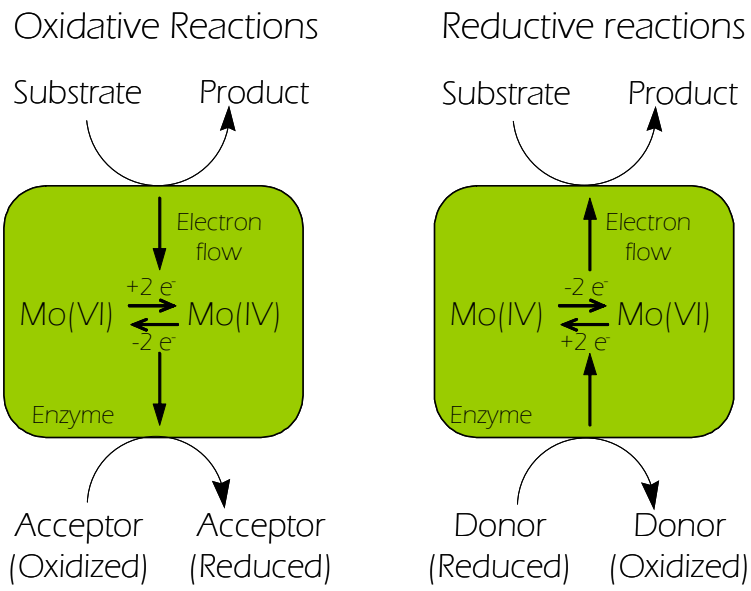

Figure I.5 *Accepted general mechanism for oxidative (left) and reductive (right) reactions catalyzed by mononuclear molybdenum-containing enzymes.*

In the last years, a few examples of other types of Mo enzymes have been reported. Preliminary characterizations suggested the presence of clusters containing Mo among other metal ions [12, 13]. Furthermore, until now, there are no clues on their function in the cell though several hypotheses such as Mo transport and storage has been proposed.

The work presented in this thesis corresponds to the study of two different systems in which the presence of Mo is the only link. In addition, the state of the art is at different stages; therefore, the work is divided in two parts. The first part involves the study of the enzyme Fdh from the SRB *D. desulfuricans* ATCC 27774. Preliminary EPR and EXAFS characterization of this protein showed that it belong to the family of the DMSO reductase (Figure I.3) and that is closely related to other Fdhs obtained from other sulphate reducing organisms [10] and from the *E coli* Fdhs. The work performed on this enzyme is a continuation of these studies and are oriented to understand the gene organization and the kinetic and EPR properties of the as-prepared and inhibited forms of this enzyme.

The second part of this work is oriented to the characterization of a novel Mo protein isolated from the sulphate reducer *D. alaskensis*. A similar protein purified from the SRB *D. aminophilus* seems to be a case in which Cu could replace Mo, and, therefore, is also included in our study. The function of both proteins are still unknown and our work was oriented to perform their primary characterization, e.g. molecular properties determination, metal analysis, gene sequencing, and type and structure of the metal clusters.

II. Molybdenum-containing proteins from Sulphate Reducing Bacteria: *revealing new features of old enzymes.*

II.1 Introduction

II.1.1 Metabolism of formate in the bacterial cell

Formate can be a substrate (equation II.1.1) or a product (equation II.1.2) of diverse reactions catalyzed by eukaryotes organisms, bacteria, and archae [14]. In addition, formate is either required or used by several cells for biosynthesis [15] (equation II.1.3, e.g. bioshynthesis of purines).

$$2HCOO^- \rightarrow 2CO_2 + H_2 + 2e^-,\ E=-420mV \qquad \text{(equation II.1.1)}$$

$$Pyruvate + CoA \rightarrow acetyl-CoA + formate,\ \Delta G^{o\prime}=-16.3kJ/mol \qquad \text{(equation II.1.2)}$$

$$Formate + H_4F + ATP \rightarrow N^{10}\text{-}formyl-H_4F + ADP + Pi,\ \Delta G^{o\prime}=+8.4\ 3kJ/mol \qquad \text{(equation II.1.3)}$$

In prokaryotes formate serves as the major electron donor to a variety of respiratory pathways which use terminal acceptors other than oxygen [16, 17]. Formate dehydrogenase catalyzes the two-electron oxidation of formate to carbon dioxide (equation II.1.1) being the key enzyme in this process. Formate dehydrogenases were identified in several both prokaryotes and eukaryotes organisms.

The best understood metabolic way for formate in prokaryotes organisms, as well as the best characterized Fdhs, corresponds to the *E coli* bacteria.

The genome of *E coli* contains three enzymes called Fdh-N, Fdh-O, and Fdh–H, which can oxidize formate in both cytoplasmic and periplasmic sides [18]. Whereas Fdh-N and Fdh-O are membrane bound enzymes with the catalytic subunit located in the periplasmic side of the cell, Fdh-H is a cytoplasmic protein (Figure II.1.1). Therefore, endogenous and exogenous formate must diffuse to periplasm and cytoplasm to be metabolized. Endogenous formate is derived primarily from pyruvate through a cleavage reaction catalyzed by pyruvate formate-lyase (PFL) [19].

The Fdh-N enzyme is expressed when cells are grown anaerobically in the presence of nitrate [20] and couples formate oxidation with nitrate reduction through the respiratory nitrate reductase [21-24]. In this system, formate is oxidized on the periplasmic side and the two electrons released are transported across the membrane to a bound menaquinone, which upon reduction takes up two protons from the cytoplasm. The electrons are transferred to Nar for the nitrate reduction in the cytoplasmic side on the membrane and the protons are released to the periplasm (Figure II.1.1). In contrast, Fdh-O is induced when cells are grown aerobically, but the enzyme is also induced under nitrate respiring conditions [25].

Fdh-H is synthesized only during fermentative conditions, forming part of the multiprotein formate hydrogen lyase complex (FHL) [19, 26, 27]. The active site of Fdh-H is located on the cytoplasmic side of the membrane (Figure II.1.1).

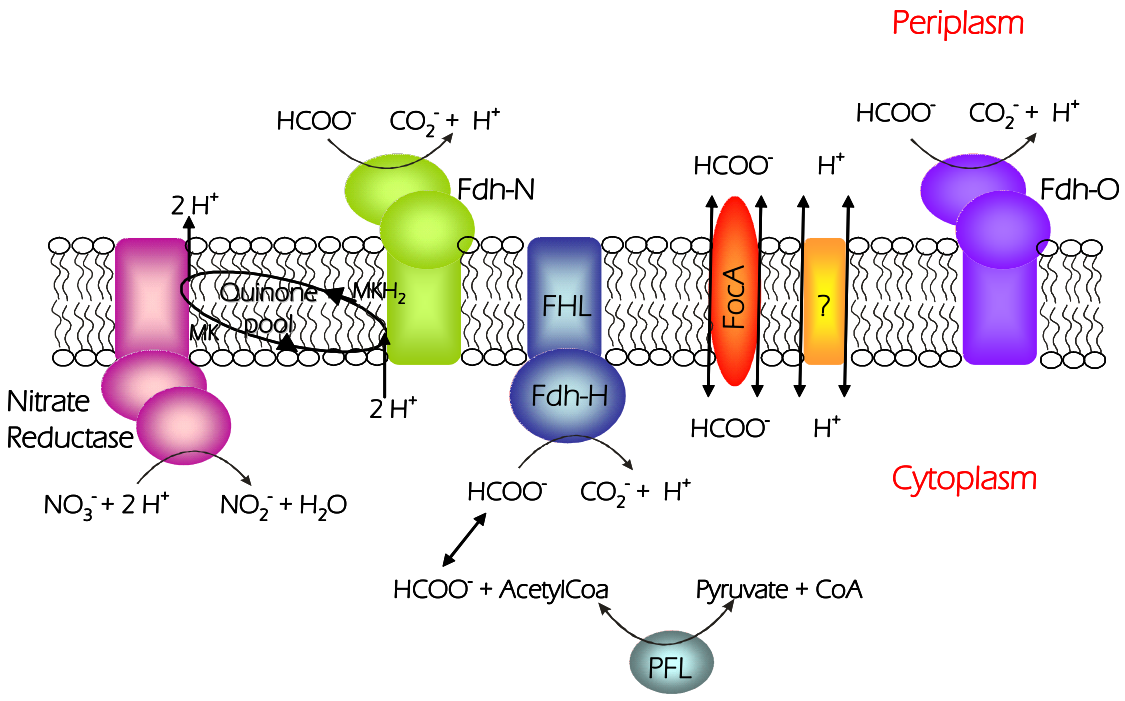

Figure II.1.1 Schematic representation of formate metabolism in *E coli.* (Adapted from reference [28])

In contrast, there is no much information on the formate metabolism in sulphate reducing bacteria. Most of the work has been performed on the genus *Desulfovibrio* and

the recent sequence of *D. vulgaris* Hildenborough genome has given important insights on the energy transduction and electron transport mechanisms [29].

In the *D. vulgaris* Hildenborough genome, three periplasmic formate dehydrogenases were identified. The detection of these Fdhs indicates that formate endogenous and exogenous must diffuse to periplasm to be metabolized [29]. As shown in Figure II.1.2, endogenous formate could generate from lactate oxidation to pyruvate, which could be then oxidized by a putative pyruvate-formate lyase (PFL) identified in its genome [29]. Subsequently, either the formate diffusing into the periplasm from cytoplasm or that from external sources is metabolized to CO_2 by any of the formate dehydrogenases. Electrons from formate oxidation would be transferred directly or indirectly to a cytochrome matrix for subsequent release to cytoplasm where sulphate is reduced (Figure II.1.2). Additional work is necessary to confirm this supposed pathway.

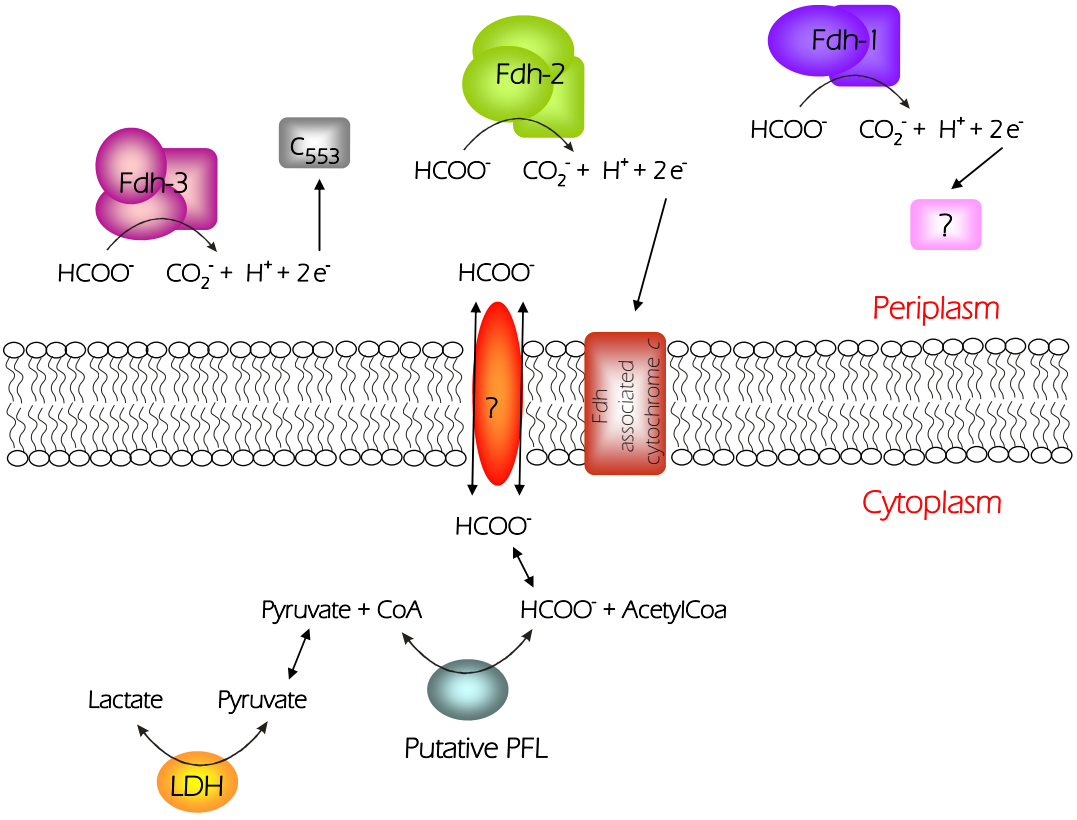

Figure II.1.2 Schematic representation of formate metabolism in *Desulfovibrio vulgaris* Hildenborough (Adapted from [29]).

II.1.2 Biochemical and structural properties of Mo- and W-Formate Dehydrogenases belonging to the DMSO reductase family

Formate dehydrogenases may be classified into two major families: NAD^+-dependent and NAD^+-independent Fdhs. According to the main properties, NAD^+-dependent Fdhs can be also divided in two subgroups. The first group includes enzymes that resemble the yeast-type Fdh and are in general insensible to oxygen. These enzymes contain two identical subunits, lack of metal cofactors and shows low affinity for formate. The second group comprises enzymes that have complex subunit structures, cofactors, and contains biologically active transition metals like molybdenum or tungsten [30-34].

NAD^+-independent Fdhs include a diverse group of microbial metalloproteins differing in factors such as physiological role, cellular location, substrate specificity, nature of physiological electron acceptor and content and type of metal cofactors [10, 35]. This group comprises a wide number of enzymes which can contain Mo or W in their active site. The most common Formate dehydrogenases belong to the big family of mononuclear Mo-enzymes and are usually found in anaerobic bacteria. Other W-Fdhs, which are usually purified from hyperthermophilic organisms and contain a pterin cofactor at the active site, have been classified in a different family called the W-enzymes [2, 36]. These enzymes are not analyzed in our study and they will not be discussed any further.

The structures of three Fdhs belonging to the dimethyl sulphoxide (DMSO) reductase family have been solved so far. Two of them are the Mo-containing Fdhs from *E coli* [37, 38] and one W-Fdh from *D. gigas* [39, 40]. These enzymes show a similar geometry coordination around Mo(W) ion (Figure II.1.3), but different subunit composition and cell location [1, 8, 10]. The biochemical and structural properties of these enzymes together with the best characterized Fdhs from sulphate-reducing bacteria are discussed in the following sections.

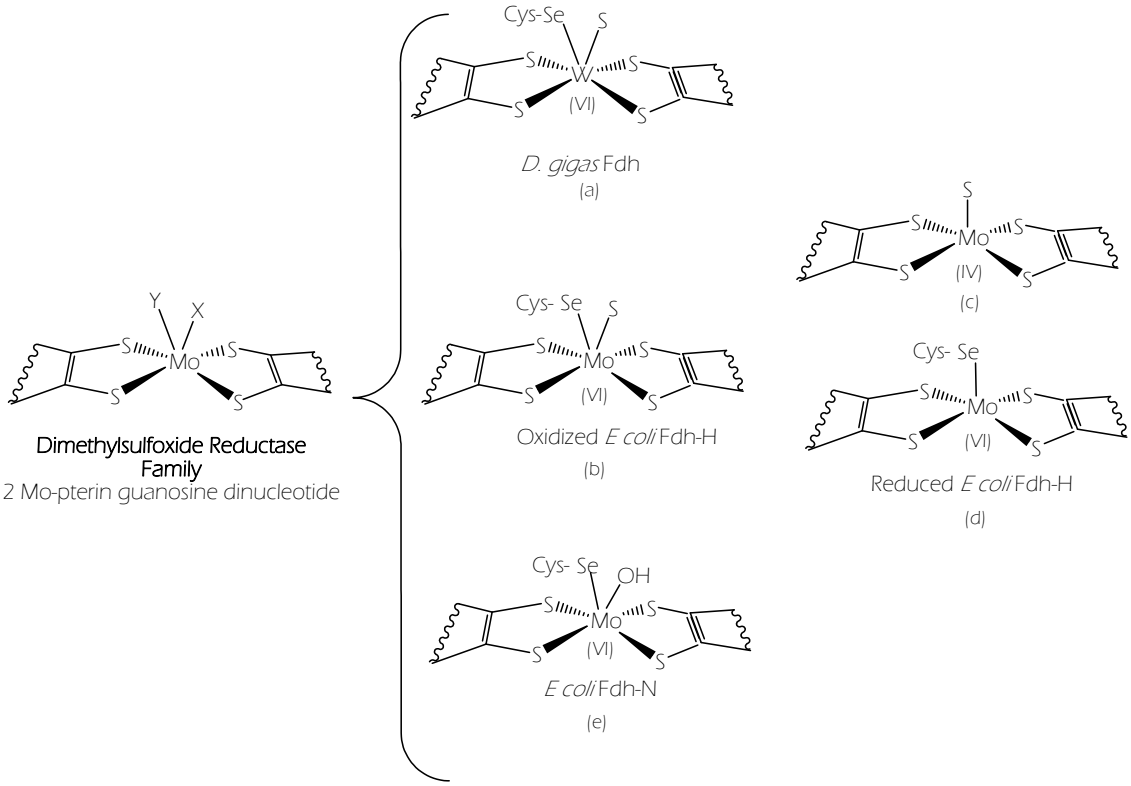

Figure II.1.3 Active site of three Fdhs belonging to the DMSO reductase family (adapted from [10]). X and Y represent ligands such as oxygen (oxo, hidroxo, water, serine, aspartic acid), sulphur (cysteine) and selenium atom (selenocysteine). The coordination around the active site of the enzymes was adapted from: (a), [39, 40]; (b), [37]; (c), [37, 41]; (d), [42]; (e), [23, 24].

II.1.2.1Formate dehydrogenases from sulphate reducing bacteria

II.1.2.1.1 W-Fdh from *Desulfovibrio gigas*

Although *D. gigas* is a strict anaerobic microorganism and Fdh is air sensitive, this enzyme can be purified under aerobic conditions since its catalytic competence can be restored [43]. This enzyme is an heterodimeric protein composed by a 110 kDa **α**-subunit and 24 kDa **β**-subunit [39, 40, 43]. The large subunit contains the W-containing active site and a [4Fe-4S] centre whereas the small subunit has 3×[4Fe-4S] clusters (Figure II.1.4).

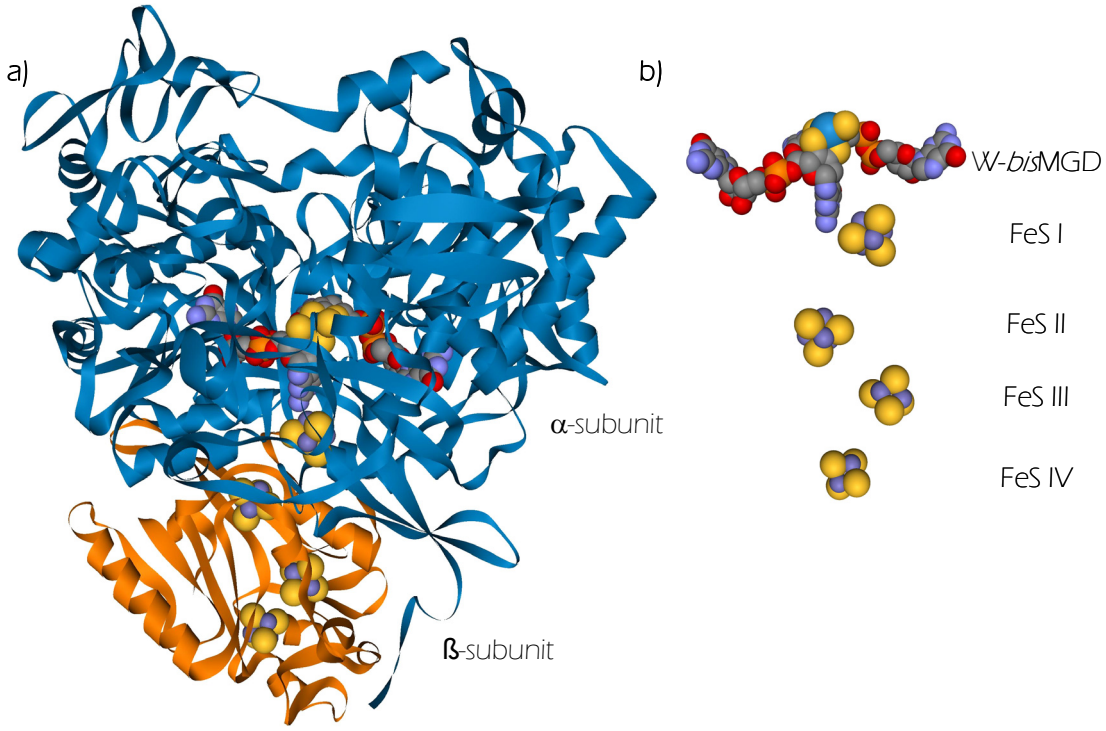

Figure II.1.4 Stereo representation of the overall structure of W-Fdh from *Desulfovibrio gigas* (a) and the redox cofactors involved in electron transfer (b) (reproduced from [35, 39, 40]).

The primary structure of the N-terminal large subunit (35 first aminoacids) shows the presence of a signal peptide with the twin arginine motif RRxFLK [44]. This feature is characteristic of Sec-independent export to the periplasm and harbored by periplasmic molybdoproteins. Amino acid sequence of small subunit lacks signal peptide suggesting that αβ complex is formed in cytoplasm before translocation to the periplasm [40]. A similar feature was observed for [NiFe] hydrogenases [45]. The amino acid sequence of the α-subunit shows the presence of conserved residues involved in the stabilization and orientation of substrate (Arg^{407}), coordination around W center ($SeCys^{158}$), enzymatic mechanism (His^{159}) and electron pathway between W and FeS I (Lys^{56}) [40].

D. gigas Fdh is the first representative W-enzyme from a mesophile whose crystal structure has been solved [39, 40]. Following the classification used for *E coli* Fdh-H [37] and *Dd* 27774 Periplasmic Nitrate Reductase [46], the large subunit was divided in four

domains (I, II, III, and IV). The W-active site is buried inside the protein and is stabilized by hydrogen bonding interactions to residues of mainly domains II, III and IV. Domain I carries the characteristic cysteine motif that binds the first [4Fe-4S] center (-$CX_2CX_nCX_mC$-). The N terminus of the large subunit wraps around the smaller subunit and contributes to the stability of the functional heterodimer. Like other Fdhs, coordination around W in the oxidized state includes four sulphurs, a SeCys and a sixth ligand that refined better as a sulphur than a oxygen atom, which is in contrast with that reported for the *E coli* enzymes (Figure II.1.5) [10].

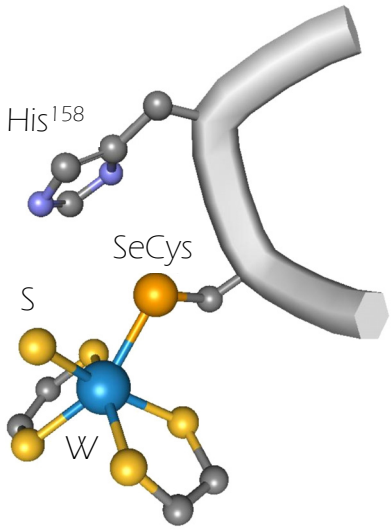

Figure II.1.5 Coordination around W atom in the oxidized Fdh from *Desulfovibrio gigas*.

II.1.2.1.2 Formate dehydrogenases from *Desulfovibrio vulgaris* Hildenborough

D. vulgaris Hildenborough contains three periplasmic Mo-Fdhs. As already observed in others Fdhs, the α-subunit of the three enzymes contains the active site and a [4Fe-4S] cluster. The β-subunit of Fdh-1 and Fdh-2 contains 2× [4Fe-4S] clusters whereas Fdh-3 has 3× [4Fe-4S] centres. Fdh-3, the best characterized *Dv*H Fdh, is a trimeric protein which contains in the third subunit four hemes type *c* [47] homologous to the soluble tetrahemic cytochrome c_3 found in *Desulfovibrio* species [48]. The physiological partner of this Fdh have been suggested to be the monohemic cytochrome c_{553} [47, 49, 50]. Fdh-2 is also a

trimeric enzyme which includes in the γ-subunit 11 *c* binding sites and have as redox partner a membrane bound cytochrome [29].

II.1.2.1.3 Formate dehydrogenase from *Desulfovibrio alaskensis* NCBI 1391

D. alaskensis Fdh is aerobically purified in two isoforms each containing Mo- or W-*bis* MGD at the active site. The protein is constituted by a 93 kDa α-subunit and a 32 kDa β-subunit. The UV-visible absorption spectrum of this enzyme is typical of an iron-sulphur protein and is very similar to that of the *D. gigas* W-Fdh which suggests a similar cofactor organization for both proteins. The EPR experiments shows at least three different [4Fe-4S] centres [51], but spin quantification of the FeS signal yields lower values than that expected for a protein containing 4 × [4Fe-4S] cluster, which suggests that the protein loses some iron during purification.

II.1.2.1.4 Formate dehydrogenase from *Desulfovibrio desulfuricans* ATCC 27774

Dd Fdh is a periplasmic trimeric enzyme which can be purified aerobically. The large subunit (~110 kDa) contains the Mo-*bis* MGD and one [4Fe-4S] centre [52]. EXAFS studies on the active centre of this enzyme show a hexacoordination around the Mo atom [53]. *Dd* Fdh, in its oxidized form, shows that Mo atom is coordinated to four sulphur atoms, an oxo-group and a Se atom. In addition, these data are consistent with a Se-S bound (Figure II.1.6a). In the reduced form of the enzyme, the oxo-group is replaced by a des-oxo ligand and the Se-S bound is reduced (Figure II.1.6b) [53].

A preliminary characterization of *Dd* Fdh [52] proposed a total of 2×[4Fe-4S] clusters. This result suggests that β-subunit contains only one [4Fe-4S] cluster which is unlike when compared with homologous Fdhs [23, 38-40]

As already observed in the closely related *Dv*H Fdh-3, the γ-subunit (~14kDa) is a cytochrome which was proposed to contain four hemes type *c* in a low spin configuration.

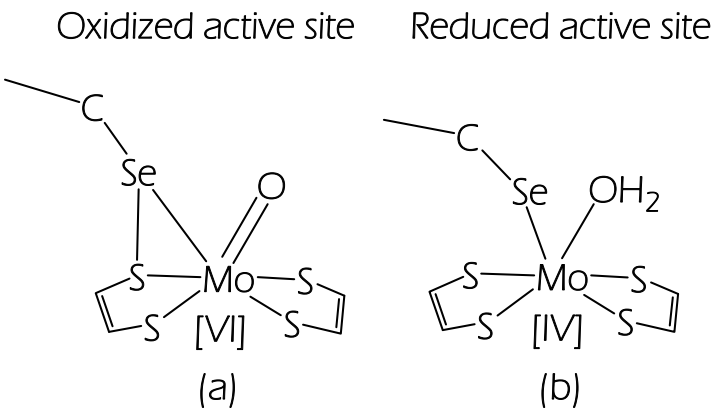

Figure II.1.6 Postulated coordination around Mo active site of *Dd* Fdh on the basis of EXAFS data [53]. Oxidized (a) and reduced state (b).

II.1.2.2 Formate dehydrogenases from *E coli*

II.1.2.2.1 Formate dehydrogenase H

Fdh-H is a monomeric cytoplasmic enzyme (79 kDa) which contains a Mo-*bis* MGD at active site and a FeS centre of the type [4Fe-4S]. The Fdh-H enzyme is extremely oxygen sensitive and needs to be purified in presence of high concentrations of azide. Despite this molecule was demosntrated to be a strong inhibitor of Fdhs, it is though to be necessary to protect inactivation by oxygen [54].

The structure of this enzyme consists of four $\alpha\beta$ domains (Figure II.1.7) [37]. Domain I coordinates the [4Fe-4S] cluster just bellow to the protein surface. Domain II coordinates the MGD^{801} and domain III coordinates MGD^{802}.

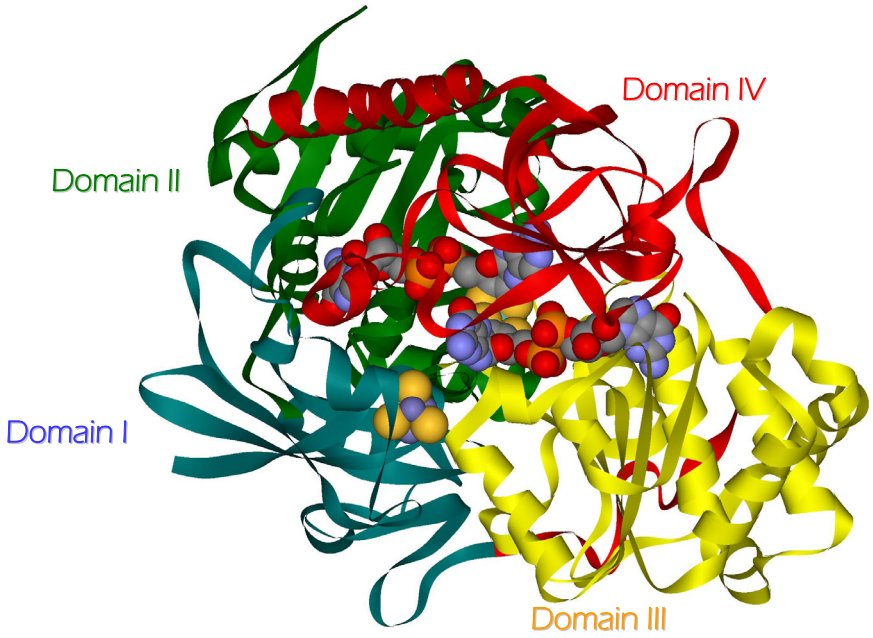

Figure II.1.7 Stereo view of *E coli* Fdh-H [37]. *Domains I, II, III and IV are shown in blue, green, yellow and red, respectively. Redox cofactors (Mo bis-MGD and [4Fe-4S] cluster) are represented as balls model.*

In the oxidized state, the Mo(VI) ion of the active site is coordinated to the four *cis*-dithiolene sulphurs of the MGD cofactors, $SeCys^{140}$ and a hydroxil ligand (Figure II.1.8). In contrast, a recent reinterpretation of the *E coli* Fdh [42] postulates a sulphur atom in the position of the hydroxyl ligand coordinated to the Mo(VI) specie.

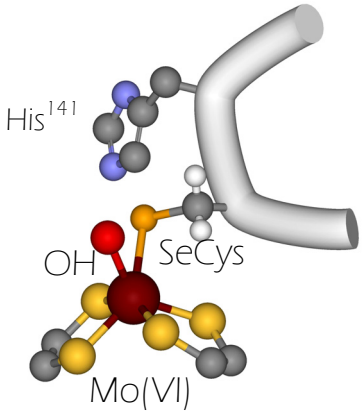

Figure II.1.8 The oxidized active site of *E coli* Fdh-H.

The X-Ray structure of the reduced enzyme shows that the coordination geometry around Mo(IV) is closely approximated by a distorted square pyramid where the sulphur atoms provide the four equatorial ligands and the selenocysteine provides the apical ligand (Figure II.1.9a) [37]. In contrast, a recent reinterpretation of these data potulates that the the apical position of the pyramid corresponds to a sulphur atom (Figure II.1.9b) [42].

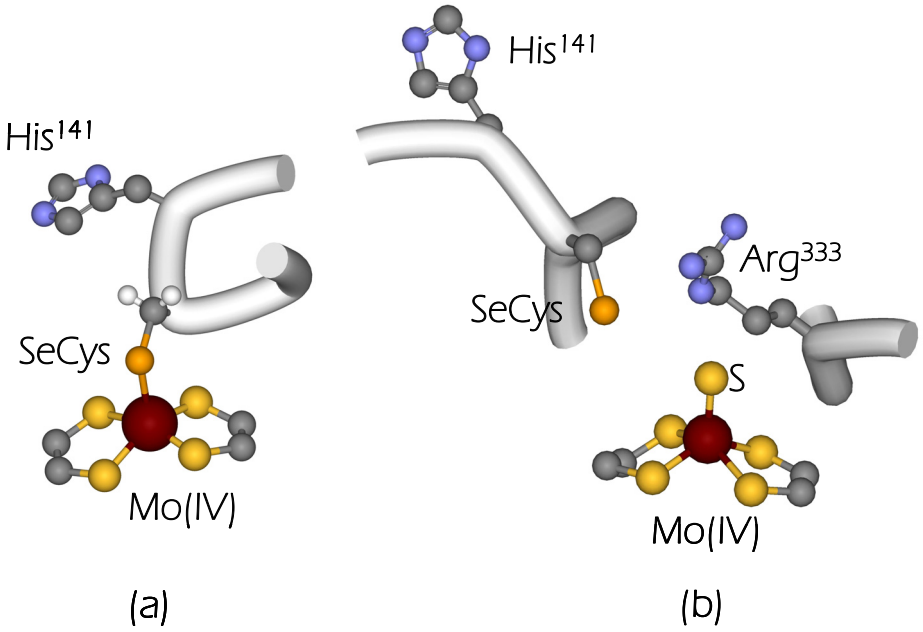

Figure II.1.9 Coordination around the reduced active site of *E coli* Fdh-H. (a) Formate reduced form as determined by Boyington J.C. *et al.* [37] (b) New interpretation by Raaijmakers & Romão [42].

II.1.2.2.2 Formate Dehydrogenase N

The enzyme Fdh-N and thedissimilatory nitrate reductase cooperate in one of the major alternative respiratory pathway: the nitrate reduction coupled to a transmembrane proton gradient (Figure II.1.1 [55]. Fdh-N is a large complex of 600 kDa with a $(\alpha\beta\gamma)_3$ structure. This enzyme is a membrane-bound protein that contains a Mo *bis*-MGD cofactor, heme and non-heme iron (Figure II.1.10) [38].

The catalytic α-subunit is located on the periplasmic side and harbours the Mo *bis*-MGD cofactor, a [4Fe-4S] cluster and the intrinsic SeCys residue. This subunit was divided into five domains (I-V). Domain I binds the [4Fe-4S] cluster, whereas domains II and III are

mainly involved in the coordination of the active site. The overall fold of this subunit is similar to the structures of *D. gigas* W-Fdh [40] and *E coli* Fdh-H [10, 23].

The β-subunit of Fdh-N has 4×[4Fe-4S] clusters and contains transmembrane helix in its C-terminal region. The N and C termini of the subunit are on the periplasmic and cytoplasmic sides, respectively. The subunit is divided into two subdomains each containing 2×[4Fe-4S] centres. This arrangement is similar to that of the small subunit of *D. gigas* W-Fdh, but the difference is that one of the subdomains only contains one [4Fe-4S] centre [39, 40].

The γ-subunit is a membrane bound cytchrome *b* with four transmembrane helices. This subunit contains two heme *b* groups (b_c and b_p) and a menaquinone reduction site. All four transmembrane helices are involved in maintaining the two heme groups; however, only three provide the heme ligands. Heme b_p, which is in the periplasmic side, receives electrons from the β-subunit. The electrons are then given to heme b_c, which is in the cytoplasmic side, to be finally transferred to the menaquinone.

Since edge-to-edge distances between redox centres (6 to11 Å) are shorter than the reported limit of physiological transfer (14 Å) [56] and than adjacent monomers (26.5 Å), the electrons transfer occurs within the monomer being each monomer a functional unit.

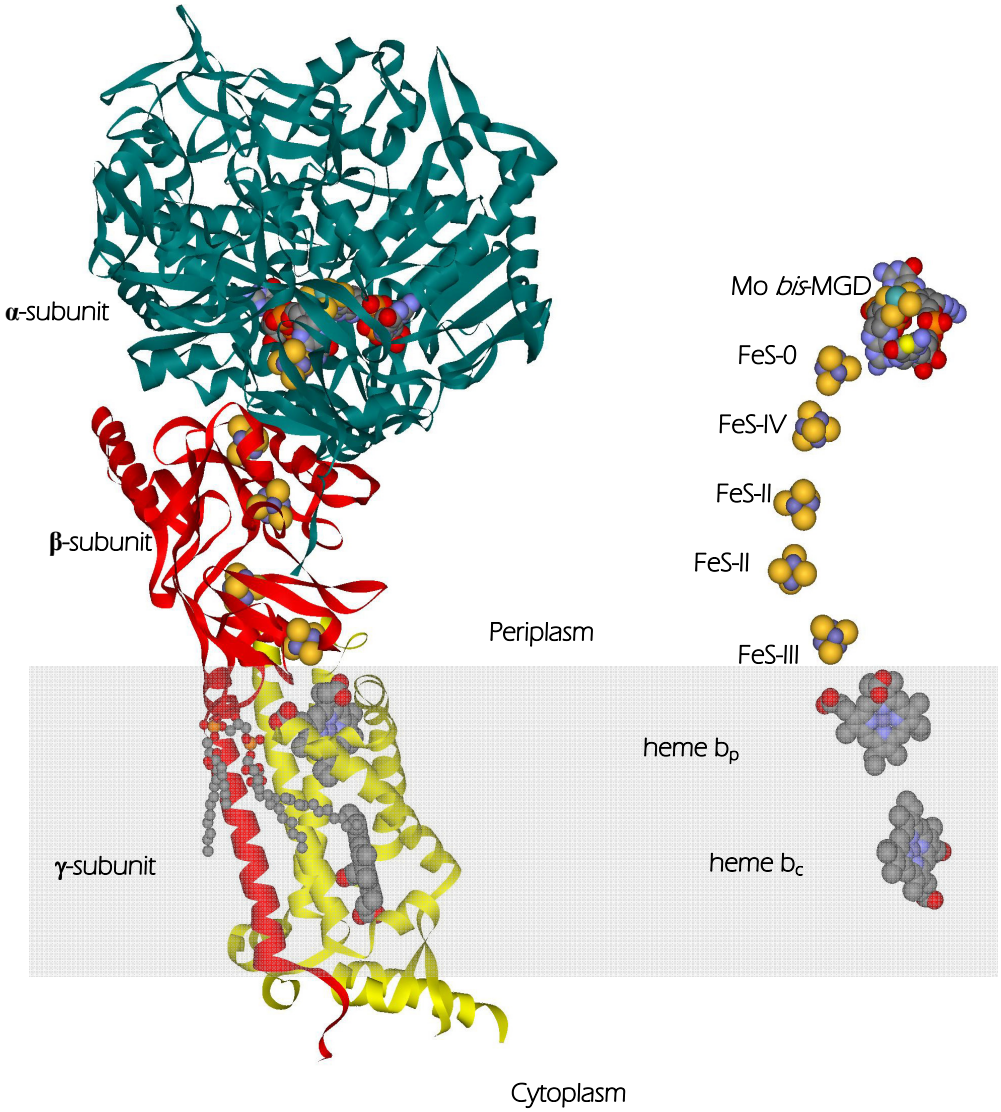

Figure II.1.10 Fdh-N from *E coli.* Left: overall stereo view with redox cofactors represented as balls model. Right: Arrangement of redox cofactors involved in electron pathway from formate to oxidized menaquinone.

II.1.3 Oxidation of formate to carbon dioxide: The proposed reaction mechanisms

Most of the enzymes containing molybdopterin are involved in catalysis of reactions in which an oxygen atom is transferred from the water to the product (equation II.1.4) [1, 57]. Fdh should be considered an oxotransferase if bicarbonate would be the direct product of formate oxidation (equation II.1.5). Nevertheless, mass spectrometric studies on *E coli* Fdh-H demonstrated that CO_2 rather than bicarbonate is the primary product of

formate oxidation (equation II.1.6) [41]. Consequently, Fdh is an exception in terms of reaction mechanism.

$$X + H_2O \Leftrightarrow XO + 2e^- + 2H^+ \qquad \text{(equation II.1.4)}$$

$$H_2O + HCOO^- \xrightarrow{Fdh} HCO_3^- + 2e^- + 2H^+ \qquad \text{(equation II.1.5)}$$

$$2HCOO^- \rightarrow 2CO_2 + H_2 + 2e^- \qquad \text{(equation II.1.6)}$$

Figure II.1.11 shows two proposed reaction mechanisms for Fdhs based on the crystal structure data of the *E coli* enzyme. The mechanism in black includes the species proposed by Boyington *et al* [37, 41] whereas the one in red the species by Raaijmakers & Romão [42]. In the mechanism of Boyington *et al.* [37, 41] the cycle begins when the formate molecule binds to the Mo(VI) site replacing the oxygen ligand. In doing this, it is though that the residues Arg^{333} and His^{141} are necessary to stabilize and to orient the substrate molecule (Figure II.1.12). The oxidation of the formate molecule implies the lost of the α-proton of formate, which is transferred to the nearby His^{141}[41], and the concomitant transfer of the two electrons to the Mo ion, after which, the CO_2 molecule is released. The next step is to shuttle electrons from the square pyramidal Mo(IV) site to the external electron acceptor through the [4Fe-4S] centre and thus catalytic cycle is completed. The residue Lys^{44}, which is well conserved in Fdhs, it is though to be essential in this process (Figure II.1.12). A similar mechanism was proposed by Raaijmakers and Romão but differs in that the formate molecule coordinates in the position of SeCys (Figure II.1.11, red arrows).

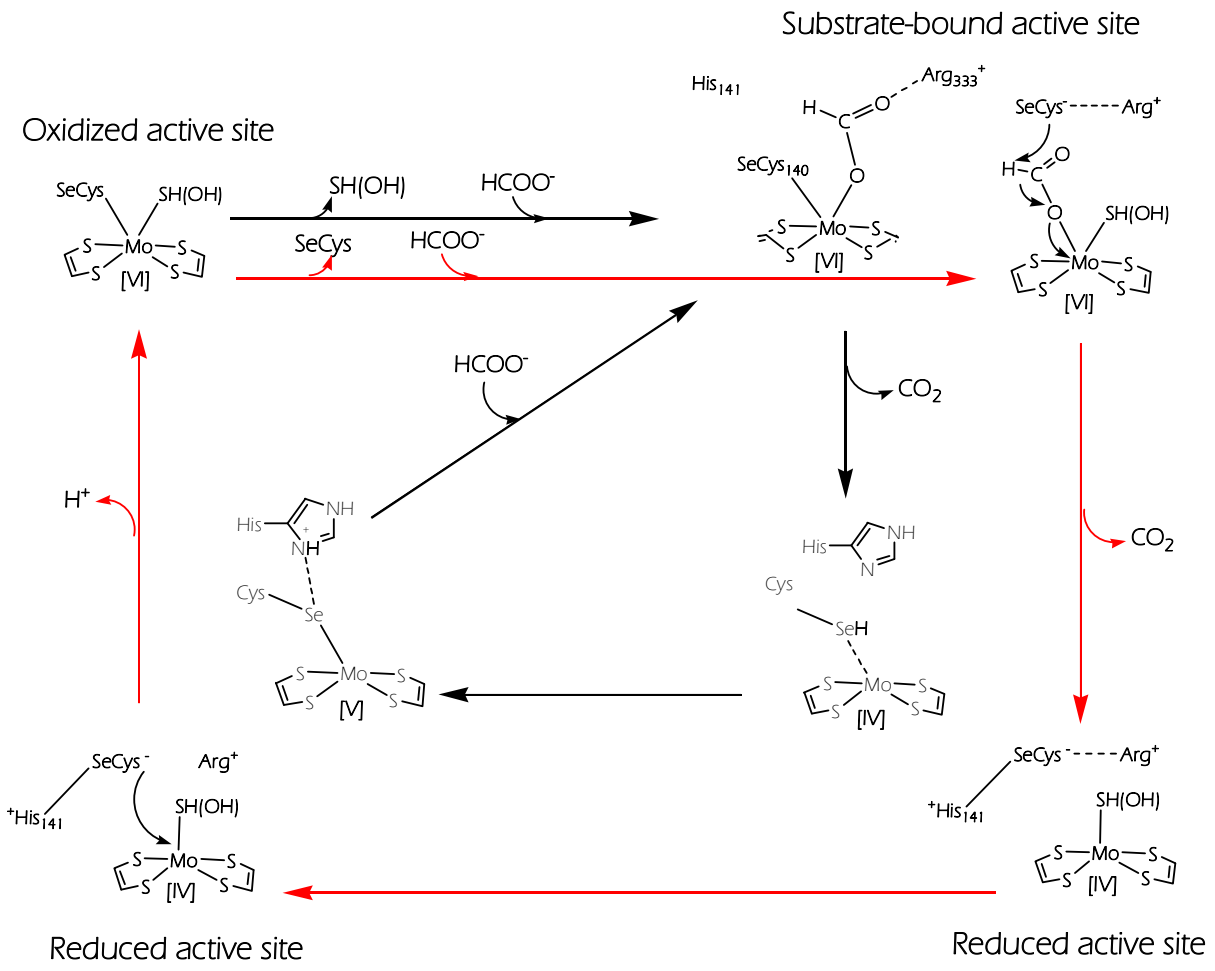

Figure II.1.11 Schematic representation of the reaction mechanism. Black line: proposed reaction mechanism for *E coli* Fdh-H by references [37, 41]. Red line: proposal for the reaction mechanism deduced from the reanalysis of the X-ray data of formate-reduced Fdh-H [42].

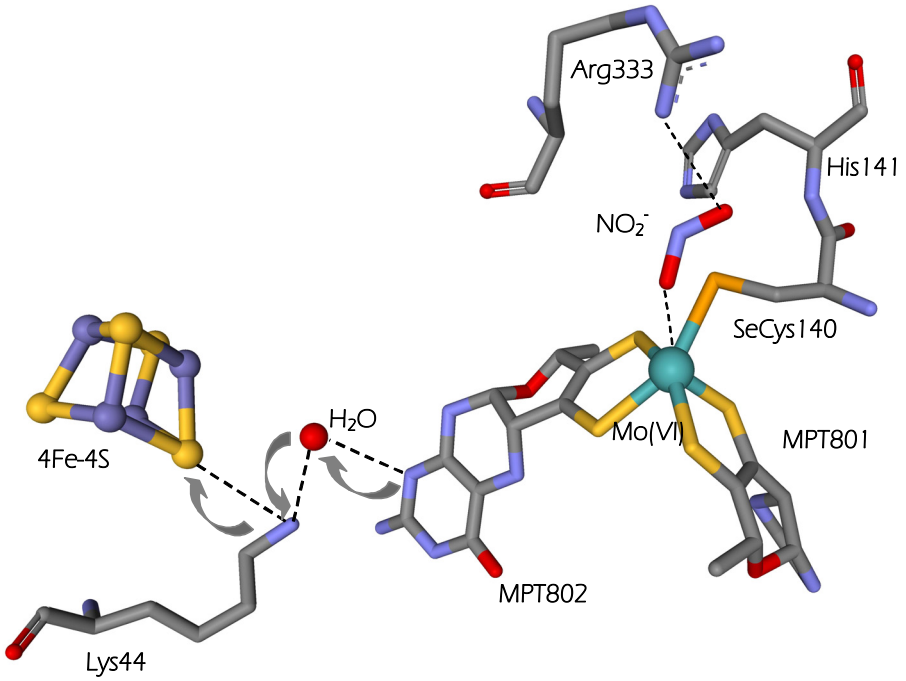

Figure II.1.12 The nitrite/formate binding site. *Nitrite molecule replaces the OH/SH ligand being stabilized by Arg*[333]*. The postulated electron transfer pathway is shown by grey arrows.*

II.1.4 Gene organization of Formate Dehydrogenases

Table II.1.1 shows operons encoding NAD^+-independent Fdhs identified in several bacteria.

The operons present variability in both composition and organization. In addition, some bacteria contain in the same genome up to three fdh-coding operons [29].

Table II.1.1 *Fdh* gene organization of several organisms.

Organism	Gene organization
Desulfovibrio desulfuricans G20	*fdhCAB*
	fdhAB
	fdhBA
	fdhABED
Desulfovibrio vulgaris Hildenborough	*fdhAB*
	fdhBACD
	fdhCEBA
Escherichia coli K12	*fdnGHI*
	hycABCDEFGHI
Sulfurospirillum multivorans	*fdhEABCD*
Desulfitobacterium hafniense	*fdhGHIE SelA SelB*
Pseudomonas fluorescens	*fdhABCE*

The *fdhA* gene (*fdhf* and *fdnG* in *E coli* Fdh-H [27] and Fdh-N [20], respectively) codifies for the catalytic subunit which contain the active site, a Mo or W*bis*-MGD, and one FeS centre.

In periplasmic enzymes, FdhA contains a signal peptide with a twin-arginine motif (SRRxFL/IK). Targeted proteins are substrate for the twin-arginine transport (Tat) system. This is a protein-targeting pathway found in the cytoplasmic membranes of many prokaryotes and the thylakoid membranes of chloroplasts [58, 59] whose function is transport fully folded proteins. In addition, the Tat translocase itself is thought to accept or reject proteins for transport through a quality control activity [60].

Another important feature in *fdhA* is the presence of a UGA codon. UGA, usually a stop codon, can also direct the incorporation of the modified amino acid selenocysteine [27, 61]. The mechanism of distinguishing between a selenocysteine insertion into a polypeptide and a termination polypeptide synthesis depends on the presence of a 40-base sequence downstream of the UGA codon [62]. This sequence fold into a stem-loop structure called SECIS element. The SECIS element contains a conserved cytosine, adjacent to the UGA codon, which prevents UGA reading. Furthermore, a bulged timine, which

interacts with a protein homologous to the elongation factor (SELB), is included (Figure II.1.13). Both cytosine and timine provide the additional information required for SeCys incorporation In *E coli*, SECIS element and *selA*, *selB*, *selC* and *selD* gene products are necessary for selenocysteine insertion [63, 64]. The presence of SECIS element was also detected in *D. gigas* W-Fdh [65].

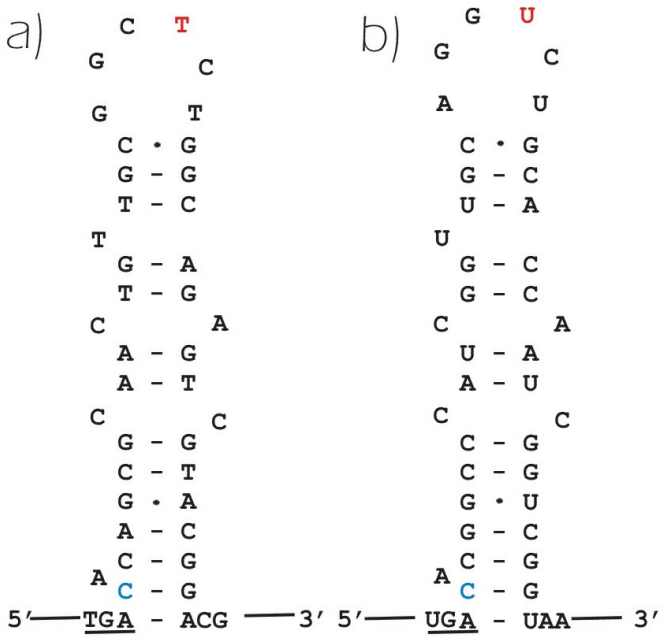

Figure II.1.13 Postulated SECIS element for: a) *D. gigas fdhA* [65] and b) *Escherichia coli* K12 *fdhF* [63]. **C**: single C that prevents UGA read through, **T**/**U**: bulged U/T that interacts with SELB.

The *fdhB* gene product (*fdnH* in *E coli*) is a ferredoxin-like protein. The *fdhB* product (FdhB) lacks signal peptide which suggests that, in periplasmic proteins, the formation of a complex between *fdhA* and *fdhB* product in the cytoplasm before translocation to periplasm [40, 45]. The number of cysteine motifs (-CXXCX$_n$CX$_m$C-) which coordinates the FeS clusters is variable.

The *fdhC* gene encodes a *c*-type cytochrome which is a part of trimeric Fdhs. Although multimeric Fdhs have been found several bacteria, the presence of low redox potential *c*-type cytochromes in Fdhs is specific to sulphate-reducing bacteria [50].

The *fdnI* gene codifies for a *b*-type cytochrome which is the transmembrane protein of membrane-associated Fdhs [23, 24, 38]. In *E coli* Fdh-N, a menaquinone reduction site was identified in the product of *fdhI gene,* which is in agreement with the menaquinol reduction function proposed for this subunit.

The function of *fdhD* and *fdhE* genes product is not completely clear. Studies on Fdh-N from *E coli* k12 suggest that in vivo role of the *fdhD* (*fdnC* in S. typhimurium) gene product is in enzyme assembly or maturation [66, 67].

II.2 MATERIALS AND METHODS

II.2.1 Cell growth and protein purification

D. desulfuricans ATCC27774 Fdh was isolated as reported before [52] but with some modifications. Cells (800 g wet weight) were suspended in 10 mM Tris-HCl buffer and ruptured in a French press at 9000 psi. After centrifugation (10000 × *g*, 45 min) and ultracentrifugation (180000 × *g*, 60 min) the supernatant was dialyzed against 10 mM Tris-HCl buffer. The soluble extract was subjected to a four step purification protocol. In the first purification step soluble extract was loaded onto an anionic exchange column (DEAE-Cellulose™, equilibrated with 10 mM Tris-HCl). The proteins were eluted using a Tris-HCl gradient (10-500 mM) and the fraction containing mainly Fdh was collected at ~200 mM. The second purification step included another anionic exchange column (Q-Sepharose, equilibrated with 10 mM Tris-HCl) in which a Tris-HCl gradient (10-250 mM) was applied. Fdh was eluted at ~200 mM ionic strength. After the first two anionic exchange chromatography, the major contaminants were Periplasmic nitrate reductase, ATP sulphurylase, Isadoxin and Split Soret. The third chromatographic step was a Hydroxyapatite column equilibrated with 100 mM Tris-HCl and eluted with a potassium phosphate linear gradient from 1 to 200mM. Fdh was eluted at 200 mM potassium phosphate. In contrast to that previously observed [52], no loss of activity was detected after the Hydroxyapatite column. In this step, Fdh co-eluted with ATP sulfurylase and Split Soret. Finally, a Superdex 200 (Pharmacia) column (equilibrated with 300 mM Tris-HCl) was used and Fdh was obtained pure as judged by SDS-PAGE. All purification procedures were performed under aerobic conditions at 4 ºC and pH 7.6. This procedure yielded approximately 30 mg of enzyme with a specific activity of 143(6) μmol/min/mg.

II.2.2 Protein and Metal quantification

A modified version of the Lowry/Biuret method [68] and Bicinchoninic Acid Kit (Sigma) were used for quantification of the protein concentration using bovine serum albumin as standard protein. In the modified Lowry/Biuret method, 0.4 ml of Biuret reagent was added to 0.1 ml of sample and incubated for 10 min at room temperature. Then, 3.5 ml of 2.3% Na_2CO_3 and 0.1 ml of Folin-Ciocalteu's phenol reagent were added and the sample was incubated for 30 min at room temperature. Finally, the absorbance was measured at 750 nm.

Mo, Se and Fe were quantified by inductively coupled plasma emission analysis in a Jobin-Yvon (Ultima) instrument using standards from Reagecom in a concentration range of 0.05-1.5 ppm.

II.2.3 Molecular weight determination

The molecular mass of the native protein was determined by gel filtration using a Superdex 200 column (1 x 30 cm) (Pharmacia) with a flow rate of 0.5 ml/min. The volume of protein or standard injected was 200 µl. The elution buffer was 50 mM potassium phosphate buffer pH 7.6 with 150 mM NaCl. The standards used were aprotinin (6.5 kDa), cytochrome c (12.4kDa), ovalbumin (47.2 kDa), aldolase (158 kDa), catalase (232 kDa) and ferritin (440 kDa) from Amersham Pharmacia.

In order to establish the protein purity and subunit composition, 15% tricine SDS-PAGE was carried out [69]. The standards used were: **α**-lactalbumin (14.4 kDa), trypsin inhibitor (20.1 kDa), carbonic anhydrase (30 kDa), ovalbumin (45 kDa), albumin (66 kDa) and phospholylase b (97 kDa) from Amersham Pharmacia. Proteins in the gel were stained with Coomassie Brillant Blue or silver stain [70].

II.2.4 Activity assays

Enzymatic assays were performed under anaerobic conditions in a final volume of 1.1ml following the reduction of benzyl viologen at 555 nm as previously described [52] but with some modifications. Enzyme (35 nM) was pre-incubated for 10 minutes at 37ºC with a solution containing 130 mM β-mercaptoethanol in 60 mM Tris-HCl, pH 7.6. Then, enzyme was reduced adding substrate (HCOONa or DCOONa) and incubating for 10 minutes. The reaction was started by the addition of 7.5 mM benzyl viologen. The addition order of the reagents constitutes the main difference with the previously employed method. Inhibition studies were performed adding azide, cyanide or nitrate together with the electron acceptor. All the procedures were performed under strict anaerobic conditions.

The absorbance changes versus time were recorded on an Agilent 8453 diode array spectroscopy system (sampling interval 0.9 nm between 190 – 1100 nm), equipped with a single-cell thermosettable holder in an open sample compartment. Experimental data were plot and fitted using least square fitted with appropriated models.

II.2.5 EPR spectroscopy

II.2.5.1 X-Band EPR spectroscopy

Spectra were recorded on a Bruker EMX spectrometer equipped with a dual-mode cavity (Model ER4116DM) and an Oxford Instrument continuous flow cryostat. Simulations of the Mo(V) signals were performed with the program Q-powa [71, 72]. FeS signals were simulated with WINEPR Simfonia v1.2 software from Bruker Instruments. Samples for EPR spectroscopy were prepared in 60 mM Tris- HCl buffer, pH 7.6. The spectra were acquired in non-saturating conditions. Mo(V) EPR experimental conditions were: Microwave frequency, 9.65 GHz; Modulation field, 100 kHz, Modulation amplitude, 5 G; Microwave power, 2 mW; Temperature, 100 K.

Mo(V) EPR signals were developed by reducing *Dd* Fdh samples (200 μM) with formate (HCOONa or DCOONa, D. 99% from Cambridge Isotopes) or sodium dithionite using a molar ratio of 30:1 or 20:1 reductant/enzyme, respectively.

Inhibited samples were prepared by dialyzing *Dd* Fdh (200 μM) against H_2O-buffer and D_2O-buffer (D. 99.9% from Cambridge Isotopes) containing inhibitors (cyanide or azide) with a final concentration of 3 mM. Then samples were reduced with sodium formate, as explained, to obtain the *formate* signal (see results). For the formate reduced samples, the inhibitors were added in anaerobic conditions to reach a concentration of 3 mM.

II.2.5.2 Q-Band EPR spectroscopy

Spectra were recorded on a Bruker ESP 300E spectrometer equipped with an ER051QG microwave bridge and a SF935 crystotat. EPR simulations were performed as described in II.2.5.1.

II.2.6 Spin quantification

EPR signals were quantified against a Cu-EDTA standard (1mM) according to the equation:

$$C_e = \frac{A_e}{A_r} \times \frac{M_r}{M_e} \times \sqrt{\frac{P_r}{P_e}} \times \frac{G_r}{G_e} \times \frac{g_{iso,r}}{g_{iso,e}} \times \left(\frac{d_r}{d_e}\right)^2 \times C_r$$

Where "C" is the spin concentration (spins/molecule), "A" is the area under the absorption EPR signal, "M" is the modulation field (G), "P" is the microwave power (W), "G" is spectrometer gain, "g_{iso}" is the isotropic g value, "d" is the diameter of the EPR tube. The sub-indices "e" and "r" stand for the experimental and reference samples, respectively.

II.2.7 Fdh operon sequence

II.2.7.1 Gene isolation strategy

In a first step, conserved sequences presents in organisms filogenetically related were used to design primers to isolate DNA sequences codifying α and β subunits. Multiple alignments of DNA sequences were performed using MACAW software [73]. The primers designed, the fragments amplified, and the annealing temperatures used in the amplification reactions are described in the Table II.2.1.

The DNA sequence located between *fdhB* and *fdhC* was amplified using a specific forward primer designed from of 3' termini of *fdhB* and a degenerated reverse primer designed from N-terminal aminoacid sequence of FdhC (Table II.2.1, primers fFdhDE and rFdhDE).

When no conserved sequences were available the genome walking technique [74, 75] was used to sequence fdh gen. For each fragment amplified, two specific primers (one for the primary PCR reaction and another for secondary PCR reaction) were designed using the sequences obained in the first strategy (Table II.2.2).

Table II.2.1 Primers used to amplify Fdh DNA fragments from fresh *Dd* cells

Primer Name	Orientation	Sequence (5'-3')	Tm (° C)	Target	Product fragment size (bp)
F1fdh	Forward	GGYGCAGAACATCCG	65	FdhA	650
R1fdh	Reverse	AGYGCCACTGCAMCCAGCG			
F2fdh	Forward	GGYGCRATGACSAAYCACTGG	60	FdhA	700
R2fdh	Reverse	TAGCGCGTTGATGCC			
F3fdh	Forward	CCAAGACCAAGAAGACCG	57	FdhA	500
R3fdh	Reverse	TCCRGSGARGCRCGG			
F5cfdh	Forward	CCCTCAACTGGATATACACCG	62	FdhB	1400
R5cfdh	Reverse	ATGGTMCCSGTVGGRCAGG			
F2betaFdh	Forward	TCAGCGTGATCTACCTGC	59	FdhC	2000
R2gamaFdh	Reverse	GATGGGYTCCTTGATGG			
fFdhDE	Forward	GGCACTTGGGCATATCTCC	60	FdhE	1000
rFdhDE	Reverse	CCTCATGCTGCCATTGC			
FdhBEf	Forward	TTCAGTCAGGTTTCAGTTTGG	60	FdhB/FdhE	300
FdhBEr	Reverse	CATTGATGCTCCCAAACC			

Table II.2.2 Specific primers used in Genome Walker technique.

Primer Name	Orientation	Sequence (5'-3')	Tm (° C)		Target	Product fragment size (bp)
			Tm1	Tm2		
eu1Ddfdh	Reverse	TAATGGTCCTTCATGAGGTTGATGACG	74	69	FdhA	400
iuDdfdh	Reverse	GGTGTAGTTGTTAACGTACTCCTTGTGG	68	63		
e2GWDdfdh	Reverse	CCGTTGTCCTTGGCTTTCATGATCC	76	71	FdhA	500
i2GWDdfdh	Reverse	ATGTCGATCCAGTGATTGGTCATTGC	74	69		
e3GWDdfdh	Reverse	CTTGATGGATAACAGCGCACTCTTCG	75	70	FdhA	500
i3GWDdfdh	Reverse	AGAAGATGGTTTCCAGACGGTTGACC	74	69		
e4GWDdfdh	Forward	GCCATGATACAGGACAAGAAAACAGG	72	67	FdhB	500
i4GWDdfdh	Forward	AGGAGGCCTGCCCCTATAATATTCCC	74	69		
e5GWFdh	Reverse	TGATCTGACACTGAACAGAACAGAAGG	71	66	FdhA	700
i5GWFdh	Reverse	AGAAGGGGCAAATGCTCGATACTTCC	75	70		
eGWGammaFdh	Forward	CAAGGGAAACCGTTGCAGTAATGAGG	75	70	FdhC	1000
iGWGammaFdh	Forward	GGGCTTCCGAAGATTTACTACCTCAGG	71	66		

II.2.7.2 DNA amplification reactions

As described in II.2.7.1, two different strategies were used for amplified the Fdh gen.

In both protocols the mixture for the PCR reaction contained 1 x PCR buffer (10 mM Tris-HCl, pH 9.0, 1.5 mM $MgCl_2$, 50 mM KCl), 0.2 mM dNTP´s, 50 pmol of the reverse and forward primer (Table II.2.1 and II.2.2), 5 U of Taq DNA Polymerase (Amersham), and template, in a final volume of 25 µl.

For the first strategy, direct PCR of boiled cell suspensions allowed rapid amplification using primers described in Table II.2.1. Briefly, a 1 ml aliquot of *Dd* culture was washed and resuspended in 50 µl of TE buffer (Tris-HCl 10 mM, 1mM EDTA; pH 7,6). Then, the cell suspension was kept in a boiling water bath for 5 min, followed by centrifugation at 10000 rpm during 5 min. Volumes between 2 to 10 µl of supernatant were used as DNA template. The program for the amplification was the following: 5 min, at 94ºC for the denaturation of the DNA, and 30 cycles of 1 min at 94 ºC, followed by 1.5 min at annealing temperature (Tm, Table II.2.1) and 3 min at 72 ºC for DNA extension. After these cycles the mixture was incubated for another 5 min at 72 ºC, and then was cooled down to 4 ºC. The temperature of the lid was 105 ºC.

The second strategy used, Genome Walker, involves the use of specific primers, DNA libraries as template, two PCR having different programmes and primers to DNA annealing temperatures (T_m1 and T_m2, Table II.2.2). The genomic DNA used for preparation of libraries was purified from *Dd* ATCC 27774 cells according to the protocol described by Wilson [76]. Libraries were prepared using four different restriction enzymes (DraI, EcoRV, PvuII and StuI from Fermentas) and the genomic DNA fragments were ligated to adaptors. All the procedures were performed following the protocol described in GenomeWalker™ kit (Clontech Laboratories).

The programme for the first PCR amplification was: 5 cycles of 25 sec at 94°C and 3 min at T_m1, followed by 20 cycles of 25 sec at 94°C and 3 min at T_m2. After these cycles the mixtures were kept for 7 min at 72 ºC.

The primary PCR mixtures were then diluted (1/20) and 1 µl of each dilution was used as template for the secondary PCR.

The programme for the second PCR was: 7 cycles of 25 sec at 94°C and 3 min at T_m1, followed by 32 cycles of 25 sec at 94°C and 3 min at T_m2. In the last step the mixtures were incubated 7 min at 72 ºC.

Fragments amplified by direct PCR from the cells and from libraries were analyzed by electrophoresis in 1-2% agarose gels and purified from using the QIAquick gel extraction kit.

II.2.7.3 Cloning and sequencing fdh gen.

The purified DNA fragments were cloned into the pCR2.1-TOPO vector using the TOPO-TA cloning kit (Invitrogen). Then, One Shot Mach1-T1 chemically competent *E coli* (Invitrogen) were transformed with these constructs. Transformants were plated on LB plates containing 100 µg/ml ampicillin and 40 mg/ml X-Gal for blue-white colour screening. Colony PCR of white colonies was done to confirm positive selection before sequencing. PCR products were analyzed by electrophoresis in 1-2% agarose gels. Isolated positive colonies were growth in LB ampicilin medium and plasmidic DNA was isolated using QIAprep Spin Miniprep Kit (Qiagen). Most of the molecular biology techniques (as transformations, isolation of agarose gel fragments, ligation of vector and DNA fragments, and preparation of DNA sequencing samples) used were performed according to manufactures' instructions.

Finally, the DNA fragments were sequenced using an ABI3700 DNA Analyzer; (Perkin-Elmer/Applied Biosystems. Stabvida, Oeiras, Portugal). The obtained sequences were submitted to GenBank (ABE73760 and ABE73761).

II.2.7.4 Analysis of protein and DNA sequences

Nucleotides sequences were translated into proteins using the TRANSLATE program at Expasy (http://www.expasy.org/tools/dna.html).

Sequence database search for homology between fragments obtained and fdh genes sequenced was performed using the BLAST programme at NCBI (http://www.ncbi.nlm.nih.gov/BLAST/)

The presence of probable signal peptide sequence in the primary sequences was analyzed using Signal P 3.0 programme (http://www.cbs.dtu.dk/services/SignalP/) [77].

The molecular weight of the mature proteins was calculated using the ProtoParam programme (http://www.expasy.org/tools/protparam.html) [78].

Multiple protein alignments were performed with CLUSTALW programme at http://npsa-pbil.ibcp.fr/cgi-bin/npsa_automat.pl?page=npsa_clustalw.html.

II.2.8 Sequencing N-Terminal Fdh Subunits

A 15% tricine SDS-PAGE [79] was used to separate approximately 2.5 ng of pure Fdh. Gel pieces containing **α**, **β**, and **γ** subunits were excised and incubated in 500µl Millipore water at 4ºC during 36 hours. After that, the solution was lyophilized and re-suspended in an appropriated volume for sequencing.

Subunits were sequenced by Edman degradation reaction, in a Protein Sequencer (Applied Biosystems, model 491, Faculdade de Ciências e Tecnologia, Universidade Nova de Lisboa, Portugal).

II.3 RESULTS

II.3.1 Molecular properties

Molecular weight determination of the as-prepared protein by exclusion molecular chromatography shows a peak corresponding to 150 kDa.

SDS gel electrophoresis shows three bands at 100 kDa, 30 kDa and 14 kDa approximately (Figure II.3.1).

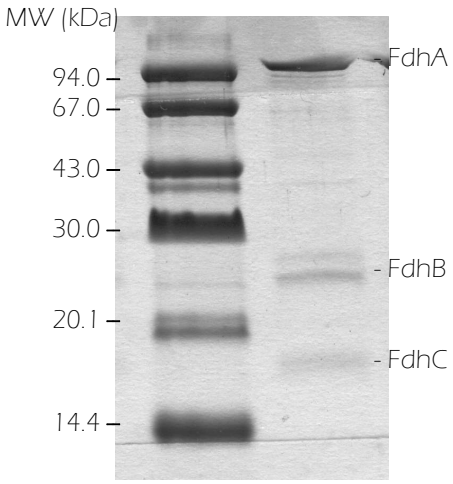

Figure II.3.1 Tricine SDS-PAGE (15%) of *Dd* Fdh after Superdex 200 column.

II.3.2 UV-visible spectroscopy

As was previously published [52], the UV- visible spectrum of the air-oxidized pure protein (Figure II.3.2) shows a Soret peak at 409 nm. This wavelength, the line shape of the **α**,**β** region (500-600 nm) as well the absence of bands in the 630-650 nm region confirms that the hemes are in the low spin state. Upon reduction with dithionite, Soret bands shifts to 416 nm and **αβ** bands develop at 552 nm and 523 nm, respectively. Metals quantification reveals the presence of 15.1±0.4 Fe/protein, 1.1±0.2 Mo/protein, and 1.8±0.6 Se/protein. These results are similar to the values previously reported [52].

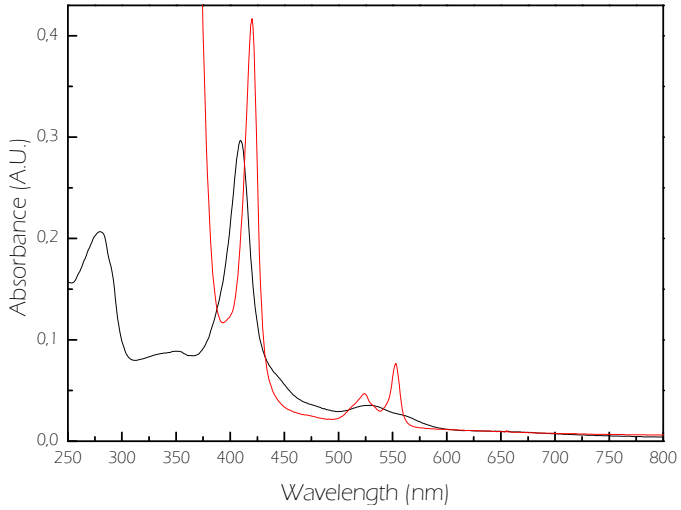

Figure II.3.2 UV-visible spectra of as-prepared *Dd* Fdh (black line) and dithionite reduced form (red line).

II.3.3 Fdh operon sequence

A genomic segment of 6895 bp was sequenced (Figure II.3.3) and found to contain a cluster of four collinearly oriented open read frames that , on the basis of similarity to others *fdh* genes, were designated as genes *fdhA*, *fdhB*, *fdhE and fdhC* (Figure II.3.4). Furthermore, two gaps located upstream and downstream of the *fdhE* gene were observed.

Figure II.3.3 Nucleotide and corresponding aminoacid sequence of the four ORF of *Dd* Fdh operon. *Underlined sequences show the putative Ribosome Binding Sites (RBS),* M *and* * *are the ORF start and end, respectively.*

```
   1 - TTGGTAAATAGTGGAGTAAAATCCGCAGCTTCATATTCTGCTCAACGGCCTGTGAAAAAG - 60

  61 - TTTTCGCAGGCCGTTTTTTGGGCGCTTTTGCGGCCGGGGCCGCCCTGTTGACAACGGAAG - 120

 121 - TGGAAAAAATTGATGGATAAATAAAATGGTAAAAGAAAAATTCAGTGATTTCGGGCGATA - 180

 181 - TTCCATACATGTTTTTTGTGATTTTTCAGCAAAAAATGGACAGCATCAAGGGGGAGTTTA - 240

 241 - AGTATCTGGCTGGAATGGTATGACAATTTACCATCTAGGGAAAAATATCACAAACACGTG - 300

 301 - AAACTATAATATAAAATGTCGAACAATCTTGCGACATCACGATTTTTGGAATATGGTGAC - 360

 361 - CGCAACTCTTTTTATTATCAAGGCGCACACATTGTCGCCAAAGCTTCTTTTGCGCGGCCG - 420

 421 - CCTGCCTCGGCCCCGCGCATGTGACAGGCACAAACAAGGAGAGGTCTCATGAAAAGCACT - 480
     -                                          M  K  S  T

 481 - CGACGGAGTTTTCTCAAAGGTGTCGGTGCAGGGGTATTATGCCTTACGCTGGGGCACCTG - 540
     - R  R  S  F  L  K  G  V  G  A  G  V  L  C  L  T  L  G  H  L

 541 - GGTTTTGACCTGGGCGAGGCCCAGGCATACGCCGGCAAACTCAAGATCGAGGGTGCCAAG - 600
     - G  F  D  L  G  E  A  Q  A  Y  A  G  K  L  K  I  E  G  A  K


 601 - GAAGTATCGAGCATTTGCCCCTTCTGTTCTGTTCAGTGTCAGATCATCGCTTACGTCAAG - 660
     - E  V  S  S  I  C  P  F  C  S  V  Q  C  Q  I  I  A  Y  V  K

 661 - GGCGGCAAGCTTGTCTCCACTGAGGGCGATCCGGACTTTCCCATCACCGAAGGCGCGCTC - 720
     - G  G  K  L  V  S  T  E  G  D  P  D  F  P  I  T  E  G  A  L

 721 - TGCGCCAAGGGCGCGGCGCTGTACTCCATGTACACCAGCGACCACCGCCTGATGAAACCC - 780
     - C  A  K  G  A  A  L  Y  S  M  Y  T  S  D  H  R  L  M  K  P

 781 - ATGTATCGCGCTCCGTTCAGCGACAAGTGGGAAGAAAAAGACTGGGACTGGACCCTTGAG - 840
     - M  Y  R  A  P  F  S  D  K  W  E  E  K  D  W  D  W  T  L  E

 841 - CAAATAGCGCGCCGCGTCAAGGACGCACGCGATAAGGATATGATCCTTAAAAACGACAAA - 900
     - Q  I  A  R  R  V  K  D  A  R  D  K  D  M  I  L  K  N  D  K

 901 - GGGCAGACGGTCAACCGTCTGGAAACCATCTTCTGGATGGGAACCTCGCACGCTTCCAAC - 960
     - G  Q  T  V  N  R  L  E  T  I  F  W  M  G  T  S  H  A  S  N

 961 - GAAGAGTGCGCTGTTATCCATCAAGCCTTGCGCGGCCTGGGTGTTGTCCATATGGACCAC - 1020
     - E  E  C  A  V  I  H  Q  A  L  R  G  L  G  V  V  H  M  D  H

1021 - CAGGCGCGGGTCTGACACAGCCCCACTGTTGCGGCTCTGGCAGAGTCGTTCGGACGCGGT - 1080
     - Q  A  R  V  *  H  S  P  T  V  A  A  L  A  E  S  F  G  R  G

1081 - GCAATGACCAACCACTGGATCGACATCAAGAATGCCGATGCGGTGCTTATTATCGGCAGT - 1140
     - A  M  T  N  H  W  I  D  I  K  N  A  D  A  V  L  I  I  G  S

1141 - AATGCCGCTGAACATCATCCCGTGGCTTTCAAATGGATCATGAAAGCCAAGGACAACGGG - 1200
     - N  A  A  E  H  H  P  V  A  F  K  W  I  M  K  A  K  D  N  G

1201 - GCCGTGCTCATGCACGTGGACCCCAAGTTCTCGCGCACATCCGCCAGGTGTGATTTCCAT - 1260
     - A  V  L  M  H  V  D  P  K  F  S  R  T  S  A  R  C  D  F  H

1261 - GTGCCCCTTCGCTCGGGTACGGACATCCCCTTCCTGGGCGGCATGCTCAACTACATCCTT - 1320
     - V  P  L  R  S  G  T  D  I  P  F  L  G  G  M  L  N  Y  I  L

1321 - GAAAACGGTTTGTACCACAAGGAGTACGTTAACAACTACACCAACGCGGCCTTTGTGGTG - 1380
     - E  N  G  L  Y  H  K  E  Y  V  N  N  Y  T  N  A  A  F  V  V
```

```
1381 - GGTGACGGCTACGCCTTTGAAGACGGGCTTTTCAGCGGCTATGATGCCGCCGCCCGCAAG - 1440
     - G  D  G  Y  A  F  E  D  G  L  F  S  G  Y  D  A  A  A  R  K

1441 - TATGACAAAAGCAAGTGGGCCTTGGCCAAGGGGCCTGACGGCGGGCCTGTCGTGGATCCC - 1500
     - Y  D  K  S  K  W  A  L  A  K  G  P  D  G  G  P  V  V  D  P

1501 - ACACACCAGAACCCGCGCTGCGTCATCAACCTCATGAAGGACCATTACTCCCGCTACACG - 1560
     - T  H  Q  N  P  R  C  V  I  N  L  M  K  D  H  Y  S  R  Y  T

1561 - CTTAAAAACGTCTCCGACGTCACGGGCGTTTCGCAGGACAACCTGCTCAAGGTGTACAAG - 1620
     - L  K  N  V  S  D  V  T  G  V  S  Q  D  N  L  L  K  V  Y  K

1621 - AACTTCTGCGCTACCGGCAGGCCGGACAAGGCGGGAACCATTCTTTACGCTCTGGGCTGG - 1680
     - N  F  C  A  T  G  R  P  D  K  A  G  T  I  L  Y  A  L  G  W

1681 - ACACAGCATACAGTAGGCGTGCAGAACATCCGCCTTTCGAGTCTTGTGCAGCTCTTGCTG - 1740
     - T  Q  H  T  V  G  V  Q  N  I  R  L  S  S  L  V  Q  L  L  L

1741 - GGCAACATAGGCATCGCCGGGGGCGGCATCAACGCGCTACGCGGCGAACCTAACGTGCAG - 1800
     - G  N  I  G  I  A  G  G  G  I  N  A  L  R  G  E  P  N  V  Q

1801 - GGCTCGACCGACCATGCCCTGCTGTACAACAACATTCCCGGCTACCACGGCACACCCCAG - 1860
     - G  S  T  D  H  A  L  L  Y  N  N  I  P  G  Y  H  G  T  P  Q

1861 - GCTCCGTGGCAGACCCTGGGCGAATACAACAAGGCCAATACCCCGGTAACGGTGGTGCCT - 1920
     - A  P  W  Q  T  L  G  E  Y  N  K  A  N  T  P  V  T  V  V  P

1921 - AACAGCGCCAACTGGTGGGGCAACAGGCCCAAGTATGTGACAAGTCTGCTCAAGGGCTGG - 1980
     - N  S  A  N  W  W  G  N  R  P  K  Y  V  T  S  L  L  K  G  W

1981 - TTCGGCGATGCCGCCACCCCCGAAAACGACTTCTGCTACAGCCTGCTGCCCAAGCTGGAG - 2040
     - F  G  D  A  A  T  P  E  N  D  F  C  Y  S  L  L  P  K  L  E

2041 - CCGGGCGTGGACTATTCGTACATGTTCGTCATGGACAGGATCTATAACAAGAAGATCAAG - 2100
     - P  G  V  D  Y  S  Y  M  F  V  M  D  R  I  Y  N  K  K  I  K

2101 - GGCGGCTTCATCATGGGTGTAAACCCCATGAACAGCTTCCCCAACACCAACAAGATGCGG - 2160
     - G  G  F  I  M  G  V  N  P  M  N  S  F  P  N  T  N  K  M  R

2161 - GCAGCCCTGGACAATCTTGACTGGCTGGTCTGTTCCGAAATCCATAATTCGGAAACCACG - 2220
     - A  A  L  D  N  L  D  W  L  V  C  S  E  I  H  N  S  E  T  T

2221 - GATAACTGGCAACGCCCCGGCGTGGGCCCCAAGACCAAGAAGACCGAGGTCTTTTTGCTG - 2280
     - D  N  W  Q  R  P  G  V  G  P  K  T  K  K  T  E  V  F  L  L

2281 - CCTTCGGCCCATCGCATCGAAAAGGCGGGAACCATCAGCAACAGCGGGCGCTGGTTGCAG - 2340
     - P  S  A  H  R  I  E  K  A  G  T  I  S  N  S  G  R  W  L  Q

2341 - TGGCACTACAAGGCCGTGGAACCCGCCGGAGAGGCGCGCAACTTCGCTGACGTGGTCGTG - 2400
     - W  H  Y  K  A  V  E  P  A  G  E  A  R  N  F  A  D  V  V  V

2401 - CCGCTCTTCAACACCATCCGCCGCATGTACAAGACAGAGGGCGGGGTACTGCCCGAAGCC - 2460
     - P  L  F  N  T  I  R  R  M  Y  K  T  E  G  G  V  L  P  E  A

2461 - GTGCTGCAGATGCACTGGACGGACAAGTATGATCCTGAAGACTGGGCCAGGCGCATCAAC - 2520
     - V  L  Q  M  H  W  T  D  K  Y  D  P  E  D  W  A  R  R  I  N

2521 - GGTTTCTTCTGGGCCGACACCAAGGTGGGCGACAAGACCTATAAGCGCGGGCAGCTTGTA - 2580
     - G  F  F  W  A  D  T  K  V  G  D  K  T  Y  K  R  G  Q  L  V

2581 - CCCGCCTTCGGCGCGCTCAAGGATGACGGAACCACGTCTTCCCTCAACTGGATATACACC - 2640
     - P  A  F  G  A  L  K  D  D  G  T  T  S  S  L  N  W  I  Y  T

2641 - GGAAGCTGGACGGAAGAAGACGGCAACAAGTCGCGGCGGCGCGATCCCAGCCAGACGCCC - 2700
     - G  S  W  T  E  E  D  G  N  K  S  R  R  R  D  P  S  Q  T  P

2701 - ATGCAGGCCAAGATAGGCCTCTTCCCCAACTGGTCGTGGTGCTGGCCGCTCAACAGGCGC - 2760
     - M  Q  A  K  I  G  L  F  P  N  W  S  W  C  W  P  L  N  R  R
```

```
2761 - ATCCTGTACAACCGCGCCTCGGTGGACATGAACGGCAAGCCCTTCAACCCCAACAGGGCT - 2820
     - I  L  Y  N  R  A  S  V  D  M  N  G  K  P  F  N  P  N  R  A

2821 - GTTATCGAATGGGACGGCAGCAAATGGGTGGGCGACGTGCCCGACGGCCCCTGGCCGCCC - 2880
     - V  I  E  W  D  G  S  K  W  V  G  D  V  P  D  G  P  W  P  P

2881 - ATGGCTGACCCCAAGGGCAAGCTGCCCTTTATCATGGTCAAGGACGGCCTTGCCCAGTTC - 2940
     - M  A  D  P  K  G  K  L  P  F  I  M  V  K  D  G  L  A  Q  F

2941 - TATGGTCCCGGCCCGGCTGACGGTCCGTTCCCCGAGCACTACGAACCTGCTGAAACGCCC - 3000
     - Y  G  P  G  P  A  D  G  P  F  P  E  H  Y  E  P  A  E  T  P

3001 - CTGGCGACCCATCCGTTCTCCAAGCAGCTCAGCAGCCCGGTATATAAATACCACAAGACC - 3060
     - L  A  T  H  P  F  S  K  Q  L  S  S  P  V  Y  K  Y  H  K  T

3061 - GACATGGACCAGATCGCGCCTCCGGCCGATCCGCGTTACCCCATAGTGCTGACCACCTAC - 3120
     - D  M  D  Q  I  A  P  P  A  D  P  R  Y  P  I  V  L  T  T  Y

3121 - AGCCTTACCGAGCACTGGTGTGGCGGCGGTGAAACGCGCAACGTGCCCAACCTGCTGGAA - 3180
     - S  L  T  E  H  W  C  G  G  G  E  T  R  N  V  P  N  L  L  E

3181 - ACAGAGCCGCAGCTTTATGTGGAAATGAGCCACGAGCTGGCCAAGGAAAAGGGCATCAAG - 3240
     - T  E  P  Q  L  Y  V  E  M  S  H  E  L  A  K  E  K  G  I  K

3241 - AACGGCGACGGGGTCGTGCTTGAAAGCGCGCGCGGCAACTGTGAGGCCATCGCCATGGTA - 3300
     - N  G  D  G  V  V  L  E  S  A  R  G  N  C  E  A  I  A  M  V

3301 - ACGGTGCGTATACGTCCCTTCACGGTTATGGGCAAAACTGTCCACCTGGTGGGTATGCCC - 3360
     - T  V  R  I  R  P  F  T  V  M  G  K  T  V  H  L  V  G  M  P

3361 - TTTGCCTTTGGCTGGACAACGCCAAAAACCGGCGACTCCACCAACAGGCTTACCGTTGGC - 3420
     - F  A  F  G  W  T  T  P  K  T  G  D  S  T  N  R  L  T  V  G

3421 - GCGTATGATCCCAATACTACCATTCCCGAGTCCAAGGCCTGCTGCGTAAACCTGCGCAAG - 3480
     - A  Y  D  P  N  T  T  I  P  E  S  K  A  C  C  V  N  L  R  K

3481 - GCTGATAAACTCACCGAAATAGGCTAACGAGAAGGGCGCGCCCTTACGGTAGGGCGCGCC - 3540
     - A  D  K  L  T  E  I  G  *

3541 - TGACAAGGAGCATACTATGCCGAAAACATTCTTAGTTGACACCACGCGGTGCACGGCATG - 3600
     -                M  P  K  T  F  L  V  D  T  T  R  C  T  A  C

3601 - TCGTGGCTGCCAGTTGGCCTGTAAGGAGTGGCATGATCTGCCTGCCAACCACACCAAGCA - 3660
     -  R  G  C  Q  L  A  C  K  E  W  H  D  L  P  A  N  H  T  K  Q

3661 - GCGCGGCACGCACCAGAATCCGCCGGATCTGAATCCCAACAACCTCAAGATTGTACGCTT - 3720
     -  R  G  T  H  Q  N  P  P  D  L  N  P  N  N  L  K  I  V  R  F

3721 - TCACGAATATATCAATGACGAAGGCAATGTGGTCTGGAACTTCTTTCCCGACCAGTGCCG - 3780
     -  H  E  Y  I  N  D  E  G  N  V  V  W  N  F  F  P  D  Q  C  R

3781 - CCATTGCCTCACGCCGCCCTGTGTGGATGTGGCAGACATGGCGGTGCCGGGAGCCATGAT - 3840
     -  H  C  L  T  P  P  C  V  D  V  A  D  M  A  V  P  G  A  M  I

3841 - ACAGGACAAGAAAACAGGGGCCGTACTGGCTACGGAAAAATCGGCCAAGCTCAGCGAGGA - 3900
     -  Q  D  K  K  T  G  A  V  L  A  T  E  K  S  A  K  L  S  E  D

3901 - CGACGCCCAGGCCATACAGGAGGCCTGCCCCTATAATATTCCCAGGCGCGATCCCGAAAA - 3960
     -  D  A  Q  A  I  Q  E  A  C  P  Y  N  I  P  R  R  D  P  E  N

3961 - CGGCCGCCTGACCAAGTGCGATATGTGCATCGACCGTGTCAGCGCGGGTATGCAGCCTAT - 4020
     -  G  R  L  T  K  C  D  M  C  I  D  R  V  S  A  G  M  Q  P  I

4021 - CTGCGTCAAGACCTGCCCGACAGGGGCCATGGTTTTCGGCGAGCGTGAAGAGGTGCTGCC - 4080
     -  C  V  K  T  C  P  T  G  A  M  V  F  G  E  R  E  E  V  L  P

4081 - CCTGGCCCAGAAACGTCTTGAAAACGCCAAAAAGCGTTGGCCCAAGGCTTTTCTGGCCGA - 4140
     -  L  A  Q  K  R  L  E  N  A  K  K  R  W  P  K  A  F  L  A  D
```

```
4141 - TATGGAAGATGTCAGCGTGATCTACCTGCTGGCCGACACCAAGGATAAGTATTACGAGTT - 4200
     -  M  E  D  V  S  V  I  Y  L  L  A  D  T  K  D  K  Y  Y  E  F

4201 - CGCGGCCTTTATGTAGAGTGCTTCAGTCAGGTTTCAGTTTGGCATTGCCATAATTGTCAA - 4260
     -  A  A  F  M  *

4261 - CTGAAATTATGCTGATGCACAGCGTTGCCGTCAGGCCTGTACCGTATTCAACGGCTTCCG - 4320

4321 - GCGTTTTGCCGGAAGCCGGATTCACGGCACAGCCGGGCGGGGCACTTGGGCATATCTCCG - 4380

4381 - GCGGAAACGCCTTTTCGCCGGAAACGGGCAGACCGCTTCGGCGGCAGGGCCTGCGATACG - 4440

4441 - GCATCAAGTGCGGCGCGCGGGAAACAGCCCGCGCGCCGCTATCACCTTTCGGACGGAGGT - 4500

4501 - TCCGGCCTCCGGGTTTGGGAGCATCAATGGCCTCATCCTGCCAAAGCGTGGCAAAAACCC - 4560

4561 - TGGCGGAGGTGGTGGAATGCCGCCCCGTGCTGGAACCCGTGCTACGGGCGTTTGAACCCC - 4620

4621 - TGCTGGCCGCCCAGGCCAATGGCCGATGATCTGGCCGACAGCATACGCGCTTCGGGGCT - 4680
     -                  M  A  D  D  L  A  D  S  I  R  A  S  G  L

4681 - GGAACTGCCTGAAGCGCAGCCCGGCGCCCTGGAGCAGGGTCTTTCATTGCTGGCCGGCGT - 4740
     -  E  L  P  E  A  Q  P  G  A  L  E  Q  G  L  S  L  L  A  G  V

4741 - ACCGTTGACGGGAGCCGCCGCCCCGTTGCGGCAAAGCGCCGAAAAACTGCTGCCGCTTTT - 4800
     -  P  L  T  G  A  A  A  P  L  R  Q  S  A  E  K  L  L  P  L  L

4801 - GGCTACGCTGGAAACCATGGCTCCTCACCTGCCCGCCCTTGAGGCTTTTTTGCTGGCTCC - 4860
     -  A  T  L  E  T  M  A  P  H  L  P  A  L  E  A  F  L  L  A  P

4861 - GGCTGGAGCAGCAAAGAAGGGCAAGGGGGCCAAAACCAGGCAGGATCCGCGCGAAGCACT - 4920
     -  A  G  A  A  K  K  G  K  G  A  K  T  R  Q  D  P  R  E  A  L

4921 - GGCCGAAGCCCTGCTGTCGGGTAACAGCGAAGAAGAAACCCGTCTGGCTGCCGCACATGA - 4980
     -  A  E  A  L  L  S  G  N  S  E  E  E  T  R  L  A  A  A  H  D

4981 - CCTCGATCCTTCAATACTGCATTTTGCCTTCAGTTTTGTGCTGGCCCCGGTTTTACGCGC - 5040
     -  L  D  P  S  I  L  H  F  A  F  S  F  V  L  A  P  V  L  R  A

5041 - AATTGTGTCAGGGAGCCTGCCTGAAGAAGGGGACGCCCCCTGGGATGCGGGCAGCCTGTG - 5100
     -  I  V  S  G  S  L  P  E  E  G  D  A  P  W  D  A  G  S  L  W

5101 - GCGGCAGGGCTATTGCCCCGTATGCGGCAGTTTTGCCACCATCGCCTGGCTCGACAAACC - 5160
     -  R  Q  G  Y  C  P  V  C  G  S  F  A  T  I  A  W  L  D  K  P

5161 - CCTGGTTGACGAAAAAAATGCCTATCTGGCTGGCGGCGGCGGCAAGAAACATCTGCACTG - 5220
     -  L  V  D  E  K  N  A  Y  L  A  G  G  G  G  K  K  H  L  H  C

5221 - CGGCCTGTGCGGCACTGACTGGAAATTCATGCGCGGAACCTGTCCTTCATGTGGCGAGAA - 5280
     -  G  L  C  G  T  D  W  K  F  M  R  G  T  C  P  S  C  G  E  K

5281 - GGGCAGCGGTGTCATCGAAATGCTGCGTGAAAGCGGCTCGGCTCACGGCGAGCGGCTGGA - 5340
     -  G  S  G  V  I  E  M  L  R  E  S  G  S  A  H  G  E  R  L  D

5341 - CTGGTGCACCAAGTGTAAAACCTATTGCCCGACAGTGGACCTGCGTGAACGCGACGGAAA - 5400
     -  W  C  T  K  C  K  T  Y  C  P  T  V  D  L  R  E  R  D  G  K

5401 - GCCGGATATGGACGCGCTGGCCCTGGGGATGATGCACCTGGATATGGTGGCGGCCCGTAA - 5460
     -  P  D  M  D  A  L  A  L  G  M  M  H  L  D  M  V  A  A  R  K

5461 - AAAGCTGCGCCCGCTCAAGGTTTCGTTCTGGAATACTTTTTAGGGCAGCGTAACGCTGAG - 5520
     -  K  L  R  P  L  K  V  S  F  W  N  T  F  *

5521 - ACTGTTCTGAAGGATTGGGAGCAGGCGCCCGCCGCAAGGGCGCTGGCCGCAAGCATGGCG - 5580

5581 - GAGGCAATGGCAGCATGAGGTTCATGCGCCGTGAGCAGCCGCGAGCGCAAAGAGTTGTGT - 5640

5641 - GTAAAAGGCCGGAAGCATGACGGGCCGGGCCAACGGGCAGAAGCGCGCCCGAAAGCCGCC - 5700

5701 - GGGCTGAAGAGAAGCGCCAGCGGCGCGTCAGAGGCCAGGCTGGCCGGATGGTCCGGCATG - 5760
```

```
5761 - CGCAGAGACACAAGGGAAACCGTTGCAGTAATGAGGATTTTTGCTCTTTGCCAAGGCTGG - 5820

5821 - CGGCCCGGCGAAGCCTGATGCACCAAAACATGTATGAGGTTTTGCGGTGCGGTCTGCTGC - 5880

5881 - GGGCAGAGAGCAAAGATGATCATTATTCAGGGCTTCCGAAGATTTACTACCTCAGGAGGA - 5940

5941 - GCTTGTTCATGAAAACCCTGGTCATCACTCTTTTTGCCCTGACGTTTCTGTGGGCTGGCG - 6000
     -        M  K  T  L  V  I  T  L  F  A  L  T  F  L  W  A  G  G

6001 - GCGCGCAGGCCCGCAGCGTCAAAGAGATGTCGCAAGCCATCAAGGAACCCATTGAAATTG - 6060
     -   A  Q  A  R  S  V  K  E  M  S  Q  A  I  K  E  P  I  E  I  E

6061 - AAGCTTCCGGCTCCAAGCGCATGAACGTCATGTTTCCCCATACCGCACACAAGGGTATTT - 6120
     -   A  S  G  S  K  R  M  N  V  M  F  P  H  T  A  H  K  G  I  S

6121 - CCTGCTTCCACTGCCACCRCGAGGAAGGCAGCGATGGCCGCTATGTRGCCTGTACCGAGT - 6180
     -   C  F  H  C  H  X  E  E  G  S  D  G  R  Y  X  A  C  T  E  C

6181 - GTCACGCCACGCCCGGCGCGCGTGAGCGCGACCCCATGAGTATGTTCATGGCGTTCCACT - 6240
     -   H  A  T  P  G  A  R  E  R  D  P  M  S  M  F  M  A  F  H  S

6241 - CCAAAAACAGCGACCGCTCGTGCCTTGGCTGCCACAAGAAGCTTGCTGCTGAAAATCCGG - 6300
     -   K  N  S  D  R  S  C  L  G  C  H  K  K  L  A  A  E  N  P  G

6301 - GCAAGTTCCCGCAGTTCAAGGGCTGCCGTCCTTGTCACATGAGCCCCGCCGCGCGTGAAG - 6360
     -   K  F  P  Q  F  K  G  C  R  P  C  H  M  S  P  A  A  R  E  A

6361 - CCGCCGAGGCCGCCAAGGCTGCCAAAAAATAGTTTGTATGCACAGTACGGCACTTGTGCC - 6420
     -   A  E  A  A  K  A  A  K  K  *

6421 - GGATGTTGGATGTCGGTCAGCCGGAGGTTGACCGGCATCCTTGCYTTTATGGACGAAAGC - 6480

6481 - YTGCCGCATAACGGGGACTTCCTGCCGTTACTGCGGGCAGACCGGGATTTTTTACGGTTC - 6540

6541 - TGCTGCGGTTTTTAGCCACAGATTGCCCGTCTGCTGTTCTATGCCTGCCTGGAGGCCCAY - 6600

6601 - CCTCGGTGCTGATTTTTGYGGCGGCGGAACGGGCAGCAATGCTTTTGATGAAGATGCCCG - 6660

6661 - AAGGCGCACGGATAAAGCGATCATGGTAGGGCAGATTTTTTAATCTGGARGCTATATGAC - 6720

6781 - TCTCTTCCTTTGTGTCACCGTAAACGAYAATGAAATTGAATAATGAGATTACAAAGAAAC - 6840

6841 - AACGTGGTGAGATTGAACGTATTTTATCAAACTGGACAAACTATCTTAACAGTGT - 6895
```

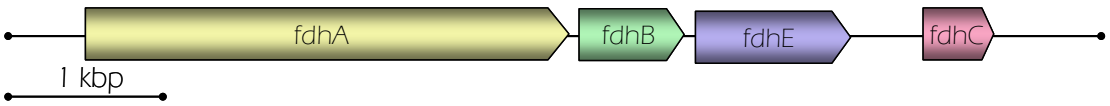

Figure II.3.4 Schematic representation of gene organization for *Dd* Fdh operon. The ORFs and its transcription senses are indicated by the arrows.

The *fdhA* gene encodes a protein of 1013 aminoacids (FdhA) with a predicted molecular mass of 112.481 kDa (Figure II.3.5). The first 29 aminoacids correspond to a signal peptide as calculated by SignalP programme. The mature protein has a deduced molecular mass of 109.36 kDa and a pI=8.17. The sequence RRSFLK (light grey, Figure II.3.5) corresponds to the twin-arginine motif (R-R-x-F-L/I-K) characteristic of Sec-

independent export to periplasm and usually found in molybdoprotein precursors [44]. Proteins targeted with twin-arginine sequence are the substrate of the Tat (twin-arginine translocation) protein export system. This system is found in the cytoplasmic membrane of most prokaryotes and is dedicated to the transport of folded proteins. During the transport cycle itself substrate proteins bind to a receptor complex in the membrane which then recruits a protein-translocating channel to carry out the transport reaction [44, 58, 80].

A comparison of the deduced amino acid sequence (FdhA) with the N-terminal sequence obtained by chemical sequencing of pure **α**-subunit (KLKIEGAKEV SSICPFC) confirms that *fdhA* gene encodes the Fdh large subunit. A multiple sequence alignment of FdhA from *Dd* and related proteins from different *Desulfovibrio* species revealed the presence of the sequence motif –CXXCX_n-CX_mC- involved in [4Fe-4S] centre binding (black circles, Figure II.3.5). FdhA also contains the $SeCys^{160}$ residue (light yellow, Figure II.3.5) codified by the TGA codon which is conserved in all Fdhs studied so far. Conserved $Histidine^{161}$ and $Arginine^{333}$, proposed to be involved in the reaction mechanism [41, 81], are also present.

Analysis of conserved domains in FdhA reveals two regions: Molybdopterin-Binding (MopB) and MopB_CT. MopB domain of the MopB superfamily of proteins, in general, bind molybdopterin as a cofactor. The MopB domain is found in a wide variety of molybdenum- and tungsten-containing enzymes, including *Ec* Fdh-H and *Ec* Fdh-N, several forms of nitrate reductase (Nap, Nas, NarG), dimethylsulfoxide reductase (DMSOR), thiosulfate reductase, formylmethanofuran dehydrogenase , and arsenite oxidase [82]. Molybdenum is present in most of these enzymes in the form of molybdopterin, a modified pterin ring with a dithiolene side chain, which is responsible for ligating the Mo.

MopB_CT_Formate-Dh-Na-like (start at approximately aminoacid 874 from N-Terminal) is the conserved molybdopterin_binding C-terminal (MopB_CT) region present in many, but not all, MopB homologs.

Figure II.3.5 Amino acid sequence alignment of the *Dd* FdhA with related proteins from different *Desulfovibrio* species. Dd27774FdhA: FdhA subunit from *D. deulfuricans* ATCC 27774, DVU2812FdnG3: large subunit from *D. vulgaris* Hilderborough (DVU2812), Dde3513DdG20FdhA4: Fdh large subunit from *D. desulfuricans* G20 (Dde3513), Q934F5DgFdhA: Fdh large subunit from *D. gigas* (Q934F5), light grey: twin arginine motif, light yellow: conserved SeCys, light blue: conserved residues probably involved in enzymatic catalysis ▼: signal peptide cleavage site, •: cysteines motifs involved in the coordination of [4Fe-4S] clusters, (*): identity, (:): strongly similar, and (.) weekly similar.

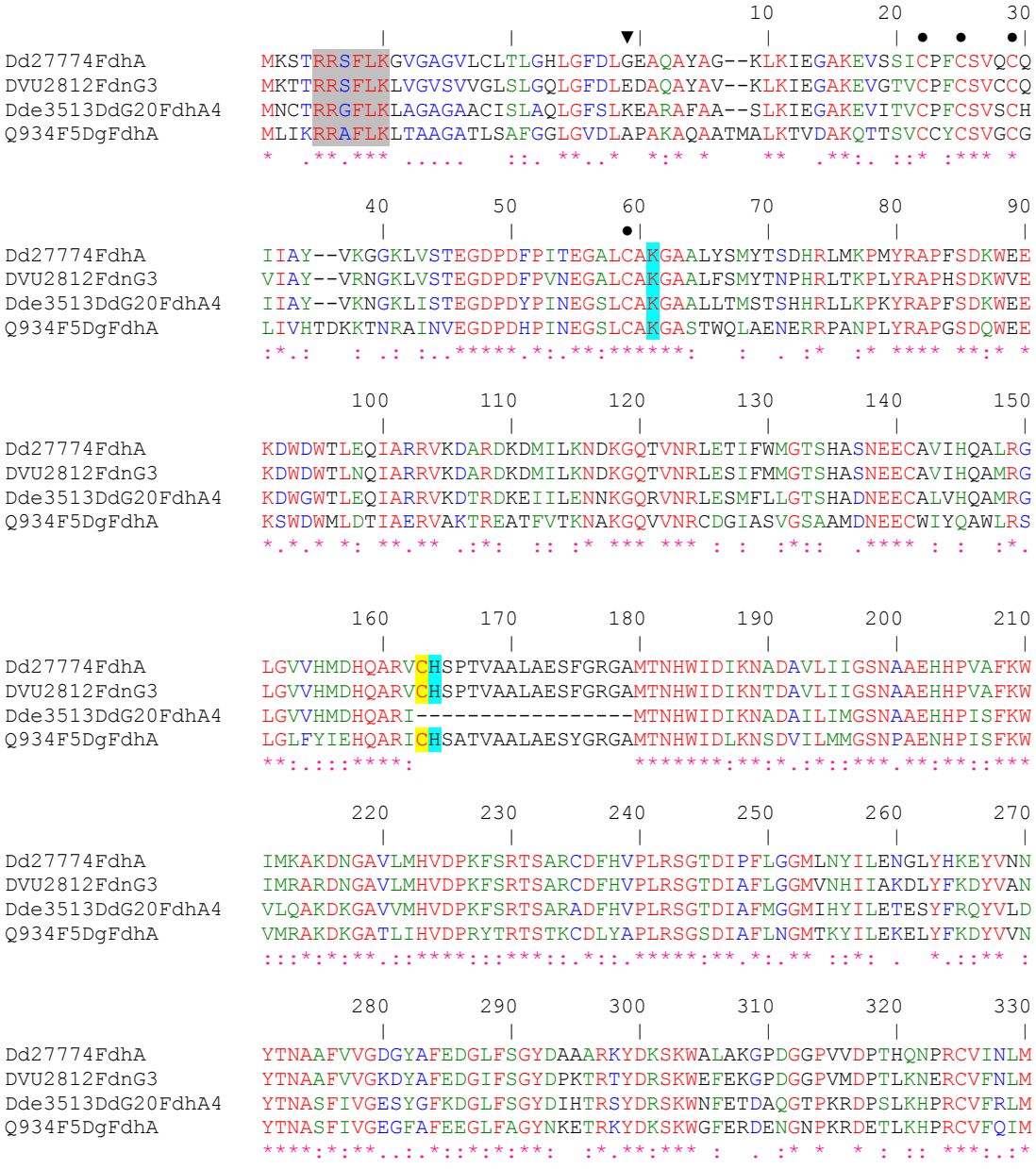

```
                          340       350       360       370       380       390
                            |         |         |         |         |         |
Dd27774FdhA           KDHYSRYTLKNVSDVTGVSQDNLLKVYKNFCATGRPDKAGTILYALGWTQHTVGVQNIRL
DVU2812FdnG3          KKHYERYTLKNVSDVTGVSEENLLRVYDAFCATGRPDKAGTILYALGWTQHTVGVQNIRT
Dde3513DdG20FdhA4     QEHYSRYTLDNVSSVTGVTKENLLKVYKAFAATGKPDKAGTMMYALGWTQHTVGVQNIRS
Q934F5DgFdhA          KKHYERYDLDKISAICGTPKELILKVYDAYCATGKPDKAGTIMYAMGWTQHTVGVQNIRA
                      :.**.** *.::* : *..:: :*:**. :.***:******::**:**************

                          400       410       420       430       440       450
                            |         |         |         |         |         |
Dd27774FdhA           SSLVQLLLGNIGIAGGGINALRGEPNVQGSTDHALLYNNIPGYHGTPQAPWQTLGEYNKA
DVU2812FdnG3          STLIQLLLGNIGVAGGGINALRGEPNVQGSTDHALLYHILPGYNAMPVAQWQTLADYNKA
Dde3513DdG20FdhA4     AAIVQLLLGNIGVAGGGINALRGEPNVQGSTDHCLLYHIIPGYMTMPMADWQTYADYNKA
Q934F5DgFdhA          MSINQLLLGNIGVAGGGVNALRGEANVQGSTDHGLLMHIYPGYLGTARASIPTYEEYTKK
                       :: ********:****:******.******** ** :  ***   . *   *  :*.*

                          460       470       480       490       500       510
                            |         |         |         |         |         |
Dd27774FdhA           NTPVTVVPNSANWWGNRPKYVTSLLKGWFGDAATPENDFCYSLLPKLEPGVDYSYMFVMD
DVU2812FdnG3          NTPVTTLKNSANWWSNRPKYVASLLKGWFGDAATPENDFCYEYLPKLEKGEDYSYMYVMD
Dde3513DdG20FdhA4     NTPVSADPQSANWWQHKPKYLTSLLKAWFGDAATAENGYCYGLLPKIEKGADHSYMFLFD
Q934F5DgFdhA          FTPVSKDPQSANWWSNFPKYSASYIKSMWPDADLNEA---YGYLPKGEDGKDYSWLTLFD
                       ***:   :***** : *** :* :*. : **   *    *  *** * * *:*:: ::*

                          520       530       540       550       560       570
                            |         |         |         |         |         |
Dd27774FdhA           RIYNKKIKGGFIMGVNPMNSFPNTNKMRAALDNLDWLVCSEIHNSETTDNWQRPGVGPKT
DVU2812FdnG3          RMYHGKLKGGFIFGVNPMNSFPNTNKMRAALDKLDWLVCSELHNSETTDNWKRPGVDPKA
Dde3513DdG20FdhA4     RMYSGKITGGFIIGLNPMNSVPNTNKVRKALDNLDWLVTAELHHSETTDNWRRPGVDPAT
Q934F5DgFdhA          DMFQGKIKGFFAWGQNPACSGANSNKTREALTKLDWMVNVNIFDNETGSFWRGPDMDPKK
                       ::  *:.* *  * **  * .*:** * ** :***:*  ::...** . *: *.:.*

                          580       590       600       610       620       630
                            |         |         |         |         |         |
Dd27774FdhA           KKTEVFLLPSAHRIEKAGTISNSGRWLQWHYKAVEPAGEARNFADVVVPLFNTIRRMYKT
DVU2812FdnG3          CKTEVFLLPSAHRVEKAGTISNSGRWLQWFDKAVEP-GQARNFADIFVPLVNKIRALYKA
Dde3513DdG20FdhA4     VKTEVFLLPSAHRVEKAGSVSNSGRWLVWHHKAVEPEGEARSFGDMFVPLINVVRDLYRK
Q934F5DgFdhA          IKTEVFFLPCAVAIEKEGSISNSGRWMQWRYVGPEPRKNAIPDGDLIVELAKRVQKLLAK
                       *****:**.*  :** *::******: *   . **  :*   .*:.* * : :: :

                          640       650       660       670       680       690
                            |         |         |         |         |         |
Dd27774FdhA           EGGVLPEAVLQMH---WT---DKYDPEDWARRINGFFWADTKVGDKTYKRGQLVPAFGAL
DVU2812FdnG3          EGGTLPDPVLKLH---WT---DKFDPEEWTRRINGFFWADTKVGDKEYKRGQLVPAFGQL
Dde3513DdG20FdhA4     EGGTMPEAVLNLD---WP---QQYDPEEWARRINGFFLKDTTVNGKEYKKGQLVPSFTAL
Q934F5DgFdhA          TPGKLAAPVTKLKTDYWVNDHGHFDPHKIAKLINGFALKDFKVGDVEYKAGQQIATFGHL
                        * :. .* ::.   *     ::**.. :: **** * .*..  ** ** :.:*  *

                          700       710       720       730       740       750
                            |         |         |         |         |         |
Dd27774FdhA           KDDGTTSSLNWIYTGSWTEEDGNKSRRRDPSQTPMQAKIGLFPNWSWCWPLNRRILYNRA
DVU2812FdnG3          KDDGSTSSLNWLYTGSYTEEDGNKSKRRDARQTPMQANIGLFPNWSWCWPVNRRILYNRA
Dde3513DdG20FdhA4     ADDGSTSSLNWLYSGSYTEEDGNKAQRRDPSQTPMQAAIGLYPKWSWCWPVNRRILYNRA
Q934F5DgFdhA          QADGSTTSGCWIYTGSYTEK-GNMAARRDKTQTDMQAKIGLYPGWTWAWPVNRRIIYNRA
                        **:*:*  *:*:**:**: ** : ***  ** *** ***:* *:*.**:****:****

                          760       770       780       790       800       810
                            |         |         |         |         |         |
Dd27774FdhA           SVDMNGKPFNPNRAVIEWDG--SKWVGDVPDGPWPPMAD-PKGKLPFIMVKDGLAQFYGP
DVU2812FdnG3          SVDVNGKPWNPKKAVIEWDG--AKWVGDVPDGPWPPMADKEKGKLPFIMNKDGFAQFYGT
Dde3513DdG20FdhA4     SVDAQGKPWNPAKAVISWNG--KKWEGDVPDGGWPPMAT-GKGRHPFIMSKHGFGQLYGT
Q934F5DgFdhA          SVDLNGKPYAPEKAVVEWNAAEKKWVGDVPDGPWPPQADKEKGKRAFIMKPEGYAYLYGP
                      *** :***: * :**:.*:.   ** ****** *** *   **: .***  .* . :**.

                          820       830       840       850       860       870
                            |         |         |         |         |         |
Dd27774FdhA           GPADGPFPEHYEPAETPLATHPFSKQLSSPVYKYHKTDMDQIAPPADPRYPIVLTTYSLT
DVU2812FdnG3          GRMDGPFPEHYEPAETPLDSHPFSKQLSSPVYKFHTSDMDQIAKAADPKYPIVLTTYSLT
Dde3513DdG20FdhA4     GRMDGPFSEHYEPVETPIDAHPFSKQLSSPVYKFVSSDMDKLARPADPRFPYVLTTYNVT
Q934F5DgFdhA          GREDGPLPEYYEPMECPVIEHPFSKTLHNPTALHFATEEKAVC---DPRYPFICSTYRVT
                      *  ***:.*:*** * *:  ***** * .*.  .  :: . :.   **::* : :** :*
```

```
                              880       890       900       910       920       930
                               |         |         |         |         |         |
Dd27774FdhA          EHWCGGGETRNVPNLLETEPQLYVEMSHELAKEKGIKNGDGVVLESARGNCEAIAMVTVR
DVU2812FdnG3         EHWCGGGETRNVPNLLETEPQLYIEMSPELAEEKGIKNGDGVIVESIRGRAEAIAMVTVR
Dde3513DdG20FdhA4    EHWCGGGETRNVPNLLEAEPQLYVELSPELAEEKGIANGDGVILESARGRVEAIAMVTVR
Q934F5DgFdhA         EHWQTGLMTRNTPWLLEAEPQMFCEMSEELATLRGIKNGDKVILESVRGKLWAKAIITKR
                     ***  *  ***.* ***:***:: *:* ***  :** *** *::** **.  * *::* *

                              940       950       960       970       980       990
                               |         |         |         |         |         |
Dd27774FdhA          IRPFTVMGKTVHLVGMPFAFGWTTPKTG-DSTNRLTVGAYDPNTTIPESKACCVNLRKAD
DVU2812FdnG3         IRPFTVMGKTVHLVGMPFAYGWTTPKCG-DSTNRLTVGAYDPNTTIPESKACLVNVRKAD
Dde3513DdG20FdhA4    IRPFTVQGKTVHLVGMPFCFGWTTPGTG-DSTNRLTPSVGDPNTSIPEYKASCVNIRKAD
Q934F5DgFdhA         IKPFAIQGQQVHMVGIPWHYGWSFPKNGGDAANILTPSVGDPNTGIPETKAFMVNVTKA-
                     *:**:: *: **:**:*: :**: *  * *::* ** .. **** *** **  **: **


Dd27774FdhA          KLTEIG-
DVU2812FdnG3         KLTEIA-
Dde3513DdG20FdhA4    TLTEIDR
Q934F5DgFdhA         -------
```

The protein encoded by *fdhB* gene is composed of 219 aminoacids and has a deduced molecular weight of 24.72 kDa. Aminoacid sequence traduced from *fdhB* is more than 60% homologous with N-terminal aminoacid chemical sequence obtained from pure β-Fdh subunit (KTFLVDTRRD QAGGGFQLK). FdhB lacks of signal peptide suggesting that αβ complex is formed in the cytoplasm being then transported to periplasm as an oligomeric structure. This feature was also observed for [NiFe] hidrogenases [45] and W-Fdh from *D. gigas* [40]. Multiple alignment of FdhB with related proteins showed the presence of three cysteines motifs (red, blue and green circles, Figure II.3.6) which are involved in the [4Fe-4S] cluster binding. This suggests the presence of four [4Fe-4S] centres in *Dd* Fdh: one in the α-subunit and three clusters in the β-subunit. Although this result is in contrast with previously published results [52], it is in agreement with the number of [4Fe-4S] clusters reported for related Fdhs [39, 83] .

Figure II.3.6 Aminoacid sequence alignment of the *Dd* FdhB with Fdh homologous subunits from related organisms. Dd27774FdhB: FdhB subunit from *D. deulfuricans* ATCC 27774, DVU2811FdnG3B: β-subunit from *D. vulgaris* Hilderborough (DVU2811), Dde3514DdG20FdhB: Fdh β-subunit from *D. desulfuricans* G20 (Dde3514), Q8GC87DgFdhB: Fdh small subunit from *D. gigas* (Q8GC87), Red, blue and green circles: cysteine motifs probably involved in the FeSII, FeIII and FeSIV cluster binding, (*): identity, (:): strongly similar, and (.) weekly similar.

```
                          10        20        30        40        50        60
                           | ●  ●  ● | ●       |         |         |         |
Dd27774FdhB         MPKTFLVDTTRCTACRGCQLACKEWHDLPANHTKQRGTHQNPPDLNPNNLKIVRFHEYIN
DVU2811FdnG3B       MPKAFLIDTTRCTACRGCQLACKEWHDLPANVTKQRGSHQNPPDLNPNNLKIVRFNERMN
Dde3514DdG20FdhB    MSKAIFIDTTRCTACRGCQLACKEWYELPANKTRQTGSHQNPPDLNPNNFKLVRFHEHMI
Q8GC87DgFdhB        MSKGFFVDTTRCTACRGCQVACKQWHGNPATPTENTGFHQNPPDFNFHTYKLVRMHEQEI
                    *.* :::*************:***:*:  **. *.: * ******:* :. *:**::*

                          70        80        90        100       110       120
                           |   ●  ●  | ●       |         |         |         |
Dd27774FdhB         DEGNVVWNFFPDQCRHCLTPPCVDVADMAVPGAMIQDKKTGAVLATEKSAKLSEDDAQAI
DVU2811FdnG3B       EKGVVIWNFFPDQCRHCVTPVCVDVADMAVPGAMIKDKKTGAVLATEKSAKLSPADAKAV
Dde3514DdG20FdhB    DDR-VVWYFFPDQCRHCVNPPCVDIANMIVDGALVHDEETGAVLTTEKSSLLSAEDFQAV
Q8GC87DgFdhB        DGR-IDWLFFPDQCRHCIAPPCKATADMEDESAIIHDDATGCVLFTPKTKDL--EDYESV
                    :   : * *********: * *   *:*   .*:::*. **.** * *:  *   * :::

                          130       140       150       160       170       180
                            ●     |         |● ●     |     ●   ●         |         |
Dd27774FdhB         QEACPYNIPRRDPENGRLTKCDMCIDRVSAGMQPICVKTCPTGAMVFGEREEVLPLAQKR
DVU2811FdnG3B       AEACPYNIPRIDPKTKRITKCDMCFDRVSAGMQPICVKTCPTGTMAFGERDEMLALAEKR
Dde3514DdG20FdhB    RDACPYDIPRRDEQTGQVKKCVMCFDRIKAGMQPACVKVCPTGTMNFGEREEMLKLARTR
Q8GC87DgFdhB        ISACPYDVPRKVAESNQMAKCDMCIDRITNGLRPACVTSCPTGAMNFGDLSEMEAMASAR
                     .****::**   :. :: ** **:**:. *::* **. ****:* **: .*:  :*  *

                          190       200       210       220       230       240
                            |         |         |         |         |         |
Dd27774FdhB         LENAKKRWPKAFLADMEDVSVIYLLADTKDKYYEFAAFM----------------------
DVU2811FdnG3B       LADAKTRFPKAHLVDVEDVSVIYLLAEEKEHYYEYAGFM----------------------
Dde3514DdG20FdhB    LEKVRKEHPRAMLADPDDVNVIFLLADDPERYHEYSVAQAEPVSRKRLFASLRRPVRAMT
Q8GC87DgFdhB        LAEIKAAYSDAKLCDPDDVRVIFLTAHNPKLYHEYAVA----------------------
                    * . :   . * * * :** **:* *.  . *:*::


Dd27774FdhB         ---
DVU2811FdnG3B       ---
Dde3514DdG20FdhB    ENS
Q8GC87DgFdhB        ---
```

Despite *fdhE* gene location between *fdhB* and *fdhC*, its product (FdhE) is not a component of Fdh. FdhE is composed by 287 aminoacids and has a calculated molecular mass of 33.03 kDa. The amino acid sequence of this protein is homologous to FdhE from *D. vulgaris* Hildenborough and *D. desulfuricans* G20 (Figure II.3.7). No signal peptide is predicted which indicates that FdhE is a cytoplasmic protein. Although the function of these proteins is unknown, they may possibly be involved in the formation of Fdh [66].

Figure II.3.7 Multiple sequence alignment of FdhE. Dd27774FdhE: FdhE protein from *D. desulfuricans* ATCC 27774, DVU2810FdnG3E: FdhE protein from *D. vulgaris* Hilderborough (DVU2810), Dde3515DdG20FdhE: FdhE protein from *D. desulfuricans* G20 (Dde3515), (*): identity, (:): strongly similar, and (.) weekly similar.

```
                          10        20        30        40        50        60
                           |         |         |         |         |         |
Dd27774FdhE       ------------------------------------MADDLADSIRASGLELPEAQPG
DVU2810FdnG3E     ------------------------------------MTVALSQTLRDAGLHLPALEGE
Dde3515DdG20FdhE  MPQSRESVSATLNAIASRRPALHSILSAFEPLLTASAALPDALADELRNGTAPLPQARSE
                                                     :.  *:: :* .   **  .

                          70        80        90       100       110       120
                           |         |         |         |         |         |
Dd27774FdhE       ALEQGLSLLAGVPLTGAAAPLRQSAEKLLPLLATLETMAPHLPALEAFLLAPAGAAKKGK
DVU2810FdnG3E     RARQGVSLLAGVALPGIAAPMRDVAGVLLPLMGGMQAVAPHMEALQAFFLCPVEPG----
Dde3515DdG20FdhE  RLAQGVPVMADAPTQWAAPLMRVAARHLLPVITAHQSLAGSRAGLEK---AFDQDD----
                     **:.::*...    *. :*  *  ***::   :::*    .*:    .

                         130       140       150       160       170       180
                           |         |         |         |         |         |
Dd27774FdhE       GAKTRQDPREALAEALLSGNSEEETRLAAAHDLDPSILHFAFSFVLAPVLRAIVSGSLPE
DVU2810FdnG3E     ----REDARDALAEAMLAGRSAD--AIAEACGVDADVLTFVTGFVLSPVLHALVAVSMPE
Dde3515DdG20FdhE  ------TALAGLMSAIVHGDAGALTRAARQHDVPEAVFAFAANAVAGPALHAMTQHHLHD
                        .  .* .*:: * :      *   .:   :: *. . * .*.*:*:.   : :

                         190       200       210       220       230       240
                           |         |         |         |         |         |
Dd27774FdhE       EGDAPWDAGSLWRQGYCPVCGSFATIAWLDKPLVDEKNAYLAGGGGKKHLHCGLCGTDWK
DVU2810FdnG3E     SGEAPWDEGGAWQEGYCPVCGAFPTIGWLDRPMLDEKNAYLAGGGGKKHLHCSMCGADWK
Dde3515DdG20FdhE  ADFA------AWREGTCPVCGSFPSIAYLGRPDPDQ-SEFLRSGGGKKHLHCSLCTHEWL
                   . *       *::* *****:*.:*.:*.:*  *: . :* .*********.:*  :*

                         250       260       270       280       290       300
                           |         |         |         |         |         |
Dd27774FdhE       FMRGTCPSCGEKGSGVIEMLRESGSAHGERLDWCTKCKTYCPTVDLRERDGKPDMDALAL
DVU2810FdnG3E     FLRGACPSCGKDASGTMEILRESEAAHGERLDWCTRCKSYCPTVDLREREAVPNLDALAL
Dde3515DdG20FdhE  FRRGACPSCGNEDPGALEYLRDPQTPW-ERIDLCRKCNTYCPGVDLRETTENPQMDAMAL
                  * **:*****:. .*.:* **:. :.  **:* * :*::*** *****    *::**:**


                         310       320
                           |         |
Dd27774FdhE       GMMHLDMVAARKKLRPLKVSFWNTF---
DVU2810FdnG3E     GMMHLDMVAARRQLRPLRPSFWNVY---
Dde3515DdG20FdhE  GMLHLDLVAAREGLMPLAPSFWNTFDDE
                  **:***:****. * **  ****.:
```

The *fdhC* gene encodes a protein of 147 aminoacids (FdhC) with a deduced molecular mass of 15.89 kDa and pI= 9.10. Analysis of the aminoacid sequence shows a putative cleavage site between aminoacids 21 and 22 (▼, Figure II.3.8). As result of this cleavage the mature FdhC protein should have a molecular mass of 13.86 kDa and pI= 8.98. The amino acid sequence of the mature protein deduced from *fdhC* is in agreement with N-terminal obtained from *Dd* Fdh γ-subunit (VKEVSQAIKEPIE). Analysis of amino acid sequence reveals that FdhC is a *c*-type cytochrome where the heme is covalently attached to the protein via two thioether bonds formed between the heme vinyl groups and the

cysteine sulphurs from the conserved -CX_2CH- peptide motif (red boxes, Figure II.3.8). Furthermore, haemic iron is coordinated at the axial positions by two amino acid side chains from the protein. The proximal ligand is provided from the histidine included into the -CX_2CH- heme binding motif and the distal ligand is probably supplied from one of the conserved Histidines (black circles, Figure II.3.8). This hexacoordination gives a low spin heme which in addition to the four heme binding sites are in agreement with data previously reported for *Dd* Fdh [52].

Figure II.3.8 Amino acid sequence alignment of the *Dd* FdhC subunit with the cytochrome c_3 from *Desulfovibrio vulgaris* Hildenborough. Dd27774FdhC: *Dd* FdhC subunit, DVU2809Cytc3: *Dv*H cytochrome C3 (locus tag DVU2809), ▼: signal peptide cleavage site, ●: histidines probable involved in the coordination of the haemic iron, red boxes: CX_2CH motif involved in heme coordination, (*): identity, (:): strongly similar, and (.) weekly similar.

```
                                          10         20         30
                    |          |▼         |          |          |●   ●
Dd27774FdhC   MKTLVITLFALTFLWAGGAQARSVKEMSQAIKEPIEIEASGSKRMNVMFPHTAHKGIS
DVU2809Cytc3  MRYLVISLFAVSLLMAGSALVGNAADAAKAPKKAIELKHGTSKRMHVMFNHTTHKDIA
              *: ***:***:::* **.* . .. : ::* *:.**:: . ****:*** **:**.*:

               40         50         60         70         80         90
               |    ●     |          |          |          ●          |
Dd27774FdhC   CFHCHHEE-GSDGRYXACT--ECHATPGARERDPMSMFMAFHSKNSDRSCLGCHKKLA
DVU2809Cytc3  CEQCHHDSPAPDKPYASCTDNDCHATPGPRERDTMSMFVAYHAKDTDRSCYGCHKKMA
              * :** :. ..*  * :**  :******.****.****:*:*:*::**** *****:*

                 100        110        120        130
                 |          |          |          |
Dd27774FdhC   AENPGKFPQFKGCRPCHMSPAAREAAEAAKAAKK
DVU2809Cytc3  AQHP----EFTGCRPCHMSQQARK--EAAASEKK
              *::*    :*.********  **:  *** : **
```

II.3.4 Kinetic Experiments

II.3.4.1 Determination of kinetic constants (K_m and V_m)

The kinetic parameters for formate and benzyl viologen were calculated using two types of plots: Michaelis-Menten and Direct Linear Plot. Figure II.3.9a shows initial rate vs. formate concentration using a constant concentration of electron acceptor (benzyl viologen, 7.5 mM). Figure II.3.9b shows the initial rate dependence on benzyl viologen

using 1mM of sodium formate. The experimental data were least square fitted to the Michaelis-Menten equation:

$$V = \frac{V_m \times S}{S + K_m} \qquad \text{(equation II.3.1)}$$

where v is the initial rate, V_m is limiting rate, S is the substrate concentration, and K_m is the *Michaelis constant*.

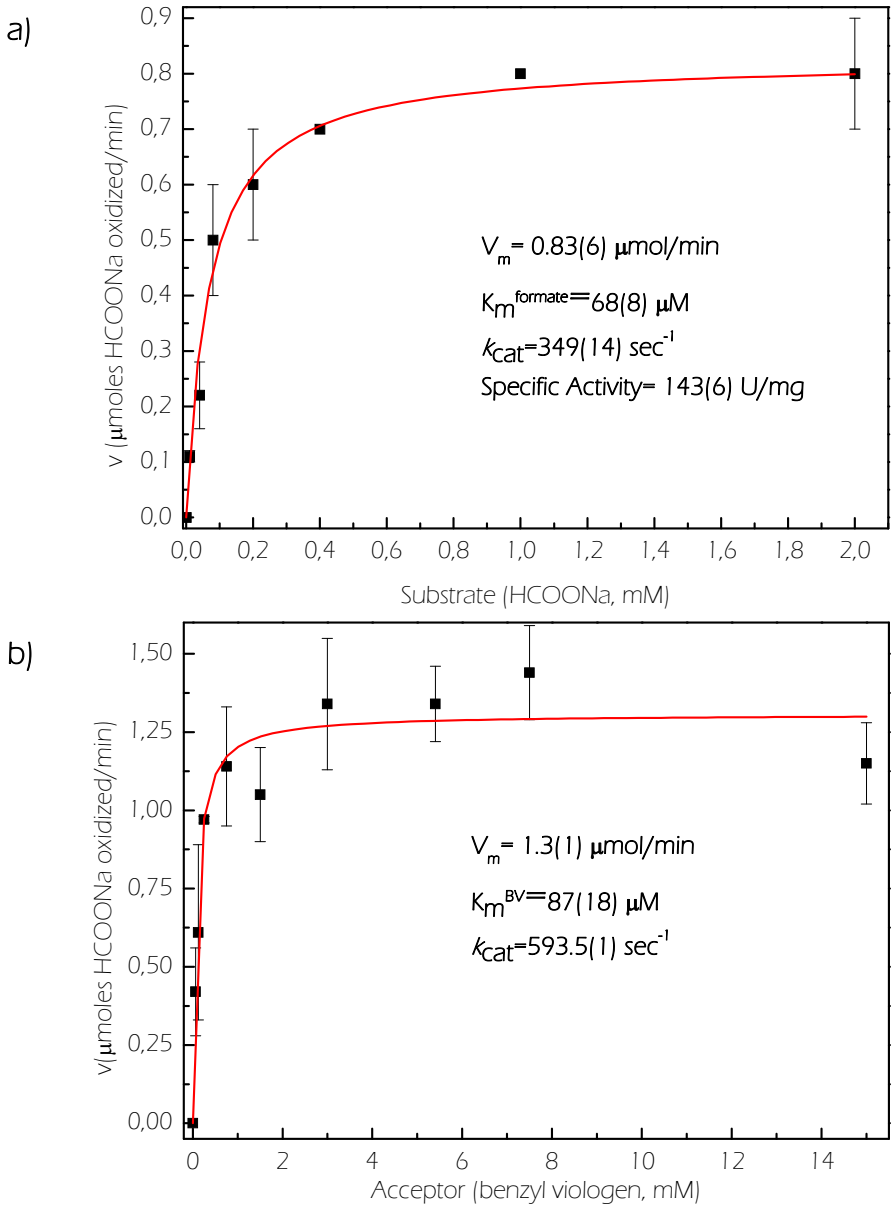

Figure II.3.9 Initial rate vs. formate concentration (a) and benzyl viologen concentration (b). The red lines show the best fit using the Michaelis-Menten model.

Figure II.3.10 shows the Direct Linear Plot for the same data plotted in Figure II.3.9.

a)

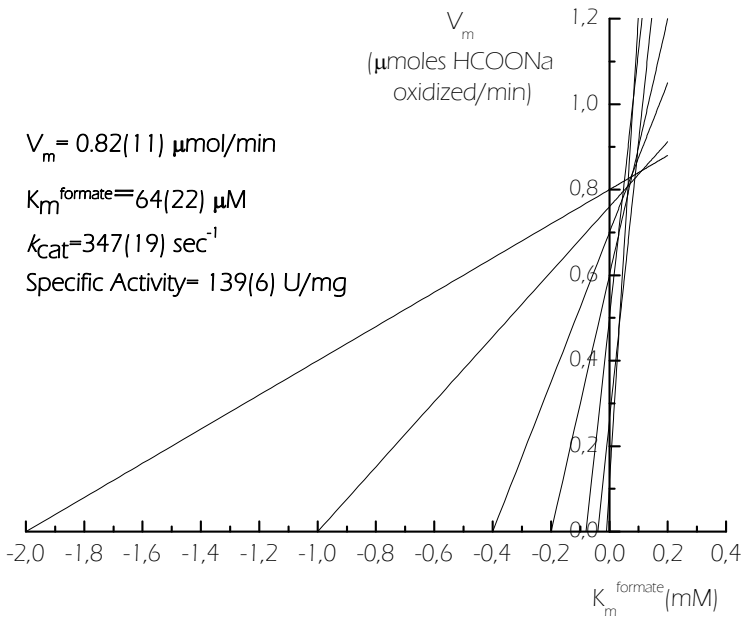

b)

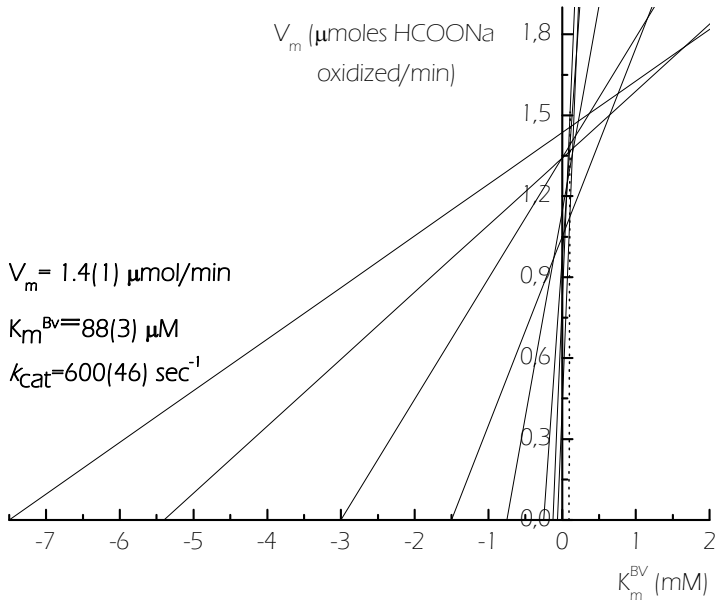

Figure II.3.10 Direct linear plot of V_m against K_m using equation II.3.2. *The slope and ordinate of each line correspond to each experimental point of Figure II.3.9 which come from the average of three independent measurements. (a) and (b) plots were constructed at benzyl viologen and formate concentration constant (7.5 mM and 1 mM, respectively)*

In this type of plot the Michaelis-Menten equation is rearranged to show the dependence of V_m on K_m (equation II.3.2):

$$V_m = v + \frac{v}{S} K_m \qquad \text{(equation II.3.2)}$$

Since v and S have been measured in the experiment, they can be treated as constants. Consequently, if V_m and K_m are considered as variables and v and S as constants, equation II.3.2 defines a straight line for each v and S set which satisfies one observation. The intersection point for two different observations defines the unique pair of K_m and V_m values that satisfies both observations exactly. The K_m and V_m values determined from Figure II.3.9 and Figure II.3.10 are included into the figures and summarized in Table II.3.1.

Table II.3.1 Kinetic constants calculated by Michaelis-Menten (MM) model and Direct Linear Plot (DLP) from experiments. Standard deviation between parentheses.

	$V_m^{formate}$ (µmol/min)	$K_m^{formate}$ (µM)	$k_{cat}^{formate}$ (sec^{-1})	Specific Activity (U/mg)	V_m^{BV} (µmol/min)	K_m^{BV} (µM)	k_{cat}^{BV} (sec^{-1})
MM	0.83(6)	68(8)	349(14)	143(6)	1.3(1)	87(18)	593.5(1)
DLP	0.82(11)	64(22)	347(19)	139(6)	1.4(1)	88(3)	600(46)

II.3.4.2 Influence of β-mercaptoethanol on the kinetic assay.

The presence of β-mercaptoethanol (130 mM) was reported as mandatory in Formate Dehydrogenases kinetic experiments [43, 52]. Although the role of the thiol has not been elucidated yet, it is thought that β-mercaptoethanol is necessary to remove the oxygen and drop the redox potential. On the other hand, β-mercaptoethanol has a denaturating effect on proteins and because of its reductant properties, could also act as a reductant of benzyl viologen. To check that both effects are not relevant and the importance of β-mercaptoethanol in the kinetic assays, a set of studies described below were carried out.

The effect of β-mercaptoethanol on substrate affinity was evaluated by comparison between kinetic parameters calculated with and without β-mercaptoethanol. Figure II.3.11

shows these data together with those obtained in presence of β-mercaptoethanol. The kinetic parameters calculated in both assays are given in Table II.3.2.

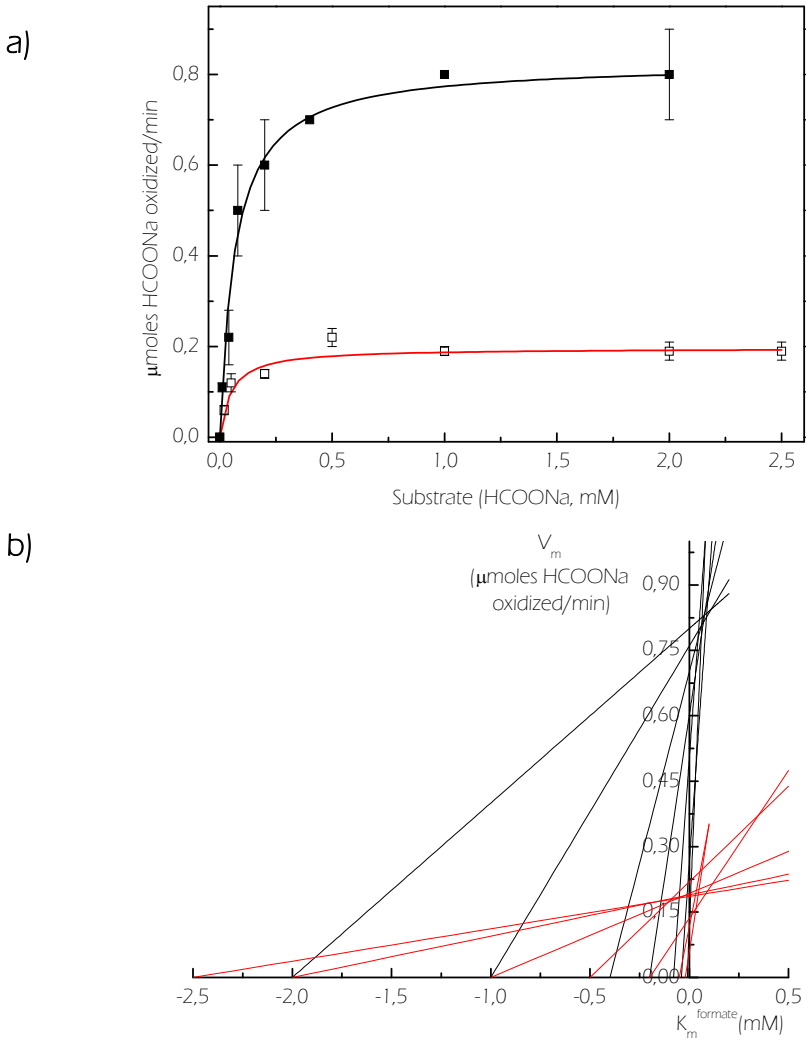

Figure II.3.11 Evaluation of the effect of β-mercaptoethanol on the substrate affinity. (a) Initial rates vs. formate concentration least square to the Michaelis-Menten model, and (b) DLP of V_m against K_m. Black and red lines correspond to assays performed with and without β-mercaptoethanol, respectively.

The data included in Table II.3.2 show that the turnover number (k_{cat}) is 4-fold larger when the thiol is present in the mixture assay. Although, the differences between the K_m values are not too significant as for k_{cat}, the presence of β-mercaptoethanol yields a slightly increase of this parameter (conclusion obtained from statistical t-test). In conclusion the presence of β-mercaptoethanol increases largely the turnover number of the enzyme but slight decrease the substrate affinity.

Table II.3.2 Kinetic constants calculated by Michaelis-Menten model and DLP from experiments with and without β-mercaptoethanol. Standard deviation between parentheses.

		$V_m^{formate}$ (μmol/min)	$K_m^{formate}$ (μM)	$k_{cat}^{formate}$ (sec^{-1})	Specific Activity (U/mg)	V_m^{BV} (μmol/min)	K_m^{BV} (μM)	k_{cat}^{BV} (sec^{-1})
With βmercaptoethanol	MM	0.83(6)	68(8)	349(14)	143(6)	1.3(1)	87(18)	593.5(1)
	DLP	0.82(11)	64(22)	347(19)	139(6)	1.4(1)	88(3)	600(46)
Without βmercaptoethanol	MM	0.196(8)	49(10)	84(3)	32(1)	n.d.	n.d.	n..d.
	DLP	0.192(70)	44(11)	83(10)	33(5)	n.d.	n.d.	n.d.

Figure II.3.12 shows the initial rates versus concentration of β-mercaptoethanol in three different conditions: 1) standard kinetic assay (■), 2) assay in absence of formate (●), and 3) assay in absence of formate and enzyme (▲).

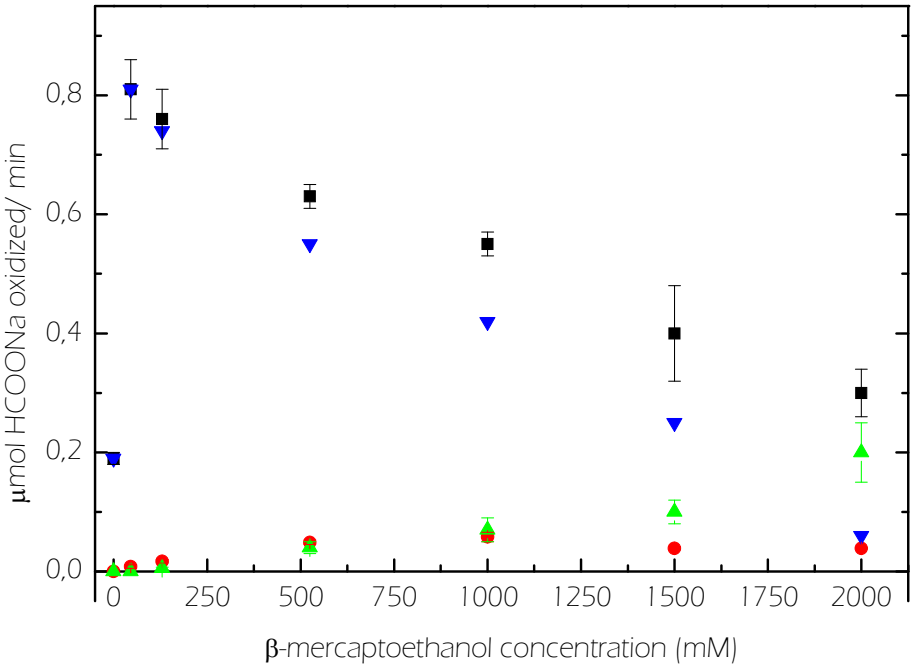

Figure II.3.12 Initial rates versus concentration of β-mercaptoethanol in different conditions. (■) standard kinetic assay; (●) assay in absence of formate; (▲) assay in absence of formate and enzyme; (▼)subtraction of initial rates in absence of formate (●) and in absence of formate and enzyme (▲) to those obtained in standard conditions (■). The concentration of benzyl viologen used was 7.5 mM.

As shown in Figure II.3.12, the data in condition 1 (■, standard kinetic assay) shows a decreasing of initial rate at higher concentrations of β-mercaptoethanol. However, this effect is not statistical significant at the assay conditions (130 mM, β-mercaptoethanol).

In addition, the data in conditions 3 (▲, assay in absence of formate and enzyme) indicate that the chemical reduction of benzyl viologen increases with the concentration of β-mercaptoethanol but this is no significant at concentrations lower than 250 mM. Therefore, the chemical reaction does not affect enzymatic initial rate in a standard reaction and becomes significant as the β-mercaptoethanol concentration increase.

II.3.4.3 Deuterioformate as substrate

Kinetic isotope effects [84] can be advantageously used to learn on enzyme mechanistic aspects that would be difficult to obtain by other methodologies. To evaluate whether the breaking of the C-H bond is the rate limiting step in the conversion of formate to CO_2, kinetic studies using deuterioformate (DCOONa) as substrate were performed. The results obtained from these experiments were analyzed and compared with those for protioformate (Figure II.3.13 and Table II.3.3).

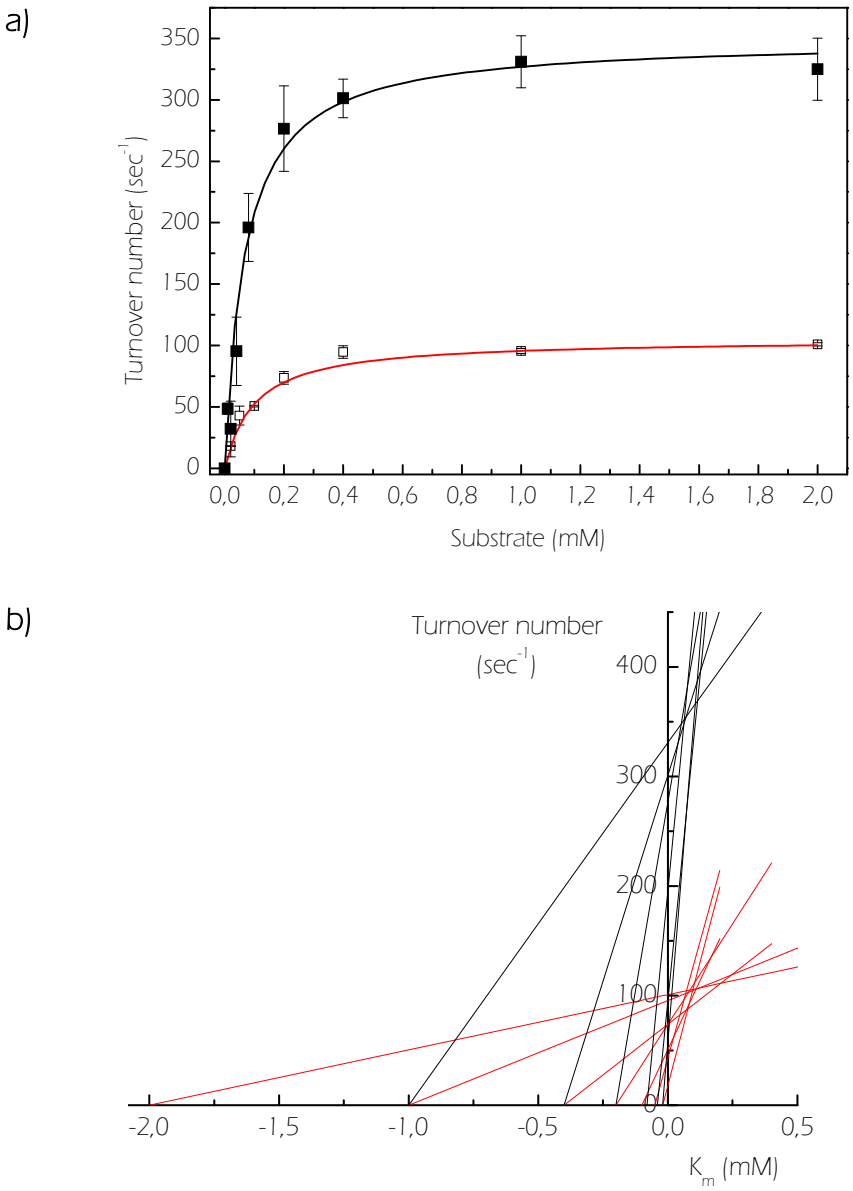

Figure II.3.13 Influence of C-H breaking in the limiting rate step. *(a) initial rates vs. formate concentration (■, HCOONa; □, DCOONa). (b) Direct linear plot of turnover number against K_m (black and red lines correspond to HCOONa and DCOONa, respectively).*

Table II.3.3. Kinetic parameters calculated for *Dd* Fdh using HCOONa and DCOONa as substrates. Standard deviation between parentheses.

		$K_m^{formate}$ (μM)	$k_{cat}^{formate}$ (sec^{-1})
HCOONa	MM	68(8)	349(14)
	DLP	64(22)	347(19)
DCOONa	MM	100(3)	105(1)
	DLP	81(20)	104(8)

A comparison of the data shown in Figure II.3.13 and in Table II.3.3 indicates that the use of DCOONa as substrate leads to an important decrease of the turnover number, which indicates that the breaking of C-H bond is the rate limiting step of formate oxidation. Furthermore, *Dd* Fdh shows an increasing of 1.5 times in the K_m parameter which is in agreement results report for *E coli* Fdh-H [85].

To check this effect in another related protein, the isotope effect was evaluated for the W-Fdh from *D. gigas*. The data obtained were least square fitted to the Michaelis-Menten model (Figure II.3.14) and kinetic constants were calculated (Table II.3.4). A comparison between constants obtained with both substrates indicates that replacement of H for D induces a similar effect on both turnover number and K_m.

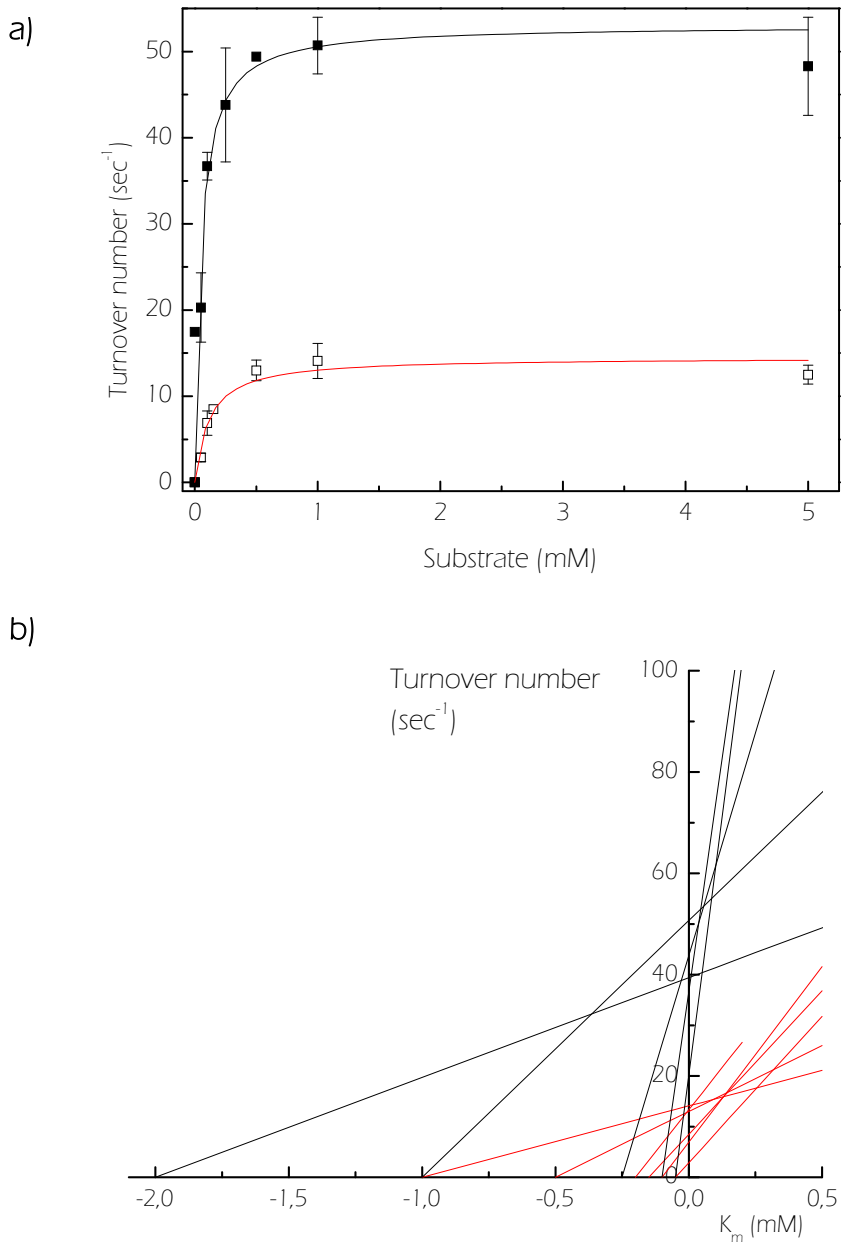

Figure II.3.14 Influence of C-H breaking in the sodium formate reduction by *Desulfovibrio gigas* Fdh. (a) turnover number vs. formate concentration (■, HCOONa; □, DCOONa), and (b) direct linear plot of turnover number against K_m (black and red lines correspond to HCOONa and DCOONa, respectively).

		$K_m^{formate}$ (μM)	$k_{cat}^{formate}$ (sec^{-1})
HCOONa	MM	49(8)	53(3)
	DLP	40(11)	51(4)
DCOONa	MM	113(10)	14(3)
	DLP	136(31)	16(2)

Table II.3.4 Kinetic parameters calculated from Michaelis-Menten and Direct Linear Plot obtained from *Desulfovibrio gigas* Fdh. The numbers in parenthesis are the standard deviations.

II.3.4.4 Inhibition studies

Azide and cyanide were demonstrated to be strong inhibitors of a number of Fdhs and other Mo-enzymes [86]. Furthermore, preliminary studies in *Dd* Fdh shows activity towards nitrate [52]. In this work, different types of experiments were carried out to characterize the inhibitory effect of azide, cyanide, and nitrate.

Figure II.3.15 shows the decay initial rate with respect to that in absence of inhibitor versus inhibitor concentration. This experiment was performed to verify the optimal inhibitor concentration and to characterize the type of inhibition.

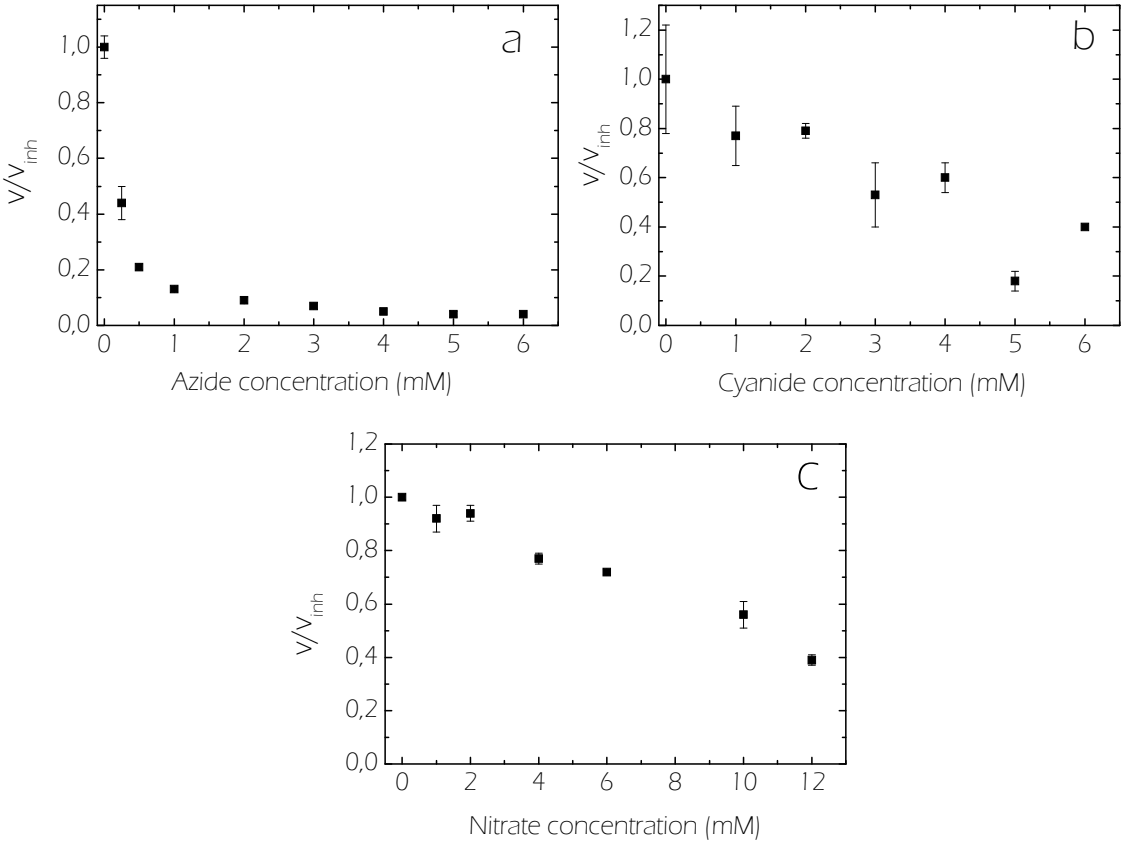

Figure II.3.15 Inhibitor concentration (a, azide; b, cyanide and c, nitrate) vs. initial rate decreasing. Concentration of formate used in the reaction mixture was 1 mM.

The data showed in this figure indicate that azide is the strongest inhibitor followed by cyanide and finally nitrate.

The type of inhibition was evaluated following conventional methods [84], i.e. by varying the substrate concentration at different inhibitor concentration. The results of these experiments are described below.

II.3.4.4.1 Inhibition by Azide

The inhibitory effect of azide was checked by means of DLP analysis, as explained in section II.3.4.1. Figure II.3.16 shows the DLP plot obtained with and without inhibitor (black and red lines, respectively). The results point to a mixed inhibition pattern which is characterized by the equations:

$$V^{app} = \frac{V_m}{1+i/K_{iuc}} \qquad \text{(equation II.3.3)}$$

$$K_m^{app} = \frac{K_m(1+K_{ic})}{1+i/K_{iuc}} \qquad \text{(equation II.3.4)}$$

$$V^{app}/K_m^{app} = \frac{V_m/K_m}{1+i/K_{ic}} \qquad \text{(equation II.3.5)}$$

where, V^{app} and K_m^{app} are the *apparent* values of V_m and K_m, i is the inhibitor concentration, K_{ic} and K_{iuc} are the competitive and uncompetitive inhibition constants, respectively.

.

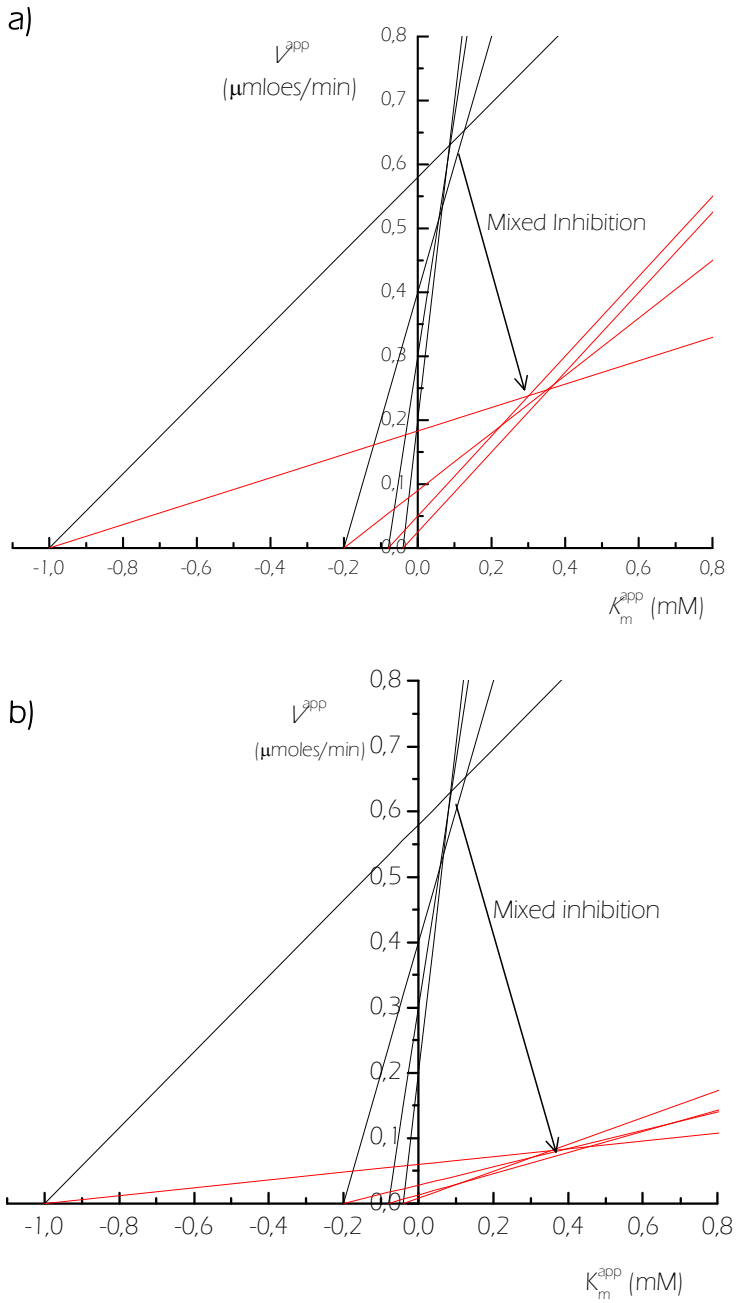

Figure II.3.16 Direct linear plots showing mixed inhibition by azide. Black and red lines correspond to the experiments with and without inhibitor. Azide concentrations used in inhibition experiments were 0.5 mM (a) and 2 mM (b).

The procedure used to evaluate the kinetic constants (K_{ic} and K_{iuc}) can be summarized as follow. The values of V^{app} and K_m^{app} were obtained from intersection points of DLP at two different concentrations of azide. Then, they were used to estimate the

constant ratio V^{app}/K_m^{app} and K_{ic} was calculated from equation II.3.5. The remaining K_{iuc} value was estimated from equations II.3.3 and II.3.4.

The K_{iuc} and K_{ic} were calculated to be 214±3 μM and 33±3 μM respectively (Table II.3.5). These values represent the median and standard deviation calculated from a set of K_{iuc} and K_{ic}. Median instead of average was estimated because intersections in DLP not cross at exactly the same point due experimental errors.

II.3.4.4.2 Inhibition by Nitrate

The inhibition effect of nitrate on the reduction of formate was evaluated by two types of plots: DLP and S/v vs. inhibitor concentration [87]. Figure II.3.17 shows the dependence S/v on inhibitor concentration where is clearly visible a competitive inhibition. At high concentrations of nitrate (20mM), DLP analysis confirms this type of inhibition by nitrate (Figure II.3.18). The effect of competitive inhibition is to decrease the apparent value of V_m/K_m by the factor $(1+ i/K_{ic})$.

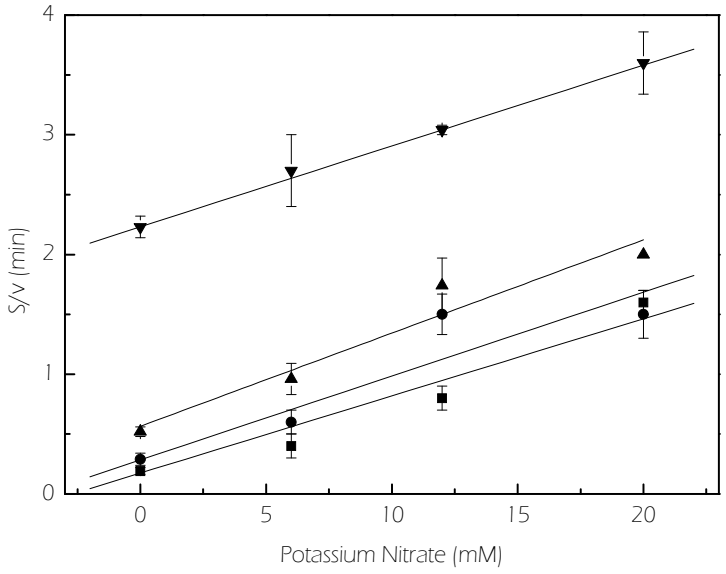

Figure II.3.17 Competitive inhibition by nitrate (Cornish-Bowden Plot [87]). Formate concentration used were: (■) 50 μM, (●) 100 μM, (▲) 200 μM and (▼) 1000 μM.

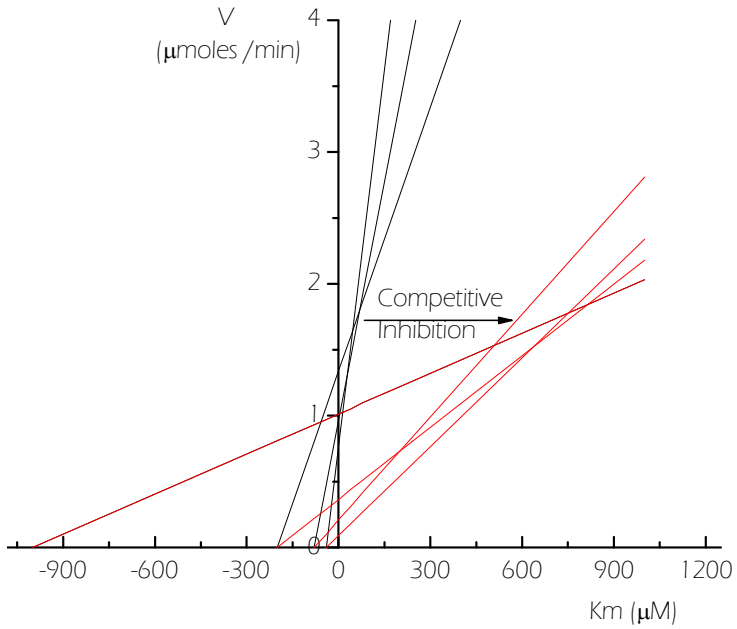

Figure II.3.18 Direct linear plot showing competitive inhibition by nitrate. Black lines: without inhibitor, red lines: 20 mM nitrate.

In this case K_{ic} was calculated by Dixon Plot [84] (Figure II.3.19) disclosing a value of 630±240 µM. (Table II.3.5).

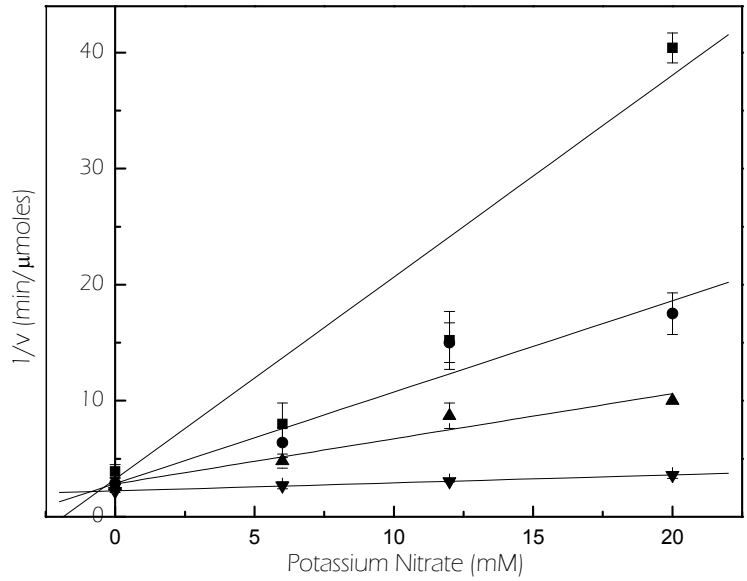

Figure II.3.19 Dixon plot for competitive inhibition by nitrate. Formate concentration used were: (■) 50 µM, (●) 100 µM, (▲) 200 µM and (▼) 1000 µM.

II.3.4.4.3 Inhibtion by Cyanide

As for azide inhibition, DLP analysis demonstrated that cyanide is a mixed inhibitor (Figure II.3.20). The K_{ic} and K_{iuc} were calculated in the same way as azide inhibition constants (Table II.3.5).

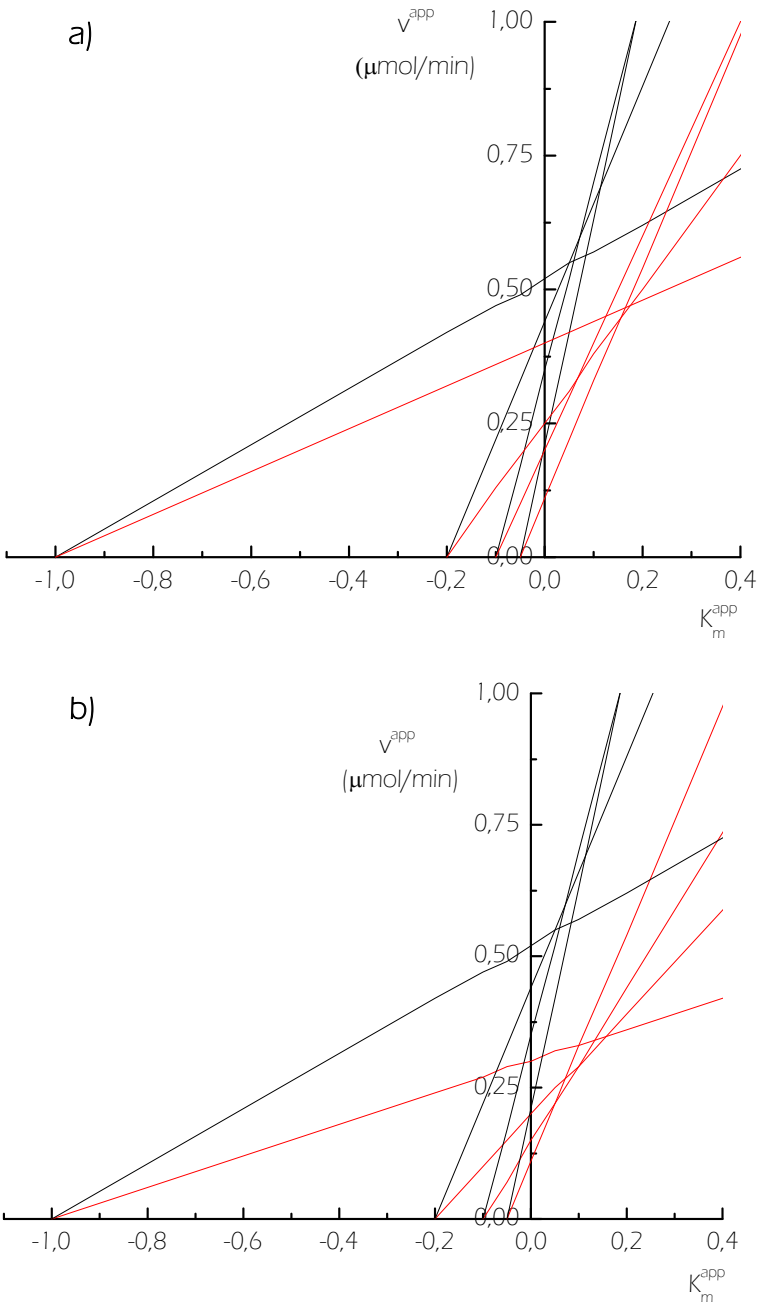

Figure II.3.20 Direct linear plots showing mixed inhibition by cyanide. Black and red lines correspond to the experiments with and without inhibitor. Cyanide concentration used in inhibition experiments was 1.25 mM (a) and 2.5 mM (b).

Table II.3.5 Inhibition constants calculated for azide, cyanide and nitrate.

	K_{iuc} (μM)	K_{ic} (μM)
Azide	214(3)	33(3)
Cyanide	1634(156)	420(127)
Nitrate	-	630(240)

II.3.5 EPR Spectroscopy

II.3.5.1 Molybdenum centre

II.3.5.1.1 As-prepared and dithionite reduced enzyme.

Figure II.3.21 shows the EPR spectra taken at 100 K of the as-prepared and dithionite reduced sample at different incubation times. As already reported [52], as-prepared *Dd* Fdh presents a rhombic EPR signal, which was called Rhombic I (Figure II.3.21a, EPR parameters in Table II.3.6). Furthermore, the dithionite reduced enzyme shows a second signal called Rhombic II and a signal from radical species (Figure II.3.21b-c, EPR parameters in Table II.3.6).

A previous redox titration performed on this enzyme [52] revealed that the intensity and line-shape of Rhombic I signal are insensitive to dithionite addition. Although some changes were detected in the different experiments carried out in this work, these are not significant and hence not analyzed. In contrast, Rhombic II species are redox active with a redox potential of -162 mV [52]. Both Rhombic II species is thought to be not relevant in catalysis, as it can be obtained only upon dithionite reduction. The radical signal observed in Figure II.3.21d, which was no observed in the previous characterization, was also observed in other closely related Fdhs [43, 88].

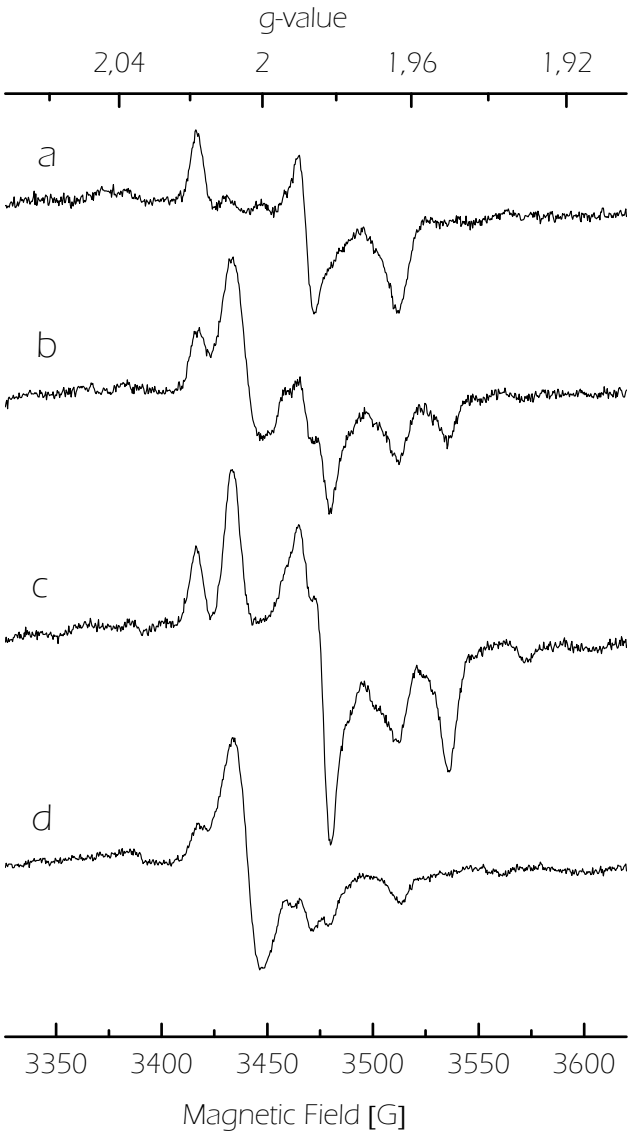

Figure II.3.21 Mo(V) EPR spectra of as-prepared and dithionite reduced enzyme. *(a) As-prepared sample, (b) Signal obtained after 10 min reduction with 10 times excess of dithionite, (c) Idem (b) but incubated 30 min, and (d) Signal obtained after 30 min with 25 times excess of dithionite. Frequency: 9.65 GHz, Microwave power: 2 mW, and Modulation Field: 10 G_{pp}, Temperature: 100K.*

Table II.3.6 EPR parameters of Rhombic I and Rhombic II signals. Linewidths (within parentheses) are given in Gauss.

Mo (V) EPR signal	g_{max}	g_{med}	g_{min}
Rhombic I	2.019(8.1)	1.989(6.9)	1.964(10.8)
Rhombic II	2.009(10.8)	1.984(6.7)	1.951(10.8)

II.3.5.1.2 Formate reduced enzyme.

The reduction of *Dd* Fdh with sodium formate yields a different signal from the dithionite reduced enzyme (Figure II.3.22a). This signal, hereafter called *formate* signal, is rhombic and shows in addition hyperfine structure, which is originated from nuclear species with I=1/2. In order to elucidate the nature of these species, EPR spectra were obtained by reducing *Dd* Fdh with sodium formate in four conditions: as-prepared enzyme reduced with (a) HCOONa and (b) DCOONa; and enzyme exchanged into D_2O buffer reduced with (c) HCOONa, and (d) DCOONa (Figure II.3.22a-d). Experiments in conditions (a) and (c) pursued to detect hyperfine splittings given by solvent exchangeable protons whereas conditions (b) and (c) splittings from the formate α-proton. Condition (d) was only for control purposes.

After reductant addition, samples were frozen immediately in liquid nitrogen followed by spectral acquisition. Then, they were thawed and incubated in anaerobic conditions for 5 minutes, after which they were immediately frozen for spectral acquisition. This procedure was repeated 6 times. Longer incubation times showed no significant changes in the spectra. The Rhombic I signal detected in the as-prepared *Dd* Fdh samples (Figure II.3.21a), which keeps line-shape and intensity on reduction with either formate or dithionite, was subtracted in all the spectra.

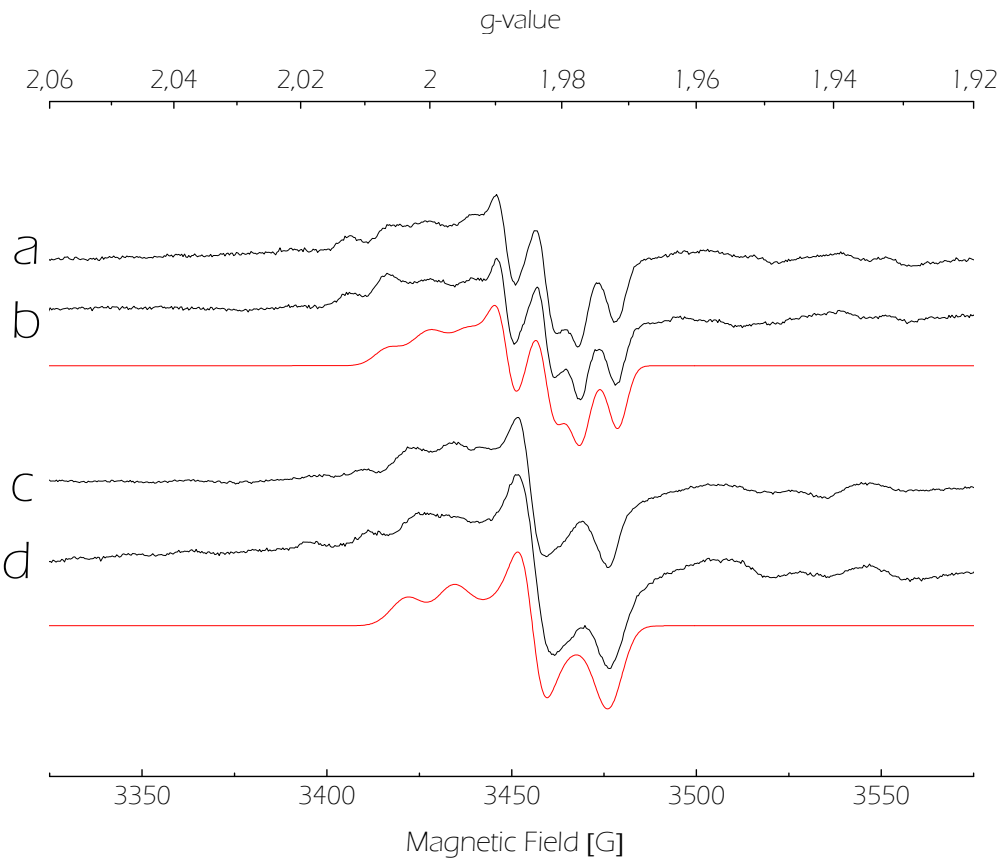

Figure II.3.22 Mo(V) EPR signals obtained after 30 minutes of formate addition to *Dd* Fdh together with simulations (red lines). a) enzyme in H_2O-buffer reduced with HCOONa, b) enzyme in H_2O-buffer reduced with DCOONa, c) enzyme exchanged into D_2O-buffer reduced with HCOONa. d) enzyme exchanged into D_2O-buffer reduced with DCOONa. Simulations (red lines) were done with parameters given in Table II.3.7. Frequency: 9.65 GHz, Microwave power: 2 mW, Modulation amplitude, 5 G; Temperature, 100 K.

Table II.3.7 EPR parameters for simulations of Mo(V) EPR signals. Linewidth are given in G between parentheses. The A values are given in $cm^{-1} \times 10^{-4}$. Indexes 1 and 2 stand for the non-solvent and solvent exchangeable protons, respectively.

EPR signal	g_{max}	g_{mid}	g_{min}	A^1_{max}	A^2_{max}	A^2_{mid}	A^2_{min}
Formate signal in H_2O -buffer	2.012 (12)	1.996 (8)	1.985 (8)	11.7	7.7	10	9.3
Formate signal in D_2O -buffer	2.012 (12)	1.996 (8)	1.984 (12)	11.7	-	-	-

Spectra in conditions (b) an (d) are similar to the spectra in conditions (a) and (c), respectively. Comparison of Figures II.3.22a and II.3.22c shows that formate signal is split by two interacting I=1/2 nuclei (EPR parameters in Table II.3.7). One of them is not solvent exchangeable and splits the g_{max} feature but not the two lowest g-values (Figure II.3.22ab). According to the proposed structure for the Mo site of *Dd* Fdh [53], the closest non-solvent exchangeable protons to the Mo atom able of giving such hyperfine coupling are situated on the β-methylene carbon of the Se-Cysteine in the oxidized form of the enzyme, which suggests that SeCys is also coordinated to the Mo(V) ion. In contrast, the second interacting nucleus is exchangeable with solvent and produces a splitting detectable at the three principal g-values. This interaction, which is more isotropic, must be produced by protons of a solvent molecule bound to the Mo, and, hence it must correspond to ligand $-OH_2$ in Figure II.1.6. The spectra taken at shorter incubation times, even those obtained immediately after reductant addition, are similar but with lower intensity. This indicates that, under these experimental conditions, splittings from formate α-proton can be neither detected nor solved.

II.3.5.1.3 Azide and cyanide inhibited enzyme.

Since azide and cyanide are inhibitors of *Dd* Fdh, their effects on *formate* signal were investigated by two different experiments. One of them aimed to detect the Mo(V) species obtained in inhibited enzyme samples followed by formate/dithionite reduction, whereas the second experiment pursued to check the effect of both inhibitors on the formate species.

For the first experiment, azide inhibited samples of as-prepared and D_2O-exchanged samples of *Dd* Fdh were reduced with DCOONa and HCOONa (Figure II.3.23a-d) and immediately frozen. In contrast to the formate signal, the intensity of these signals reaches the maximal value immediately after reductant addition (~ 10% of the total molybdenum). The spectra of Figure II.3.23 show a nearly axial symmetry with resonance lines split with a

solvent exchangeable proton at g_{mid} and g_{min} when the enzyme is incubated with HCOONa. This confirms that the splitting at g_{mid} and g_{min} is originated from the formate α-proton. Similar spectra were obtained on dithionite reduction. Surprisingly, this signal corresponds to the *2.094* signal obtained in *Ec* Fdh-H on dithionite/formate reduction. A simulation of the *2.094* signal in *Ec* Fdh-H is shown in Figure II.3.23e for comparison.

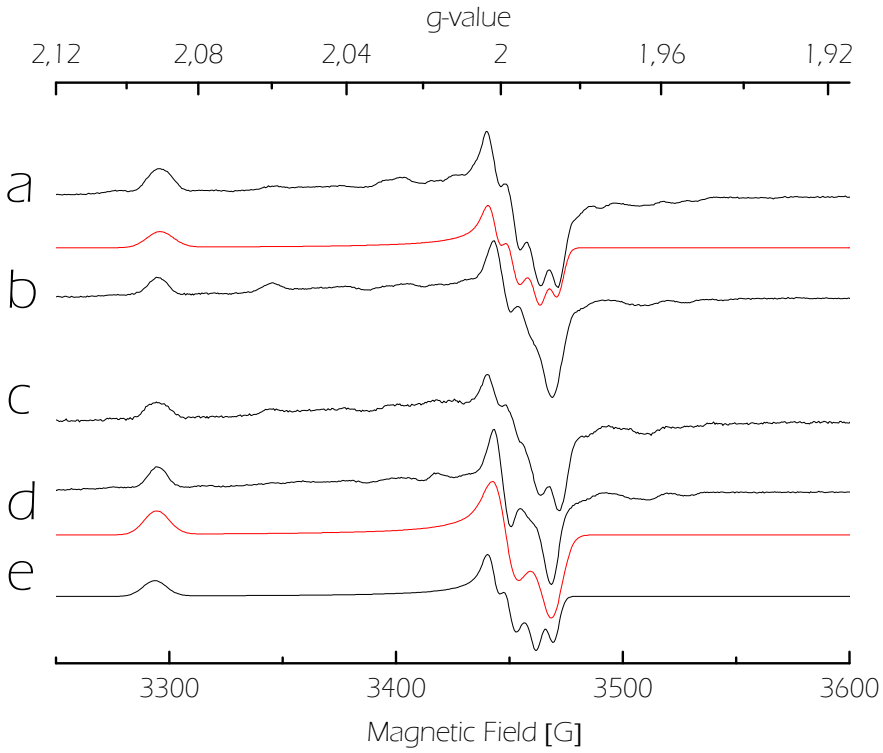

Figure II.3.23 EPR signals of azide inhibited samples (black lines) obtained after 15 seconds of formate reduction to *Dd* Fdh together with simulations (red lines). a) Inhibited enzyme in H_2O-buffer reduced with HCOONa, b) Inhibited enzyme in H_2O-buffer reduced with DCOONa, c) Inhibited enzyme exchanged into D_2O-buffer reduced with HCOONa, d) Inhibited enzyme exchanged into D_2O-buffer reduced with DCOONa, and e) *2.094* signal from *E coli* Fdh-H. S. Experimental conditions: Microwave frequency, 9.65 GHz; Modulation field, 100 kHz, Modulation amplitude, 5 G; Microwave power, 2 mW; Temperature, 100 K.

Table II.3.8 EPR parameters for simulations of Azide signals. Linewidth (between parentheses) and A are given in G and $cm^{-1} \times 10^{-4}$, respectively.

EPR signal	g_{max}	g_{mid}	g_{min}	A_{max}	A_{mid}	A_{min}
Dd Fdh Azide signal (HCOONa)	2.092 (20)	2.000(9)	1.989 (9)	nd	7.0	7.0
Dd Fdh Azide signal (DCOONa)	2094(11)	2.000(9)	1.988 (9)	nd	nd	nd
2.094 signal	2.094	2.000	1.989	2.5	6.3	7.0

The EPR spectra taken at longer incubation times (15 min) reveal additional information. As-prepared sample reduced with DCOONa (Figure II.3.24a) yielded a spectrum similar to that of Figure 3.23b after longer incubation times (Figure II.3.24b). In contrast, D_2O-exchanged samples reduced with HCOONa (Figure II.3.24c) yielded a similar spectrum to that of Figure 3.23d (Figure II.3.24d). These results indicates that the proton which originates the resonance lines split at g_{mid} and g_{min} is solvent exchangeable. Similar results were obtained in *Ec* Fdh-H [11].

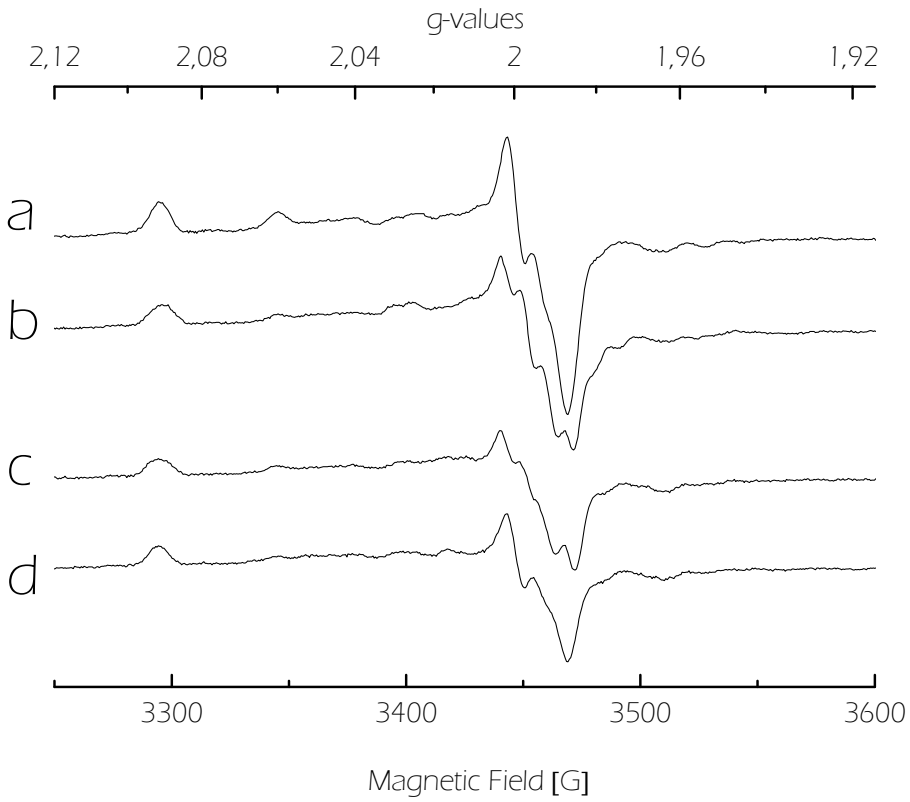

Figure II.3.24 EPR signals of azide inhibited samples obtained at different incubation times with sodium formate. *a) Inhibited enzyme in H_2O-buffer reduced 15 sec with DCOONa, b) Inhibited enzyme in H_2O-buffer reduced 15 min with DCOONa, c) Inhibited enzyme exchanged into D_2O-buffer incubated 15 sec with HCOONa, d) Inhibited enzyme exchanged into D_2O-buffer incubated 15 min with HCOONa. Frequency: 9.65 GHz, Modulation field: 100 kHz, Modulation amplitude: 5 G, Microwave power: 2 mW, and Temperature, 100 K.*

For the second experiment, azide or cyanide were added to samples showing the *formate* signal. The *2.094* signal was also detected under these conditions and no signs of both the *formate* signal and the Rhombic I signal, even in the sample obtained immediately after inhibitor addition, were observed (not shown).

Similar results were obtained by cyanide as inhibitor (data no shown).

II.3.6.2 Iron-sulphur clusters

Figure II.3.25 shows the EPR spectra taken at 20 K and at 40 K. Both signals have EPR parameters and relaxation behaviours typical of [4Fe-4S] clusters in a low spin configuration (s=1/2). The signal observed at 40 K is called FeS I whereas the broader signal, which is observed at temperatures lower than 20 K, is called FeS II.

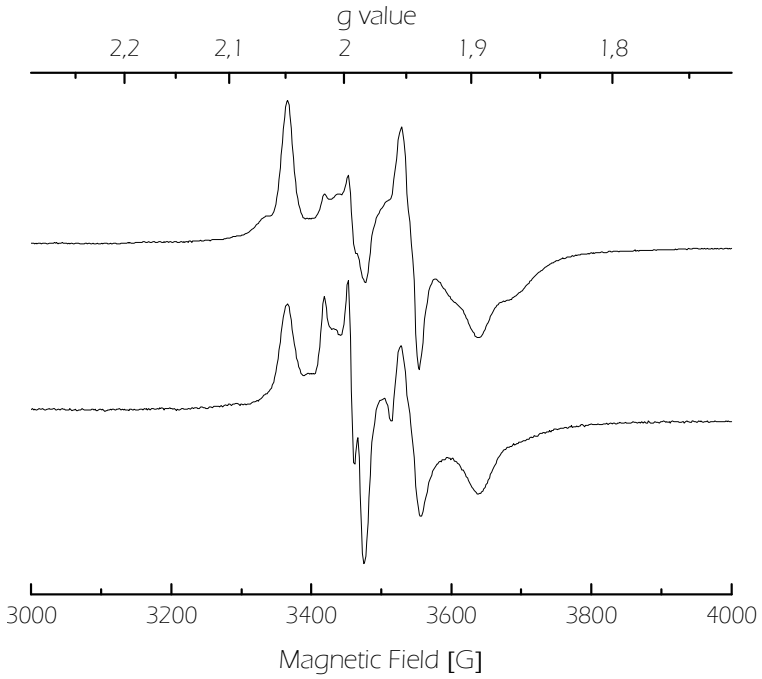

Figure II.3.25 EPR spectra of the reduced FeS clusters in *Dd* Fdh at 20 K and 40K. Frequency: 9.65 GHz, Modulation field: 100 kHz, Modulation amplitude: 10 G, and Microwave power: 2 mW.

Note that g_{mid} of the FeS I signal feature shows a shoulder, which is marked with an asterisk, and can be originated from either magnetic coupling between centres or from a different centre. To elucidate the origin of the shoulder at g_{mid}, EPR measurements at Q-band were performed (Figure II.3.26). These results show a better resolution of the shoulder indicating that the FeS I signal is composed by one major rhombic component and one minor axial component. The simulation of this spectrum was achieved assuming a ratio 0.84:0.16 between both components (Figure II.3.26, EPR parameters Table II.3.9). The simulation of the X-band spectrum at 10 K indicates a ratio 1:1 between FeS I and FeS II

signal. EPR saturation studies of FeS I signal at 30 K (Figure II.3.27) show that both components have the same saturation behaviour, which points to a single centre in two different conformations instead of different centres.

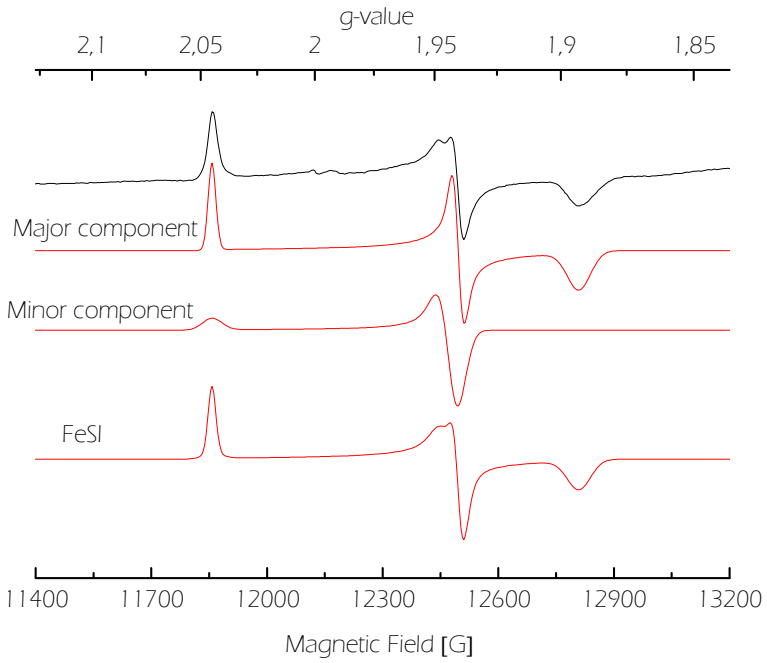

Figure II.3.26 Q-band spectra of the reduced FeS clusters in *Dd* Fdh at 10 K together with its simulations (red lines). Frequency: 33.94 GHz, Modulation field: 100 kHz, Modulation amplitude: 5G, and Microwave power: 4.256 x 10^{-2} mW.

Table II.3.9 EPR parameters for simulations of FeS I signals. Linewidth (between parentheses) are given in G.

EPR signal	g_{max}	g_{mid}	g_{min}
Major component	1.893 (60)	1.9405 (25)	2.045 (20)
Minor component	1.943 (50)	1.943 (50)	2.045 (50)

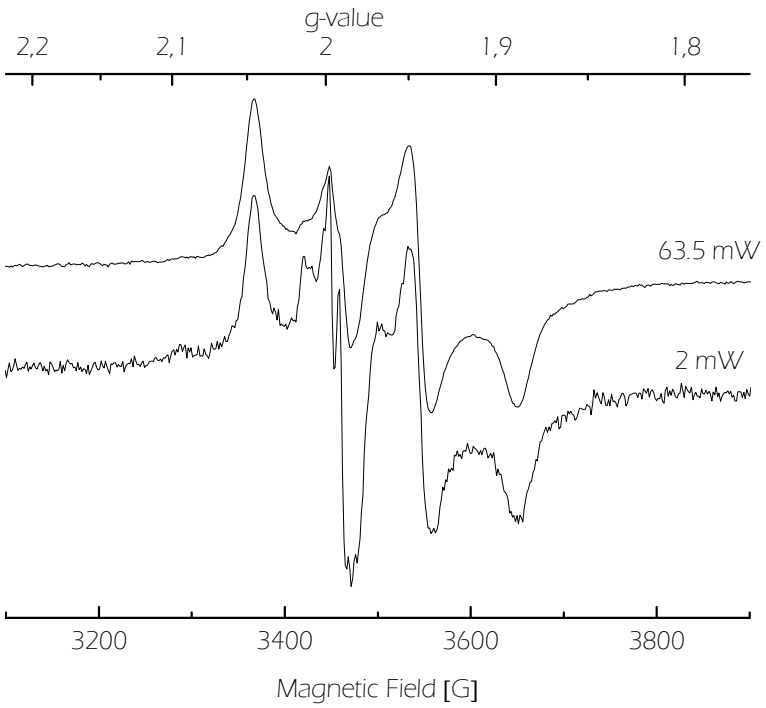

Figure II.3.27 FeS I EPR signal at 63.5 mW and 2 mW. Frequency: 9.65 GHz, Modulation field: 100 kHz, Modulation amplitude: 10 G, and Temperature: 40 K.

Spin quantification of the spectra at 20 and 40 K taking into account the protein concentration yielded values close to 2 spins/protein and 1 spin/protein, respectively. This calculation performed considering the iron content (~15 Fe/protein) raise to values close to 4 spins/protein and 2 spins/protein.

II.3.5.3 Heme centres

The EPR signal associated with heme groups, which is typical of Fe^{3+} ions in a low spin configuration, is similar to that previously reported (Figure II.3.28) [52]. This signal was simulated in reference [52] assuming four different hemes, which is in line with the histidine motifs observed in the amino acid sequence determined for the small subunit (see section II.3.3)

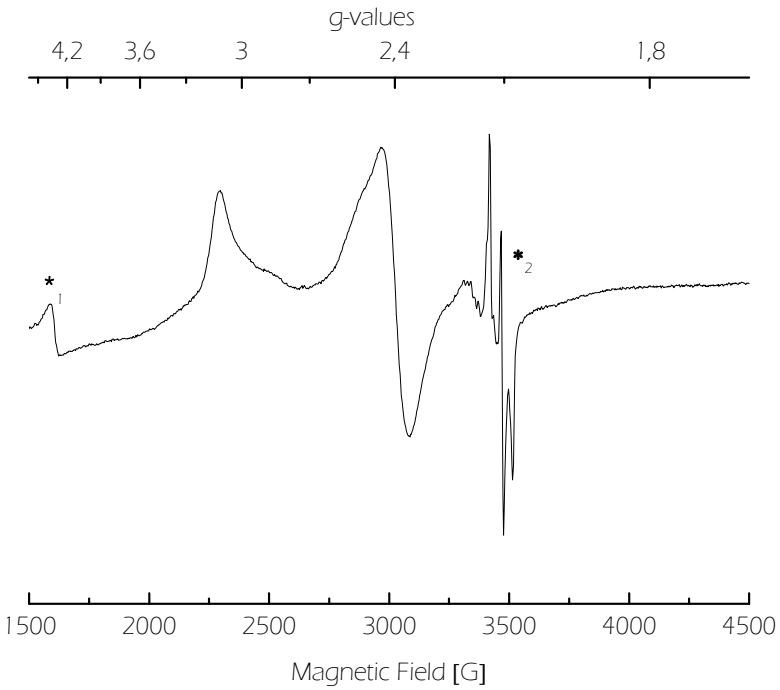

Figure II.3.28 EPR spectrum of the as-prepared *Dd* Fdh associated with the four different heme groups. The peaks marked with an asterisk correspond to adventitious iron (*g*~4.3) and Mo signals (*g*~2). Frequency, 9.65 GHz; Modulation field, 100 kHz; Modulation amplitude, 10 G; Microwave power, 2 mW, and Temperature: 20 K.

II.4. DISCUSSION

II.4.1 Gene organization of *Desulfovibrio desulfuricans* ATCC 27774 Fdh

The *fdh* cluster contains four well identified open read frames that were designated *fdh*A, *fdhB, fdhE,* and *fdhC*. Two gaps upstream and downstream of *fdhE* could indicate the presence of additional genes involved in the Fdh assembling, however, no homology with another annotated sequences have been identified. Futhermore, no termination-like sequences were found between genes suggesting that *fdh* genes are more likely expressed as an operon.

Table II.4.1 shows the sequence identity percentage between *Dd* Fdh and several related Fdhs. All the three *Dd* Fdh subunits revealed high identity percentage with the homologous enzyme from *D. vulgaris* Hildenborough.

Table II.4.1 Sequence identity percentage between *Dd* Fdh subunits and another related Fdhs. Accession number of subunits from different microorganisms are: a, YP_012024, YP_012023 and YP_012021; b, YP_390001 and YP_390002; c, Q934F5 and Q8GC87; d, YP_387213 and YP_387214; e, YP_011694 and YP_011693; f, YP_009809 and YP_009810; g, YP_387309 and YP_387308; h, P24183, P24184 and P24185 ; i, P32176, P32175 and P32174; j, P07658.

	Dd Fdh subunits		
	α	β	γ
*Dv*H Fdh-3[a]	83	79	54
*Dd*G20 Fdh[b]	73	69	n.p.
Dg W-Fdh[c]	53	50	n.p.
*Dd*G20 Fdh[d]	53	49	n.p.
*Dv*H Fdh[e]	50	58	33
*Dv*H Fdh[f]	50	53	n.p.
*Dd*G20 Fdh[g]	48	53	n.p.
Ec K12 Fdh-N[h]	44	25	12
Ec K12 Fdh-O[i]	43	24	12
Ec K12 Fdh-H[j]	18	n.p.	n.p.

Figure II.4.1 shows the organization of the *fdh* genes in several bacteria. As shown in this figure, the organization of *Dd fdh* genes highly resembles to that of *D. vulgaris* Hildenborough *fdh-3* operon.

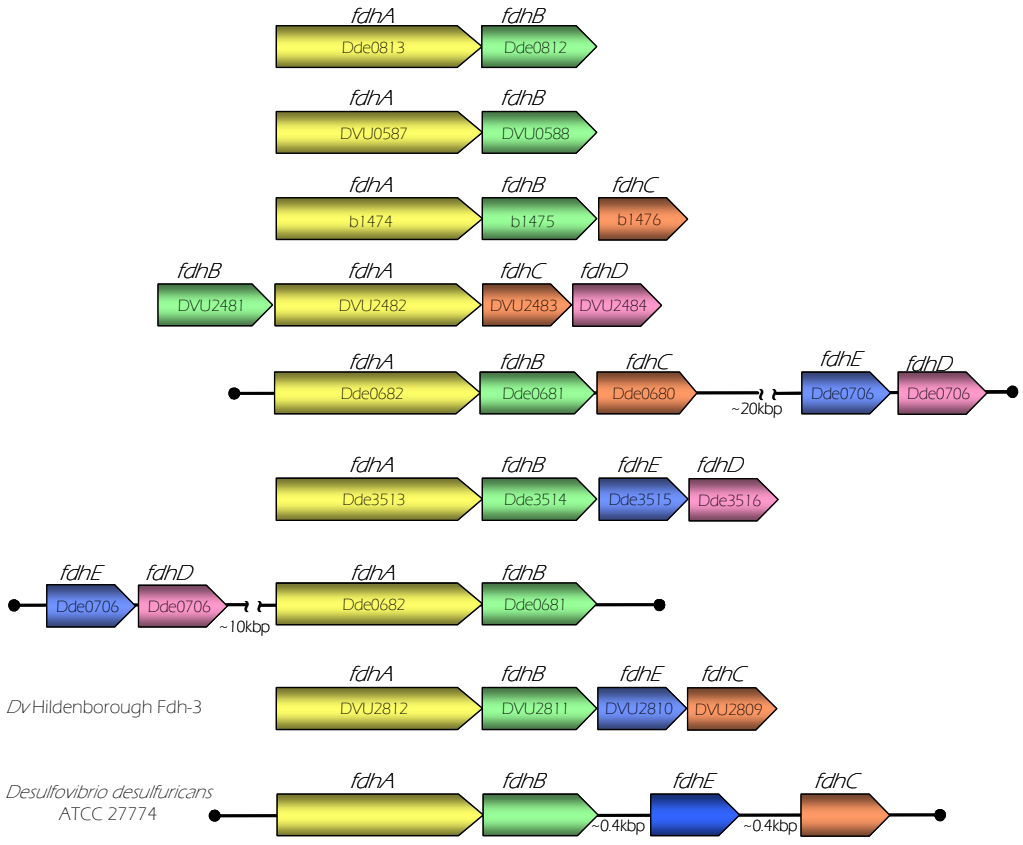

Figure II.4.1 Schematic representation of the *fdh* gene organization in diverse bacteria. Dde: *D. desulfuricans* G20, DVU: *D. vulgaris* Hildenborough, b14XX: *Escherichia coli* K12.

The first gene of the operon, *fdhA*, codifies to FdhA, which is the subunit containing the active site. A putative ribosome binding site sequence as well as promoter-like regions is located 9 nucleotides upstream of the ATG codon (Figure II.3.4).

Alignment of FdhA subunit with sequences from different organisms reveals highly conserved residues (Figure II.3.6). As already described for another Fdhs [27, 38, 40, 47], FdhA sequence contains a -$CX_2CX_nCX_mC$- motif which is likely associated with the [4Fe-4S] centre detected by EPR spectroscopy. The position of this motif is consistent with the

sequence of related proteins like *Ecoli* Fdh-H [37], *Ecoli* Fdh-N [38], *D. gigas* W-Fdh [40], and *Dd* ATCC 27774 Nap [46, 82].

On the basis of structural data, a Lys residue (Lys^{44} in *Ec* Fdh-H [41] and Lys^{56} in *D. gigas* Fdh [40]) has been proposed to be essential in the electron transfer between the active site and the [4Fe-4S] centre (Figure II.4.2). This residue is also conserved in *Dd* Fdh (Lys^{56}) which gives some additional support to this hypothesis.

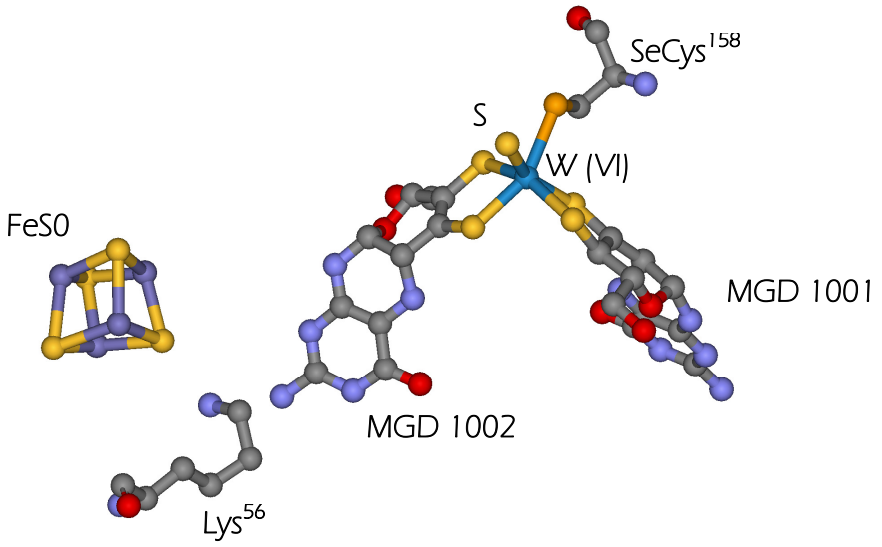

Figure II.4.2 Tungsten catalytic site of *D. gigas* Fdh [39, 40]. Lys^{56} makes a bridge between the pterin and the first [4Fe-4S] cluster which could be the electron transfer pathway of formate oxidation.

In the reaction mechanism proposed for *Ec* Fdh-H, the formate molecule is presumably oriented and stabilized by hydrogen bonding through carbonyl oxygen of formate to both Arg^{333} and His^{141}. Furthermore, it is supposed that His^{141} is involved in the formate proton abstraction. Both residues are also conserved in *Dd* Fdh (Arg^{334} and His^{162}).

An interesting feature of *Dd* Fdh is the presence of SeCys in its sequence. Three results confirm this fact: a) Metal analysis of *Dd* Fdh [52] reveals one Se atom per protein molecule, b) The TGA codon, at 565 bp downstream ATG codon, is in good agreement with the conserved position of SeCys in the Fdhs sequenced so far, c) Analysis of 40 nucleotides downstream of TGA suggests the presence of a stem loop similar to the

proposed for *D. gigas fdhA* [65], *Ec fdhF* [27] and *fdhG* [20]. These 40 nucleotides could be the selenocysteine insertion sequence (SECIS) necessary to decode the TGA codon (Figure II.4.3).

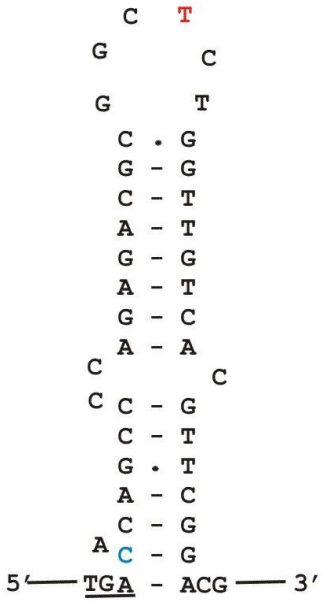

Figure II.4.3 Postulated SECIS element for *Desulfovibrio desulfuricans fdhA*. **C**: single C that prevents UGA read through, **T**: bulged T that interacts with SELB (See section II.1.4).

A putative RBS (AAGGAG) was found 37 bp downstream to the stop codon of *fdhA*. In addition, ATG and TAG codons were identified at 12 and 669 bp upstream of this RBS, respectively. This ORF reveals the presence of a second gene (*fdhB*) which codifies to FdhB. The amino acid sequence of this subunit contains three -$CX_2CX_nX_mC$- motifs in conserved positions when compared with related Fdhs [38, 40].

The analysis of the 1732 nucleotides downstream to the *fdhB* stop codon reveals the presence of several ORFs. However, only one shows a significant homology with annotated proteins. This ORF seems to codify for a protein called FdhE, which seems to be involved in the formation of Fdh. Based on the cellular locations of this protein as well as results obtained from immunoprecipitation assays, it was concluded that *fdhE* does not define any structural gene [66, 67].

The putative RBS sequence, which is 430 bp downstream from the stop codon of *fdhE*, is part of an ORF that codifies for a tetraheme *c*- type cytochrome (FdhC). This Fdh subunit is the last component of the electron transfer pathway from formate to the electron acceptor. The presence of four conserved His located out of the -CX_2CH- motifs should provide the remaining axial ligands for the four hemes of FdhC. This hexa-coordinated iron site is in line with the low spin heme detected by EPR spectroscopy [52].

II.4.2 Kinetic properties

To establish the best conditions of the enzymatic assays, a set of optimization studies were performed. The key step of the reaction was demonstrated to be the previous reduction of the enzyme with its natural substrate. This procedure is essential to eliminate the lag phase observed in the previously reported conditions [52]. This activation also produces a shortening of the first order phase, which decreases from 30 min to a few seconds. The improvement of the assay kinetic conditions allowed a carefully study of the kinetic properties of *Dd* Fdh.

There are a few reports about kinetic properties of Fdh containing Mo or W at the active site. In general, these enzymes display a Michaelian behaviour and the kinetic parameters vary widely among the different organisms. The kinetic parameters for several Fdhs are shown in Table II.4.2.

Table II.4.2 Kinetic parameters of Fdhs isolated from diverse sources

Source	Metal	$K_m^{formate}$ (mM)	$k_{cat}^{formate}$ (sec^{-1})
Desulfovibrio desulfuricans	Mo	0.06(2)	347(19)
Desulfovibrio gigas	W	0.051(4)	54(1)
Escherichia coli K12	Mo	13.3	1367
Syntrophobacter fumaroxidans 1	W	0.04	3792
Syntrophobacter fumaroxidans 2	W	0.01	5625

The differences in kinetic constants could be a consequence of factors such as variability subunit composition, metal contents, and redox cofactors among others.

Several studies leading to establish the relevance of β-mercaptoethanol in the kinetic assay were performed. As shown in section II.3.4.2 (Figure II.3.11), the presence of thiol in the reaction mixture increases approximately four times the turnover number. However, one point that needs to be elucidated is the function of the thiol in the assay. It is though that β-mercaptoethanol breaks a disulfide bridge present in the *D. gigas* Fdh structure, which would allow the opening and movement of the formate entry cleft [40]. Additional work should be necessary to confirm this hypothesis.

II.4.2.1 Influence of the C-H break in the rate liming-step

The effect of C-H break on the oxidation of formate was evaluated using DCOONa as substrate. A 3-fold decrease in the turnover number was observed for both enzymes (*D. gigas* and *Dd* Fdh) when DCOONa is used instead of HCOONa (section II.3.4.3, Table II.3.3). This result shows a primary isotope effect indicating that the break of the C-H bond is the rate limiting-step. Although a detailed analysis of this effect can become complicated, the basic idea could be summarized as follow. At room temperature, the C-H bond is in its vibrational ground state (n=0), which corresponds to the *zero point energy* of the bond

$$E_n = h\,\nu \qquad \text{(equation II.4.1)}$$

where, h is the Planck constant and ν is the fundamental vibrational frequency.

The fundamental vibrational frequency of the chemical bond between two atoms (in this case C-H or C-D) is given by

$$\nu = \frac{1}{2\pi}\sqrt{\frac{k}{\mu}} \qquad \text{(equation II.4.2)}$$

where, k is the spring constant for the bond and μ is the reduced mass (m_C and $m_{H/D}$ stand for the masses of the carbon and hydrogen/deuterium atoms, respectively)

$$\mu_{CH/CD} = \frac{m_C m_{H/D}}{m_C + m_{H/D}}$$

This is shown in Figure II.4.4 in which the *zero point energy* (equation II.4.1) corresponding to the C-D bond is lower than that of the C-H bond. It means that the lower the *zero point energy*, the higher is the energy necessary to overcome the activation energy for the bond cleavage, which results in lower turnover numbers.

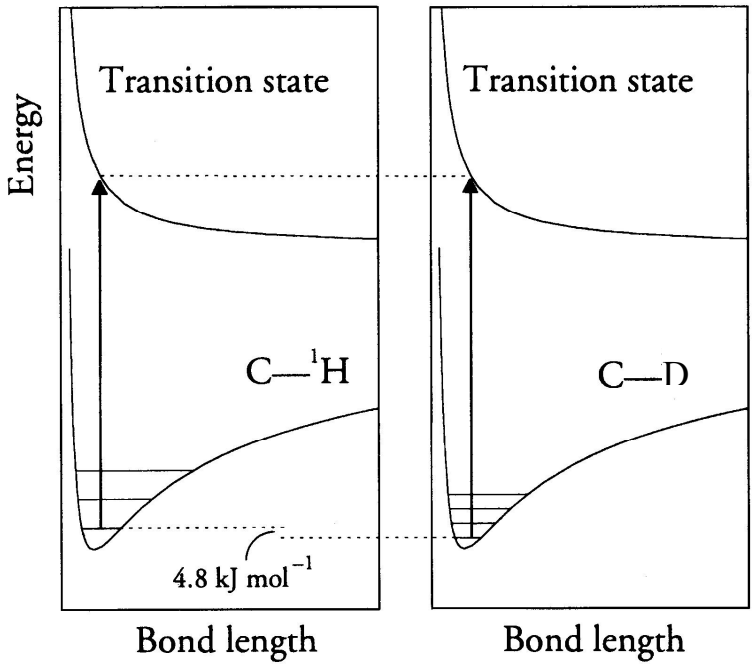

Figure II.4.4. Potential energy as a function of the distance between the atoms involved in a C-H bond (left) and C-D bond (reproduced from reference [84]). The difference between the energies of the fundamental vibrational state is indicated.

II.4.2.2 Effect of inhibitors

Three different compounds were tested as inhibitors. Azide, which shows a mixed inhibition pattern, is the strongest inhibitor with K_{ic} lower than $K_m^{formate}$. Similar results were observed for the *E coli* Fdh-H [85]. Cyanide is also a mixed inhibitor with K_{ic} and K_{iuc} around 1.63±0.16 mM and 0.42±0.12 mM, respectively. It has been postulated that the inhibition by cyanide in Fdh from *Methanobacterium formicicum* removes a sulphur ligand coordinated to molybdenum atom releasing thiocyanate [89]. This hypothesis is unlikely for *Dd* Fdh because cyanide seems to be a more reversible inhibitor than irreversible.

Fdh is inhibited in a competitive manner by nitrate with K_{ic}=0.63± 0.24 mM. This is not surprising owing to the high homology between the Fdh and Nitrate reductases active sites [10]. In addition, although with a very small specific activity, it was reported that *Dd* Fdh reduces nitrate to nitrite [52]. Despite the similar active site observed in the Mo-containing enzymes, it is not common to find examples of crossed reactivities. The correlation between the structural and kinetic properties of these enzymes could give some clues on the substrate preference developed by a given enzyme.

II.4.3 EPR of redox cofactors

II.4.3.1 The Fdh active site centre

II.4.3.1.1 The *formate* species

The Mo(V) EPR signal obtained upon dithionite reduction (Rhombic II signal) is different from that of the formate reduced enzyme (*formate* signal) (Figure II.3.21b-c and Figure II.3.22, respectively). The hyperfine splittings detected for the *formate* signal (Figure II.3.22 see EPR parameters in Table II.3.7) suggest that both the SeCys and a hydroxyl/water ligand are coordinated to molybdenum, which is in agreement with that proposed for the oxidized and dithionite reduced forms of *Dd* Fdh [53]. Therefore, these data in conjunction with the rhombic simetry of this signal suggest a distorted hexa-coordinated site for the *formate* species. Our current interpretation for the structure of this species is similar to that

shown in Figure II.4.5 for the oxidized form of *Ec* Fdh-H, in which ligand X should correspond to an oxygenic species. *Formate* species could also correspond to a Mo(V)-substrate complex. However, this possibility is tentatively excluded because formate, in such a case, should occupy a seventh coordination position, which is unlikely for a member of the DMSO family [10].

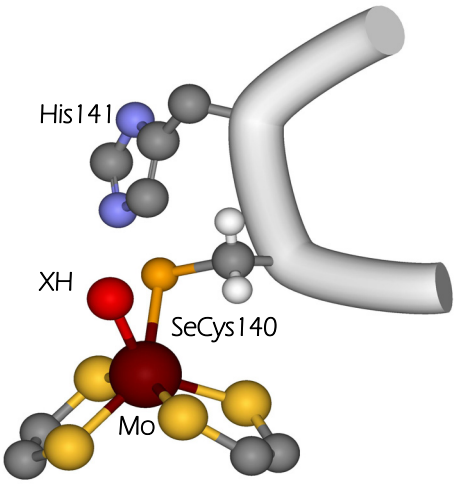

Figure II.4.5 Coordination around Mo centre for *E coli*. Data obtained from EPR experiments on *Dd* Fdh suggests a similar coordination around Mo centre to that proposed for Mo(VI) from *E coli Fdh-H,* where ligand X should correspond to an oxygenic species.

II.4.3.1.2 The *2.094* species. Effects of the inhibitors on the coordination around Mo(V) centre

When azide (cyanide) inhibited samples are reduced with formate or dithionite, or when formate reduced samples are incubated with any of the two inhibitors, the *2.094* signal is developed (Figure II.3.23). The *formate* signal is converted into the *2.094* signal suggesting that the inhibitor molecules change the coordination geometry of the active site. Furthermore, the fact that the two different inhibitor molecules yield the same EPR signal indicates that azide (as well as cyanide) is not bound to the Mo active site, which is in contrast with that proposed for the azide-inhibited form of *Ec* Fdh-H [37, 41]. Finally, as this

signal can be obtained with any of the reductans (formate or dithionite), the formate molecule is not bound to Mo in the *2.094* species.

The magnitude of the hyperfine coupling of the proton from formate suggests that it is bound to a molybdenum ligand. Furthermore, this proton is solvent exchangeable, which suggests that this ligand could be a hydroxyl/water molecule. Mo(V) EPR signals having nearly axial symmetry, such as the one observed for the *2.094* signal, are usually given by penta-coordinated Mo sites as those found in the proteins of the XO family of enzymes [1]. Figure II.4.6 shows a tentative proposal for the structure of the *2.094* species, in which a hydroxyl ligand occupies the apical position. This hypothesis is in agreement with the recent reevaluation of the X-Ray data of formate reduced *Ec* Fdh-H by Raaijmakers and Romão [42], which show that a Selenium atom does not occupy the apical position. These authors postulated for this position a sulphur ligand but, as also stated by them, the resolution is not good enough and could also correspond to an oxygenic species. A pentacoordinated site for the *2.094* species was also proposed [37, 41] but with the apical position been occupied by a SeCys ligand.

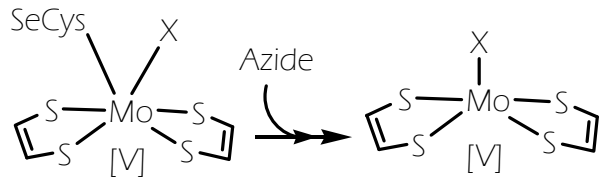

Formate species *2.094* species

(a) (b)

Figure II.4.6 Proposed coordination around Mo(V) centre. (a) Hexacoordinated structure proposed on the basis of EPR data from *Dd* Fdh. (b) Pentacoordinated structure in agreement with re-evaluation of crystallographic data obtained from *E coli* Fdh-H [42].

II.4.4.1.3 Involvement of *formate* and *2.094* species in the reaction mechanism of formate oxidation

Figure II.1.11 shows the two proposed reaction mechanisms for *Ec* Fdh-H. The mechanism in black was proposed by Khangulov *et al* [37, 41], in which the *2.094* species is the intermediate in the reoxidation from Mo(IV) to Mo(VI) [37]. The mechanism in red is a new proposal by Raaijmakers and Romão [42] from the reevaluation of the X-Ray data.

The data now collected for *Dd* Fdh demonstrate that the *2.094* species is detected because of the presence of azide (or cyanide) in the protein solution and hence its detection in *Ec* Fdh-H is due to the enzyme needs to be purified in the presence of azide to preserve inactivation by oxygen [85]. In contrast, *Dd* Fdh, like other formate dehydrogenases from sulphate reducing bacteria that can be purified under aerobic conditions without loss of activity, yields the distinct *formate* signal on formate reduction. In this context, the *formate* signal detected in *Dd* Fdh could be also considered as a potential reaction intermediate.

In contrast to any unspecific reductant (e.g. dithionite), formate, the natural substrate of the enzyme, is a specific reductant of Fdhs. For example, formate cannot reduce benzyl viologen like dithionite, as well as cannot reduce Mo-containing enzymes of the same family, e.g. nitrate reductases. It means that the reduction of the enzyme by formate must be driven by a specific reaction and its reducing effect must necessarily be accomplished through an interaction between the formate and the Mo active site. Under these conditions, the electrons given to the enzyme by formate are distributed along the electron transfer pathway according to their relative values of redox potentials. Furthermore, as discussed above, both the *2.094* and *formate* species do not correspond to a substrate-bound forms, and hence they should correspond to Mo(V) species obtained after CO_2 release. Given the above, it is evident that both *formate* and *2.094* species are produced by the specific interaction of the enzyme with substrate. However, whether they correspond to a reaction intermediate or to Mo(V) species in equilibrium with Mo(VI) and

Mo(IV) cannot be concluded with the present data and additional work is necessary to elucidate this point. In any case, these results show that EPR properties of the Mo(V) ions depend on the preparation of the sample and hence their structures. The presence of reduced species showing pyramidal coordination seem to depend on the presence of azide (or cyanide) in the medium whereas hexacoordianted ones are obtained without inhibitors. These results are supported by EXAFS data taken in dithionite reduced *Dd* Fdh (Figure II.1.6, [53]) which showed hexacoordianted Mo sites. Unfortunately, none of these studies were carried out using formate as reductant. This experiment could be useful to clarify this hypothesis.

II.4.3.2 The [4Fe-4S] clusters

The analysis of the amino acid sequence shows that the large subunit of *Dd* Fdh contains one [4Fe-4S] cluster, whereas the β-subunit contains three additional centres of the same type. This cluster composition seems to be conseved in other closely related Fdhs from sulphate reducing bacteria [10]. All these centres are aligned along an electron transfer zig-zag pathway. Nevertheless, spin quantification by EPR taking into account the protein concentration yields 2 spins/protein. This suggests that only two iron sulphur clusters are in the $[4Fe\text{-}4S]^{1+}$ (s=1/2) reduced form whereas two are in the diamagnetic $[4Fe\text{-}4S]^{2+}$ redox state. However, taking into account the iron content (15 Fe/protein) and considering that the haemic iron was determined to be 4 Fe/protein [52], it is evident that the protein lose some Fe from [4Fe-4S] centres during purification. Recalculation of the spin concentration of the spectra at 40 K and 20 K taking into account this facts yields 4 spins/protein and 2 spins/protein, respectively. This would indicates that the four FeS centres are in the $[4Fe\text{-}4S]^{1+}$ reduced form. In summary, there are 4 FeS centres of which two should give the FeS I signal and the remaining two the FeS II signal. Similar results were obtained in the closely related *D. gigas* Fdh [39, 40]

II.5 References

1. Hille R, *The Mononuclear Molybdenum Enzymes*. Chem Rev, 1996. 96(7): p. 2757-2816.
2. Johnson MK, C. RD, and Adams MW, *Tungstoenzymes*. Chem. Rev., 1996. 96: p. 2817-2840.
3. Moriwaki Y, Yamamoto T, and Higashino K, *Distribution and pathophysiologic role of molybdenum-containing enzymes*. Histol Histopathol, 1997. 12(2): p. 513-524.
4. Zumft WG, *Cell biology and molecular basis of denitrification*. Microbiol. Mol. Biol. Rev., 1997. 61(4): p. 533-616.
5. Hamilton WA, *Microbially influenced corrosion as a model system for the study of metal microbe interactions: a unifying electron transfer hypothesis*. Biofouling, 2003. 19(1): p. 65-76.
6. Einsle O, Tezcan FA, Andrade SLA, Schmid B, Yoshida M, Howard JB, and Rees DC, *Nitrogenase MoFe-Protein at 1.16 A Resolution: A Central Ligand in the FeMo-Cofactor*. Science, 2002. 297(5587): p. 1696-1700.
7. Dobbek H, Gremer L, Kiefersauer R, Huber R, and Meyer O, *Catalysis at a dinuclear [CuSMo(==O)OH] cluster in a CO dehydrogenase resolved at 1.1-A resolution*. PNAS, 2002. 99(25): p. 15971-15976.
8. Romao MJ, Knablein J, Huber R, and Moura JJ, *Structure and function of molybdopterin containing enzymes*. Prog Biophys Mol Biol, 1997. 68(2-3): p. 121-144.
9. Romao MJ and Huber R, *Structure and function of the xanthineoxidase family of molybdenum enzymes*. Springer-Verlag ed. in Metal Sites in Proteins and ModelssRedox Centers, Structure and Bonding. Vol. 90. 1998, Berlin, Germany. 69-96.
10. Moura JJ, Brondino CD, Trincao J, and Romao MJ, *Mo and W bis-MGD enzymes: nitrate reductases and formate dehydrogenases*. J Biol Inorg Chem, 2004. 9(7): p. 791-799.
11. Romao MJ, Cunha CA, Brondino CD, and Moura JJ. ed. MIB Syst. Vol. 39. 2002. 539-570.
12. Bursakov SA, Gavel OY, Di Rocco G, Lampreia J, Calvete J, Pereira AS, Moura JJ, and Moura I, *Antagonists Mo and Cu in a heterometallic cluster present on a novel protein (orange protein) isolated from Desulfovibrio gigas*. J Inorg Biochem, 2004. 98(5): p. 833-840.
13. Fenske D, Gnida M, Schneider K, Meyer-Klaucke W, Schemberg J, Henschel V, Meyer AK, Knochel A, and Muller A, *A new type of metalloprotein: The Mo storage protein from azotobacter vinelandii contains a polynuclear molybdenum-oxide cluster*. Chembiochem, 2005. 6(2): p. 405-413.
14. Ferry JG, *Formate dehydrogenase*. FEMS Microbiol Rev, 1990. 7(3-4): p. 377-382.
15. Maden BE, *Tetrahydrofolate and tetrahydromethanopterin compared: functionally distinct carriers in C1 metabolism*. Biochem J, 2000. 350 Pt 3: p. 609-629.
16. Richardson DJ, *Bacterial respiration: a flexible process for a changing environment*. Microbiology, 2000. 146(3): p. 551-571.
17. Unden G and Bongaerts J, *Alternative respiratory pathways of Escherichia coli: energetics and transcriptional regulation in response to electron acceptors*. Biochim Biophys Acta, 1997. 1320(3): p. 217-234.

18. Böck A and Thanbichler M, *EcoSal-Escherichia coli and Salmonella*. in Cellular and Molecular Biology, ed. R Curtiss. Vol. 3.6.1.1. 2004, Washington, D.C.: ASM Press.

19. Sawers RG and Clark DP, *EcoSal–Escherichia coli and Salmonella*. in Cellular and Molecular Biology, ed. I Curtiss, R. 2004, Washington, D.C.: ASM Press.

20. Berg BL, Li J, Heider J, and Stewart V, *Nitrate-inducible formate dehydrogenase in Escherichia coli K-12. I. Nucleotide sequence of the fdnGHI operon and evidence that opal (UGA) encodes selenocysteine*. J. Biol. Chem., 1991. 266(33): p. 22380-22385.

21. Enoch HG and Lester RL, *The purification and properties of formate dehydrogenase and nitrate reductase from Escherichia coli*. J. Biol. Chem., 1975. 250(17): p. 6693-6705.

22. Richardson D and Sawers G, *STRUCTURAL BIOLOGY: PMF Through the Redox Loop*. Science, 2002. 295(5561): p. 1842-1843.

23. Jormakka M, Byrne B, and Iwata S, *Formate dehydrogenase–a versatile enzyme in changing environments*. Curr Opin Struct Biol, 2003. 13(4): p. 418-423.

24. Jormakka M, Byrne B, and Iwata S, *Proton motive force generation by a redox loop mechanism*. FEBS Lett, 2003. 545(1): p. 25-30.

25. Sawers G, Heider J, Zehelein E, and Bock A, *Expression and operon structure of the sel genes of Escherichia coli and identification of a third selenium-containing formate dehydrogenase isoenzyme*. J. Bacteriol., 1991. 173(16): p. 4983-4993.

26. Sawers RG, Ballantine SP, and Boxer DH, *Differential expression of hydrogenase isoenzymes in Escherichia coli K-12: evidence for a third isoenzyme*. J. Bacteriol., 1985. 164(3): p. 1324-1331.

27. Zinoni F, Birkmann A, Stadtman TC, and Bock A, *Nucleotide Sequence and Expression of the Selenocysteine-Containing Polypeptide of Formate Dehydrogenase (Formate-hydrogen-lyase-Linked) from Escherichia coli*. PNAS, 1986. 83(13): p. 4650-4654.

28. Sawers RG, *Formate and its role in hydrogen production in Escherichia coli*. Biochem Soc Trans, 2005. 33(Pt 1): p. 42-46.

29. Heidelberg JF, *et al.*, *The genome sequence of the anaerobic, sulfate-reducing bacterium Desulfovibrio vulgaris Hildenborough*. Nat Biotechnol, 2004. 22(5): p. 554-559.

30. Friedebold J and Bowien B, *Physiological and biochemical characterization of the soluble formate dehydrogenase, a molybdoenzyme from Alcaligenes eutrophus*. J. Bacteriol., 1993. 175(15): p. 4719-4728.

31. Jollie DR and Lipscomb JD, *Formate dehydrogenase from Methylosinus trichosporium OB3b. Purification and spectroscopic characterization of the cofactors*. J. Biol. Chem., 1991. 266(32): p. 21853-21863.

32. Karzanov VV, Bogatsky Yu A, Tishkov VI, and Egorov AM, *Evidence for the presence of a new NAD+-dependent formate dehydrogenase in Pseudomonas sp. 101 cells grown on a molybdenum-containing medium*. FEMS Microbiol Lett, 1989. 51(1): p. 197-200.

33. Chistoserdova L, Laukel M, Portais J-C, Vorholt JA, and Lidstrom ME, *Multiple Formate Dehydrogenase Enzymes in the Facultative Methylotroph Methylobacterium extorquens AM1 Are Dispensable for Growth on Methanol.* J. Bacteriol., **2004**. 186(1): p. 22-28.

34. Laukel M, Chistoserdova L, Lidstrom ME, and Vorholt JA, *The tungsten-containing formate dehydrogenase from Methylobacterium extorquens AM1: Purification and properties.* Eur. J. Biochem., **2003**. 270(2): p. 325-333.

35. Brondino CD, Rivas MG, Romão MJ, Moura JJG, and Moura I, *Structural and Electron Paramagnetic Resonance (EPR) Studies of Mononuclear Molybdenum Enzymes from Sulfate-Reducing Bacteria.* Acc. Chem. Res., **2006**: 39(10): p. 788-96.

36. Hagen WR and Arendsen AF, *The Bio-Inorganic Chemistry of Tungsten.* Structure and Bonding, **1998**. 90: p. 161-192.

37. Boyington JC, Gladyshev VN, Khangulov SV, Stadtman TC, and Sun PD, *Crystal Structure of Formate Dehydrogenase H: Catalysis Involving Mo, Molybdopterin, Selenocysteine, and an Fe4S4 Cluster.* Science, **1997**. 275(5304): p. 1305-1308.

38. Jormakka M, Tornroth S, Byrne B, and Iwata S, *Molecular Basis of Proton Motive Force Generation: Structure of Formate Dehydrogenase-N.* Science, **2002**. 295(5561): p. 1863-1868.

39. Raaijmakers H, Teixeira S, Dias JM, Almendra MJ, Brondino CD, Moura I, Moura JJ, and Romao MJ, *Tungsten-containing formate dehydrogenase from Desulfovibrio gigas: metal identification and preliminary structural data by multi-wavelength crystallography.* J Biol Inorg Chem, **2001**. 6(4): p. 398-404.

40. Raaijmakers H, Macieira S, Dias JM, Teixeira S, Bursakov S, Huber R, Moura JJ, Moura I, and Romao MJ, *Gene sequence and the 1.8 A crystal structure of the tungsten-containing formate dehydrogenase from Desulfovibrio gigas.* Structure, **2002**. 10(9): p. 1261-1272.

41. Khangulov SV, Gladyshev VN, Dismukes GC, and Stadtman TC, *Selenium-containing formate dehydrogenase H from Escherichia coli: a molybdopterin enzyme that catalyzes formate oxidation without oxygen transfer.* Biochemistry, **1998**. 37(10): p. 3518-3528.

42. Raaijmakers HC and Romao MJ, *Formate-reduced E. coli formate dehydrogenase H: the reinterpretation of the crystal structure suggests a new reaction mechanism.* J Biol Inorg Chem, **2006**. 11(7): p. 849-854.

43. Almendra MJ, Brondino CD, Gavel O, Pereira AS, Tavares P, Bursakov S, Duarte R, Caldeira J, Moura JJ, and Moura I, *Purification and characterization of a tungsten-containing formate dehydrogenase from Desulfovibrio gigas.* Biochemistry, **1999**. 38(49): p. 16366-16372.

44. Berks BC, *A common export pathway for proteins binding complex redox cofactors?* Mol Microbiol, **1996**. 22(3): p. 393-404.

45. Rodrigue A, Chanal A, Beck K, Muller M, and Wu L-F, *Co-translocation of a Periplasmic Enzyme Complex by a Hitchhiker Mechanism through the Bacterial Tat Pathway.* J. Biol. Chem., **1999**. 274(19): p. 13223-13228.

46. Dias JM, Than ME, Humm A, Huber R, Bourenkov GP, Bartunik HD, Bursakov S, Calvete J, Caldeira J, Carneiro C, Moura JJ, Moura I, and Romao MJ, *Crystal structure of the first dissimilatory nitrate reductase at 1.9 A solved by MAD methods*. Structure, **1999**. 7(1): p. 65-79.

47. Sebban C, Blanchard L, Bruschi M, and Guerlesquin F, *Purification and characterization of the formate dehydrogenase from Desulfovibrio vulgaris Hildenborough*. FEMS Microbiol Lett, **1995**. 133(1-2): p. 143-149.

48. Czjzek M, Payan F, Guerlesquin F, Bruschi M, and Haser R, *Crystal structure of cytochrome c3 from Desulfovibrio desulfuricans Norway at 1.7 A resolution*. J Mol Biol, **1994**. 243(4): p. 653-667.

49. Sebban-Kreuzer C, Dolla A, and Guerlesquin F, *The formate dehydrogenase-cytochrome c553 complex from Desulfovibrio vulgaris Hildenborough*. Eur J Biochem, **1998**. 253(3): p. 645-652.

50. ElAntak L, Dolla A, Durand MC, Bianco P, and Guerlesquin F, *Role of the tetrahemic subunit in Desulfovibrio vulgaris hildenborough formate dehydrogenase*. Biochemistry, **2005**. 44(45): p. 14828-14834.

51. Brondino CD, Passeggi MC, Caldeira J, Almendra MJ, Feio MJ, Moura JJ, and Moura I, *Incorporation of either molybdenum or tungsten into formate dehydrogenase from Desulfovibrio alaskensis NCIMB 13491; EPR assignment of the proximal iron-sulfur cluster to the pterin cofactor in formate dehydrogenases from sulfate-reducing bacteria*. J Biol Inorg Chem, **2004**. 9(2): p. 145-151.

52. Costa C, Teixeira M, LeGall J, Moura JJG, and Moura I, *Formate dehydrogenase from Desulfovibrio desulfuricans ATCC 27774: Isolation and spectroscopic characterization of the active sites (heme, iron-sulfur centers and molybdenum)*. J. Biol. Inorg. Chem., **1997**. 2: p. 198-208.

53. George GN, Costa C, Moura JJG, and Moura I, *Observation of Ligand-Based Redox Chemistry at the Active Site of a Molybdenum Enzyme*. J. Am. Chem. Soc., **1999**. 121 (11): p. 2625-2626.

54. Axley MJ, Grahame DA, and Stadtman TC, *Escherichia coli formate-hydrogen lyase. Purification and properties of the selenium-dependent formate dehydrogenase component*. J. Biol. Chem., **1990**. 265(30): p. 18213-18218.

55. Berg BL and Stewart V, *Structural Genes for Nitrate-Inducible Formate Dehydrogenase in Escherichia coli K-12*. Genetics, **1990**. 125(4): p. 691-702.

56. Page CC, Moser CC, Chen X, and Dutton PL, *Natural engineering principles of electron tunnelling in biological oxidation-reduction*. Nature, **1999**. 402(6757): p. 47-52.

57. Holm RH, *Metal-centered oxygen atom transfer reactions*. Chem. Rev., **1987**. 87(6): p. 1401-1449.

58. Berks BC, Palmer T, and Sargent F, *The Tat protein translocation pathway and its role in microbial physiology*. Adv Microb Physiol, **2003**. 47: p. 187-254.

59. Mori H and Cline K, *Post-translational protein translocation into thylakoids by the Sec and DeltapH-dependent pathways*. Biochim Biophys Acta, **2001**. 1541(1-2): p. 80-90.

60. DeLisa MP, Tullman D, and Georgiou G, *Folding quality control in the export of proteins by the bacterial twin-arginine translocation pathway*. PNAS, **2003**. 100(10): p. 6115-6120.

61. Stadtman TC, *Selenocysteine*. Annu Rev Biochem, **1996**. 65: p. 83-100.

62. Liu Z, Reches M, Groisman I, and Engelberg-Kulka H, *The nature of the minimal 'selenocysteine insertion sequence' (SECIS) in Escherichia coli*. Nucleic Acids Res., 1998. 26(4): p. 896-902.

63. Zinoni F, Heider J, and Bock A, *Features of the Formate Dehydrogenase mRNA Necessary for Decoding of the UGA Codon as Selenocysteine*. PNAS, 1990. 87(12): p. 4660-4664.

64. Bock A, Forchhammer K, Heider J, Leinfelder W, Sawers G, Veprek B, and Zinoni F, *Selenocysteine: the 21st amino acid*. Mol Microbiol, 1991. 5(3): p. 515-520.

65. Macieira S, *Isolation of the genes of aldehyde oxidoreductase amd formate dehydrogenase and Biochemical characterization of coproporphyrinogen-III oxidase*, in *Chemistry Department*. 2002, New University of Lisbon: Lisbon.

66. Schlindwein C, Giordano G, Santini CL, and Mandrand MA, *Identification and expression of the Escherichia coli fdhD and fdhE genes, which are involved in the formation of respiratory formate dehydrogenase*. J. Bacteriol., 1990. 172(10): p. 6112-6121.

67. Stewart V, Lin JT, and Berg BL, *Genetic evidence that genes fdhD and fdhE do not control synthesis of formate dehydrogenase-N in Escherichia coli K-12*. J. Bacteriol., 1991. 173(14): p. 4417-4423.

68. Peterson GL. in Enzyme Structure, ed. CHW Hirs and SN Timasheff. Vol. I. 1983, New York: Academic Press. 95-119.

69. Laemmli UK, *Cleavage of structural proteins during the assembly of the head of bacteriophage T4*. Nature, 1970. 227(5259): p. 680-685.

70. Blum H, Beier H, and Gross HJ, *Improved silver staining of plant proteins, RNA and DNA in polyacrylamide gels*. Electrophoresis, 1987. 8: p. 93-99.

71. Nilges MJ. 1979, University of Illinois: Urbana, IL.

72. Maurice AM. 1980, University of Illinois: Urbana, IL.

73. Schuler GD, Altschul SF, and Lipman DJ, *A workbench for multiple alignment construction and analysis*. Proteins Struct. Funct. Genet., 1991. 9(3): p. 180-190.

74. Siebert PD, Chenchik A, Kellogg DE, Lukyanov KA, and Lukyanov SA, *An improved PCR method for walking in uncloned genomic DNA*. Nucleic Acids Res., 1995. 23(6): p. 1087-1088.

75. Siebert PD, Chen S, and Kellogg DE, *The Human GenomeWalker DNA Walking Kit: A new PCR for walking in uncloned genomic DNA*, in *CLONOTECHniques*. 1995. p. 1-3.

76. Wilson K, *Preparation of genomic DNA from bacteria*. in Current protocols in molecular biology., ed. FM Ausubel, et al. Vol. 1. 1994, New York, NY: John Wiley & Sons. 2.4.1-2.4.5.

77. Bendtsen JD, Henrik Nielsen H, von Heijne G, and Brunak S, *Improved prediction of signal peptides: SignalP 3.0*. J. Mol. Biol., 2004. 340: p. 783-795.

78. Gasteiger E, Hoogland C, Gattiker A, Duvaud S, Wilkins MR, Appel RD, and Bairoch A, *Protein Identification and Analysis Tools on the ExPASy Server*. in The Proteomics Protocols Handbook, Humana Press, ed. JM Walker. 2005. 571-607.

79. Shagger H and Von Jagow H, *Tricine-sodium dodecyl sulfate-polyacrylamide gel electrophoresis for separation of proteins in the range from 1 to 100 kDa*. Anal. Biochem., 1987. 166: p. 368-379.

80. Stanley NR, Palmer T, and Berks BC, *The Twin Arginine Consensus Motif of Tat Signal Peptides Is Involved in Sec-independent Protein Targeting in Escherichia coli*. J. Biol. Chem., 2000. 275(16): p. 11591-11596.

81. Gladyshev VN, Boyington JC, Khangulov SV, Grahame DA, Stadtman TC, and Sun PD, *Characterization of Crystalline Formate Dehydrogenase H from Escherichia coli*. J. Biol. Chem., 1996. 271(14): p. 8095-8100.

82. Gonzalez PJ, Correia C, Moura I, Brondino CD, and Moura JJ, *Bacterial nitrate reductases: Molecular and biological aspects of nitrate reduction*. J Inorg Biochem, 2006. 100(5-6): p. 1015-1023.

83. ElAntak L, *Analyse Génomique Fonctionnelle par RMN de Cytochromes c_3 de la Bactérie Desulfovibrio vulgaris Hildenborough*. 2004, Université de Provence- Aix Marseille I: Marseille.

84. Cornish-Bowden A, *Fundamentals of Enzyme Kinetics*. 2nd ed. 2001, London: Portland Press.

85. Axley MJ and Grahame DA, *Kinetics for formate dehydrogenase of Escherichia coli formate-hydrogenlyase*. J. Biol. Chem., 1991. 266(21): p. 13731-13736.

86. Blanchard JS and Cleland WW, *Kinetic and chemical mechanisms of yeast formate dehydrogenase*. Biochemistry, 1980. 19(15): p. 3543-3550.

87. Cornish-Bowden A, *A simple graphical method for determining the inhibition constants of mixed, uncompetitive and non-competitive inhibitors*. Biochem J, 1974. 137(1): p. 143-144.

88. Prince RC, Liu C, Morgan TV, and Mortenson LE, *Formate dehydrogenase from Clostridium pasteurianum Electron paramagnetic resonance spectroscopy of the redox active centers*. FEBS Lett, 1985. 189(2): p. 263-266.

89. Barber MJ, May HD, and Ferry JG, *Inactivation of Formate Dehydrogenase from Methanobacterium formicicum by Cyanide*. Biochemistry, 1986(25): p. 8150-8155.

III. Molybdenum-containing proteins from Sulphate Reducing Bacteria: *studying proteins with novel cofactors.*

III.1. INTRODUCTION

Several years ago two Mo- and Fe-containing proteins were isolated from the sulphate reducing bacteria *D. africanus* [1] and *D. salexigens* [2]. Preliminary characterization of these proteins identified molybdenum and iron in both of them. More recently a similar protein was purified from *D. gigas*, which contains Cu in addition to Mo and Fe [3]. At present, the information on these proteins is scarce. These proteins have received the generic name of *Blue* proteins and questions such as the type of metallic cofactors included in their structure and function remain elusive.

The protein isolated from *D. africanus* appears to be a complex multimer of high molecular weight (112 kDa) composed of 10 subunits (11.5 kDa) each one containing labile sulphide, 5-6 molybdenum atoms and approximately 20 iron atoms. The UV-visible spectrum shows peaks at around 615, 410 and 325 nm with a protein peak at 280 nm. The millimolar extinction coefficients at 615, 410 and 280 nm are 48.4, 64.4 and 14, respectively. The protein is composed by 106 amino acid residues per subunit and the N-terminal sequence, which has been determined up to 26 residues, is characterized by its degree of hydrophobicity. The protein isolated from *D. salexigens* has an approximate molecular weight of 110 kDa and is composed by subunits of approximately 13.25 kDa. Three molybdenum and 20 iron atoms are found associated with each subunit. This protein shows an absorption spectrum similar to that observed for the *Blue* protein isolated from *D. africanus*. Finally, the *Blue* protein isolated from *D. gigas* has a molecular weight of approximately 162.5 kDa and is composed by 11-12 identical subunits of 14.75 kDa. Metals analysis shows the presence of 3.8±0.1 Fe/monomer, 0.5±0.1 Mo/monomer, and surprisingly, 0.6±0.1Cu/monomer. The UV-visible spectrum of as-prepared is similar to the absorption spectra described above and the millimolar extinction coefficients were calculated to be 15.1 and 7.8 $mM^{-1}cm^{-1}$ at 400 and 615 nm, respectively. The sequence of

this protein shows an 18.5% homology with a Zn resistance associated protein from *D. vulgaris* Hildenborough.

The work carried out in this part deals with the characterization of two proteins isolated from *D. aminophilus* and *D. alaskensis,* respectively, belonging to the *Blue* proteins family. In addition to the molecular characterization, EXAFS studies of both proteins are reported and discussed in comparison with studies performed the *D. gigas* enzyme. All these results suggest that this family of proteins contains heteronuclear metallic clusters that show no resemblance with other clusters with a well-known function present in biology.

III.2. MATERIALS AND METHODS

III.2.1 Growth media and culture conditions

D. aminophilus and *D. alaskensis* cells were grown at 37°C under anaerobic conditions using the lactate/sulphate and adapted Postgate C, respectively (Table III.2.1).

Table III.2.1 Growth media composition (per litre). Left column: *D. aminophilus* medium. Right column: *D. alaskensis* medium.

Lactate/sulphate medium	Adapted Postgate C medium (supplemented with 45 µM of $Na_2MoO_4.2H_20$)
1.0 g NaCl	25.0 g NaCl
0.4 g $CaCl_2$. 2 H_2O	0.04 g $CaCl_2.2H_2O$
2.0 g Yeast extract	1.0 g Yeast extract
6.0 ml Sodium lactate 60% (w/v)	4.615 ml Sodium lactate 60% (w/v)
2.8 g Na_2SO_4	4.5 g Na_2SO_4
1.0 g NH_4Cl	1.0 g NH_4Cl
0.5 g K_2HPO_4	0.5 g KH_2PO_4
0.06 g $FeCl_2$. 4 H_2O	0.004 g $FeSO_4.7$ H_2O
0.4 g $MgCl_2$. 6 H_2O	0.06 g $MgSO_4.7H_2O$
0.5 g KCl	0.3 g Sodium Citrate.$2H_2O$
0.5 g Na_2S	
1.0 ml Widdel solution [4]	
The pH was adjusted to7.2	The pH was adjusted to 7.5.

III.2.2 Purification procedures

All the purification procedures carried out to isolate *Blue* protein from both organisms were performed aerobically at 4°C and pH 7.6. The purity of protein after each step was followed by electronic absorption spectrum and 15% tricine SDS-PAGE [5, 6].

In a typical preparation, 400 g (wet weight) of *D. aminophilus* cells were suspended in 10 mM Tris-HCl buffer and passed through a Manton Gaulin press at 9000 psi. Then, protease inhibitor cocktail (1 tablete/50 ml of Complete EDTA-free inhibitor from Roche) and DNAse were added. A cell-free extract was obtained by centrifugation of the cellular suspension at 16000 x g for 60 min, then the pellet was discarded and the supernatant was ultra-centrifuged at 180000g for 30 min to remove any membrane contamination. A clear supernatant containing soluble proteins (soluble extract) was dialyzed against 10 mM Tris-HCl overnight and loaded onto a DEAE-52 column equilibrated with 10 mM Tris-HCl. A linear Tris-HCl gradient (10-250 mM) was applied with a total volume of 2l. The fraction containing *Blue* protein was collected at an ionic strength of 100-150 mM. This fraction was then loaded onto a hydroxyapatite (HTP) column, equilibrated with 100 mM Tris-HCl and *Blue* protein was eluted at 450 mM potassium phosphate buffer (1-500 mM K_2HPO_4/KH_2PO_4 gradient). In the last step, the fraction was concentrated in a Diaflow apparatus with YM10 membrane and loaded onto a Superdex 200 gel filtration column equilibrated with 300 mM Tris-HCl. Pure *Blue* Protein was eluted with the same buffer a flow rate of 2 ml/min in the second peak. A global purification scheme is shown in Figure III.2.1.

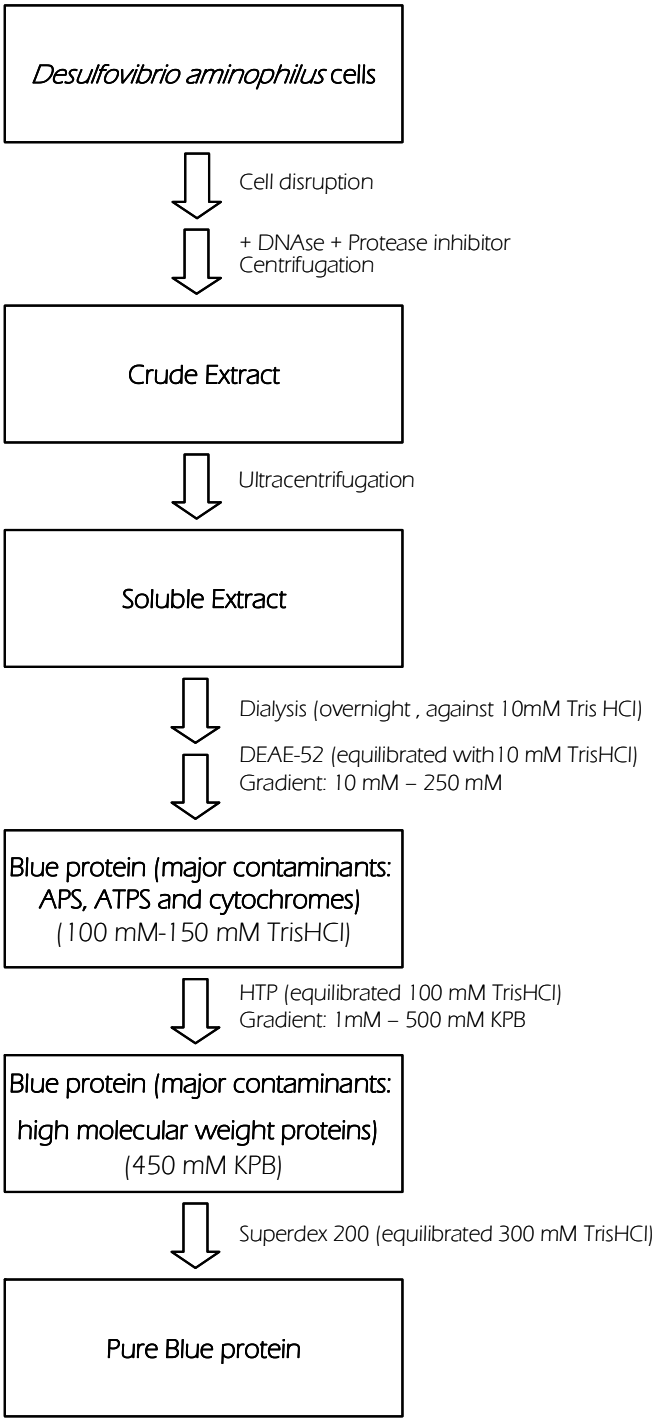

Figure III.2.1 Purification scheme of *Blue* protein from *Desulfovibrio aminophilus*.

D. alaskensis cells were collected at the end of logarithmic phase by centrifugation at 8000 × *g* during 15 min at 4 °C (Beckman Avanti^{TM} J-25 centrifuge). Periplasmic fraction was obtained following protocol described by Brondino *et al* [7]. Briefly, pellet of cells was resuspended in 10 mM Tris-HCl buffer (10ml buffer/g cell) containing deoxyribonuclease

and ribonuclease and incubated during 1 hour at 4ºC. All cell-free extract was obtained by centrifugation of the cellular suspension at 5000 × *g* for 40 min. The supernatant containing mostly periplasmic proteins was collected and dialyzed overnight against 10 mM Tris-HCl. Periplasmic fraction was loaded onto an anionic exchange column (DEAE 52 cellulose, Whatman 5×45 cm) equilibrated with 10 mM Tris-HCl. *Blue* protein fraction containing mainly haemic contaminants was collected in the flowthrough. The next step was performed on HTP column equilibrated with 10 mM Tris-HCl. Proteins were eluted using a KH_2PO_4/K_2HPO_4 buffer gradient (5-500 mM); the fraction containing pure *Blue* protein was collected at 150 mM ionic strength. Figure III.2.2 shows a general scheme of the purification procedure described above.

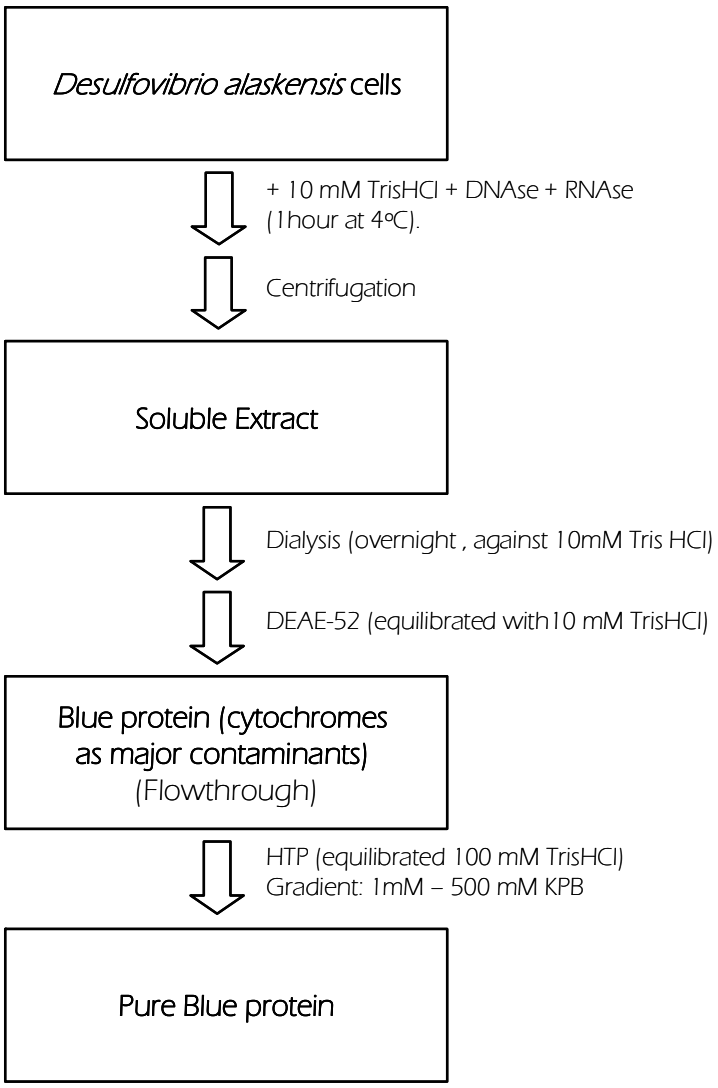

Figure III.2.2 Purification scheme of *Desulfovibrio alaskensis Blue* protein.

III.2.3 Protein and Metal quantification

Quantification of metals and protein concentration were carried out as described in section II.2.2.

Mo, Cu and Fe were quantified by inductively coupled plasma emission analysis in a Jobin-Yvon (Ultima) instrument using the Reagecom 23 ICP multielements as standard solution in a concentration range of 0.05 to 1.5 ppm.

The valence state of Cu ions was determined by a modified version of the Hanna *et al.* method [8, 9] which is a simple colorimetric test to measure Cu(I) in proteins. Briefly, samples or standard solutions (100 µl) were reduced by adding 300 µl of 20 mM sodium ascorbate (in 0.1 M sodium phosphate, pH 6.0), and incubated for 10 min. Another sample was prepared without addition of reductant. Then, 600 µl of a 2,2' – biquinoline solution (0.5 mg/ml), prepared in glacial acetic acid, was added, and the solution was incubated for 10 min prior to measure absorbance at 546 nm. The calibration curve was prepared with copper (II) acetate (0 to 48 µM Cu (II) acetate).

III.2.4 Molecular mass determination and subunit composition

The molecular mass of the as-prepared *Blue* protein and the subunit composition were determined as described in section II.2.3.

Molecular weight of *Blue* protein subunits was determined using a matrix-assisted laser desorption/ionization time-of-flight (MALDI-TOF) mass spectrometer. A volume of 10 µl of salt free sample (approximately 10 pmol of protein) was mixed with 10 µl of matrix solution (10 mg of α-CHCA dissolved in 1 ml of H_2O/acetonitrile/TFA). Then, 1µl of sample was spotted on the 100 well MALDI-TOF-MS sample plate and dried on air.

The molecular weight was then analyzed by MALDI-TOF mass spectrometer (Applied Byosystems, Foster City, USA) model voyager DE-PRO biospectrometry workstation, equipped with a nitrogen laser radiating at 337 nm. MALDI mass spectra were acquired as recommended by the manufacturer. Measurements were taken in reflector positive ion mode, with a 20 kV accelerating voltage. Three close external calibrations were performed

with the monoisotopic peaks of 16952, and 12361 m/z corresponding to apomyoglobin, and cytochrome *C* respectively. Mass spectral analysis for each sample was based on the average of 300 laser shots.

Mass spectrometry acquisition and data analysis were performed in collaboration with Prof. JJ Calvete (IBV, Valencia, Spain) and Prof. JL Capelo-Martinez (FCT-UNL, Caparica, Portugal).

III.2.5 Quantification of labile sulphide

Labile sulphide was determined according to the modified method of Fogo [10]. Briefly, 600 µl of 1% zinc acetate and 50 µl of 7% sodium hydroxide were added to 50 µl of sample and incubated during 2.5 hours at room temperature. After centrifugation, 150 µl of 0.1% N,N-dimethylenephenylenediamine hydrochloride in 5M of HCl and 150 µl of 10 mM ferric chloride in 1M of HCl were added to each tube and vigorously vortexing. Finally, the samples were incubated during 1 hour and the absorbance was determined at 670 nm. The tubes were stoppered and open only for the time necessary for each addition of reagents.

III.2.6 Determination of N-terminal and internal amino acid sequences

N-terminal sequence from both proteins was determined by automated Edman degradation in an Applied Biosystem model 477A protein sequencer coupled to an Applied Biosystem 120 analyzer following the manufacturer's instructions. A total of approximately 1 nmol of *Blue* protein was used.

Proteolytic digestion of *Blue* protein from *D. aminophilus* was performed during 16 hours at 37 ºC. Degradation with endoproteinase Lys-C was carried out at an enzyme to substrate ratio 1:50 in 25 mM Tris-HCl buffer pH 8.5 and 1 mM EDTA. Cleavage with Asp-N was performed at an enzyme to substrate ratio 1:75 in 25 mM Tris-HCl buffer pH 8.5. For cleavage of Met-Xaa bonds, a small crystal of CNBr was dissolved in a protein solution (25 mg/ml in 70% formic acid) and the mixture was incubated 8 hours at room temperature.

Peptides were separated using a reverse-phase HPLC on Lichrosorber RP-18 (Merck) column (25 x 0.4 cm, C18, 5 mm particle size) and eluted at 1 ml/min with a linear gradient of 0.1% (v/v) trifluoroacetic acid in water (solution A) and acetonitrile (solution B) (0% A-70% B during 2 hours). Detection was performed at 220 nm. Peaks were collected manually and dried in a Speed-Vac (Savant, Holbrook NY, USA). The *D. aminophilus* subunits were separated as described in section II.2.8 and using a reverse-phase HPLC column. Peptides and isolated subunits were sequenced as described above. To perform in-gel enzymatic digestion *Blue* protein was loaded in 15% SDS gel and the protein bands was excised and digested with chymotrypsin using a ProGest digestor (Genomic Solutions, Chelmsford, MA, USA) following the manufacture's instructions. The peptide mixture was dried and a SpeedVac (Savant, Holbrook, NY, USA). Digests were analyzed using an Applied Biosystems Voyager-DE Pro MALDI-TOF mass spectrometer.

Studies on *D. aminophilus Blue* protein were performed at the Laboratory of Prof. JJ Calvete (IBV, Valencia, Spain). Sequencing of N-terminal of the *D. alaskensis Blue* protein was carried out in collaboration with Prof. J Lampreia (FCT-UNL, Caparica, Portugal).

III.2.7 DNA sequencing strategies

III.2.7.1 *Desulfovibrio aminophilus Blue* Protein DNA sequencing

Two different strategies were used to amplify the DNA sequence coding *Blue* protein: multiplex and inverse PCR.

Multiplex PCR [11, 12] uses a combination of several different pairs of primers in the same amplification reaction. Primer sequences and annealing temperatures are described in Table III.2.2. The DNA used as template (100ng and 200ng) was purified using the phenol-chloroform extraction protocol [13].

Inverse PCR [14] was used for amplification of DNA sequences that flank the region of the known sequence. Genomic DNA (1 µg) was digested by the endonuclease Eco130I from Fermentas (40 units of enzyme, during 2 hours at 37ºC) using the buffer supplied by

the restriction enzyme in a final volume of 50 µl. The endonuclease was inactivated by 20 min incubation at 65ºC. Then, fragments were circularized using T4 DNA ligase in final volume of 500 µl (2.5 units of T4 DNA ligase from Invitrogen, 2 hours at room temperature). Under low DNA concentration, self-ligation is induced giving a circular DNA product. After ligation reaction, DNA was purified by precipitation using 70% of ethanol and centrifuged during 10 min at 14000 rpm. The DNA was resuspended and digested by an endonuclease known to cut once within the known internal sequence (10 units of CaiI from Fermentas, in a final volume of 10 µl, during 2 hours at 37ºC). This gave a linear product with known terminal sequences, suitable for PCR. The primers used in the amplification reaction were designed pointing away from the recognition site of the second restriction enzyme. Primers sequences and annealing temperatures are described in Table III.2.2.

Amplification reactions were loaded using the PCR mixture and programmes described in first strategy described at section II.2.7.2.

The DNA fragments were isolated, cloned, sequenced, and analyzed following the procedures described in II.2.7.2, II.2.7.3 and II.2.7.4.

Table III.2.2 Primers used in *Desulfovibrio aminophilus Blue* protein sequencing

Primer Name	Orientation	Sequence	Tm (° C)	Method	Product fragment size (bp)
NTer2	Forward	G P G P/H G M ggy ccb ggy cmb ggy atg			
Ctp14	Reverse	L F D Q G E A cts ttc gay cag ggy gar gc	56	multiplex PCR	255
LysTrp	Reverse	E H R K A V ag cac cgc aag gcc gt			
LysC2	Forward	A E L D A V g gcb gar cts gay gcb gt			
CNBr21	Reverse	G H G Y G H G ggy cay ggy tay ggy cay gg	54	multiplex PCR	300
CNBr25	Reverse	G P G G G M ggy ccb ggy ggy ggy atg			
AB1d1	Forward	V E R Q Q S P D L N gtt gag cgt cag cag agc ccg gac ctg aa	68	iPCR	218
AB1u1	Reverse	D K L F A E H K ac aag ctc ttc gcc gag cac cgca			

III.2.7.2 *Desulfovibrio alaskensis Blue* Protein DNA sequencing

Since the N-terminal *D. alaskensis Blue* protein showed to be highly homologous to the Zinc Resistance-associated Protein from *D. desulfuricans* G20, two primers were designed from known proteins sequence upstream (PAS) and downstream (Ribonucleotido Reductase, large subunit) to the homologous protein (Table III.2.3). Direct PCR of boiled cell, amplification reactions, PCR mixture and programmes were performed as described section II.2.7.2 (first strategy). The amplified DNA fragments were isolated, cloned, sequenced, and analyzed following the procedures described in sections II.2.7.2, II.2.7.3 and II.2.7.4.

Table III.2.3 Primers used in the sequencing of *Desulfovibrio alaskensis Blue* protein.

Primer Name	Orientation	Sequence (5'-3')	Tm (° C)	Product fragment size (bp)
DalaF1blue	Forward	CCTTACGGACACGGATACG	55	400
DalaR1blue	Reverse	CACCCATATGGTAGCCG		
Ddg20f2pas	Forward	CGATATTGCTTCATGTGCGTGTATGG	66	1000
Ddg20Rrr	Reverse	CGATGTCATCAGGTCGTAAAATTCACG		

III.2.8 EXAFS data collection and analysis

EXAFS measurements were conducted at the Stanford Synchrotron Radiation Laboratory in collaboration with Prof. Graham N. George (University of Saskatchewan, Canada)

Samples analyzed were in a concentration of approximately 1 mM Cu, Mo or Fe. During data collection, the samples were maintained at a temperature of approximately 10 K using an Oxford instruments liquid helium flow cryostat.

III.3 RESULTS

III.3.1. Protein purification

Blue protein from *D. aminophilus* was purified by a three purification step procedure. The protein bound weakly to the first column, (anionic exchange chromatography) which is in agreement with the high pI calculated from its sequence (9.64). The major contaminants after this step were ATP sulphurylase, APS reductase and heme containing proteins. *Blue* protein bound tightly to the second chromatographic column (HTP) and eluted at 400 mM phosphate buffer. Finally, the protein was obtained pure, as judged by SDS-PAGE, by molecular exclusion chromatography (Superdex 200).

The electrophoretic pattern shows two bands separated by approximately 2 KDa (Figure III.3.1a). UV-visible spectrum of pure protein shows three characteristic bands at 320 nm, 409 nm and 615 nm and an A_{280}/A_{615} ratio of 3.4 (Figure III.3.1b).

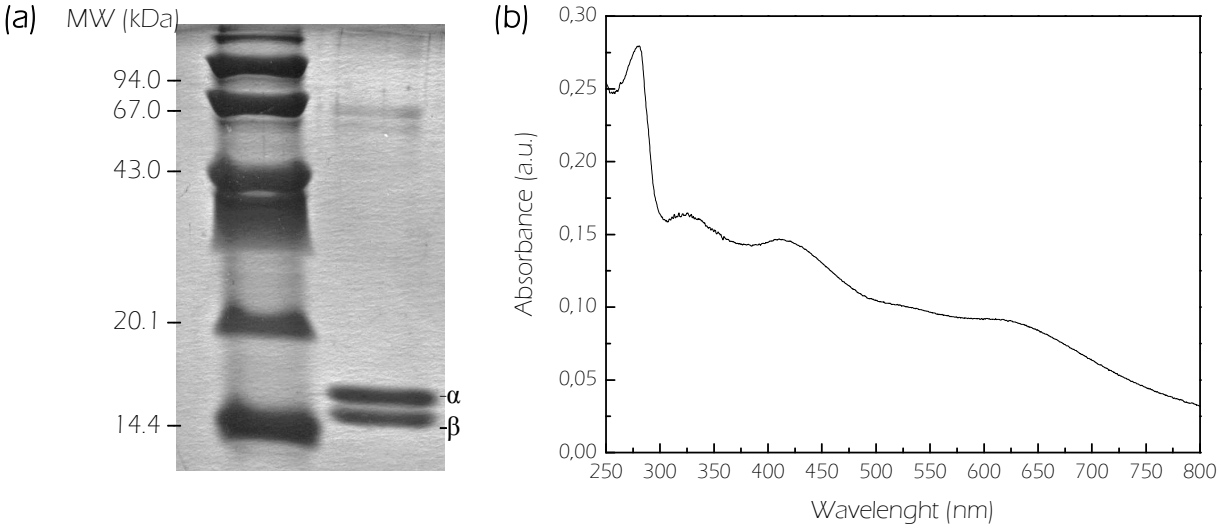

Figure III.3.1 Electrophoretic pattern (a) and UV-visible spectra (b) of pure *Blue* Protein from *Desulfovibrio aminophilus*.

Blue protein from *D. alaskensis* was purified using a two step purification protocol. As expected from its high pI (9.24), this protein was not absorbed by the anionic exchange column DEAE 52. UV-visible spectrum of this fraction revealed the presence of mainly

proteins containing hemes which were isolated by a HTP column. As judge by SDS-PAGE, the protein was in a high purity grade after this step (Figure III.3.2a). The as-prepared protein from *D. alaskensis* shows three characteristic peaks at 320 nm, 409 nm and 570 nm. The peak observed at 409 nm is increased by a cytochromic contaminant. The A_{280}/A_{570} ratio for the pure protein was 3.5 (Figure III.3.2b).

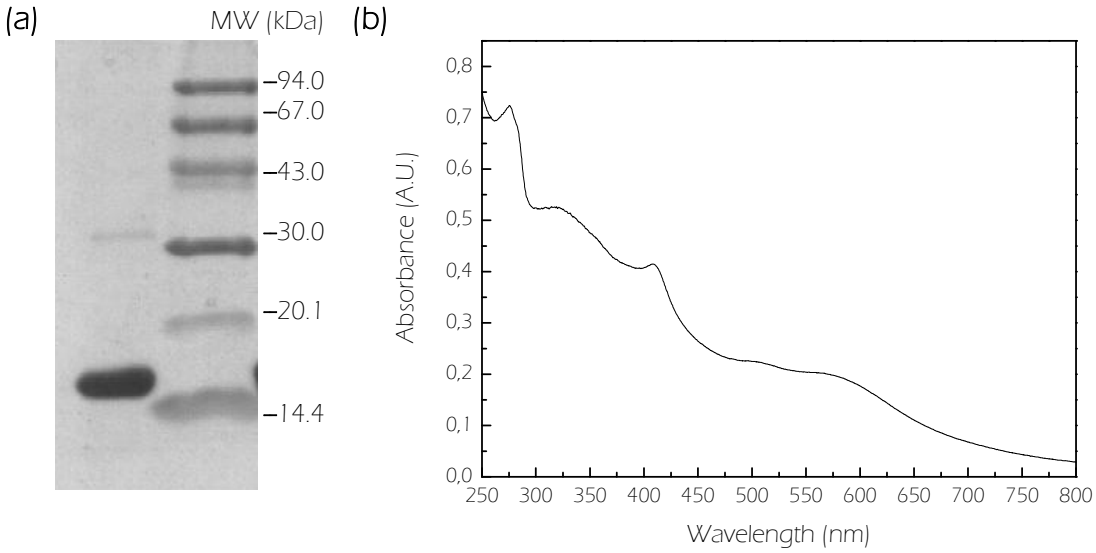

Figure III.3.2 Electrophoretic pattern (a) and UV-visible spectra (b) of pure *Blue* Protein from *Desulfovibrio alaskensis*.

III.3.2. Determination of molar extinction coefficients

The extinction coefficients calculated for the *Blue* proteins from *D. aminophilus* and *D. alaskensis* in Tris-HCl 50 mM pH 7.6 are listed in Table III.3.1.

Table III.3.1 Extinction coefficients for *Blue* Proteins from *Desulfovibrio aminophilus* and *Desulfovibrio alaskensis*. Values in M^{-1} cm^{-1}

	ε_{275}	ε_{320}	ε_{615}	ε_{570}
D.alaskensis	18730	12812		4999
D.aminophilus	21538	10607	6720	

III.3.3 Molecular weight determination

In order to determine the *D. aminophilus Blue* protein molecular weight, a first approach was performed by using SDS-PAGE. The calculated values for the two bands observed (13.7±1.2 and 15.5±1.2 kDa, Figure III.3.1a) are in agreement with those obtained by mass spectrometry (13.5 and 15.4 kDa, Figure III.3.3). A single elution peak of approximately 200 kDa was found by gel-exclusion chromatography on Superdex 200 indicating that *Blue* Protein is a multimer of 14-16 subunits.

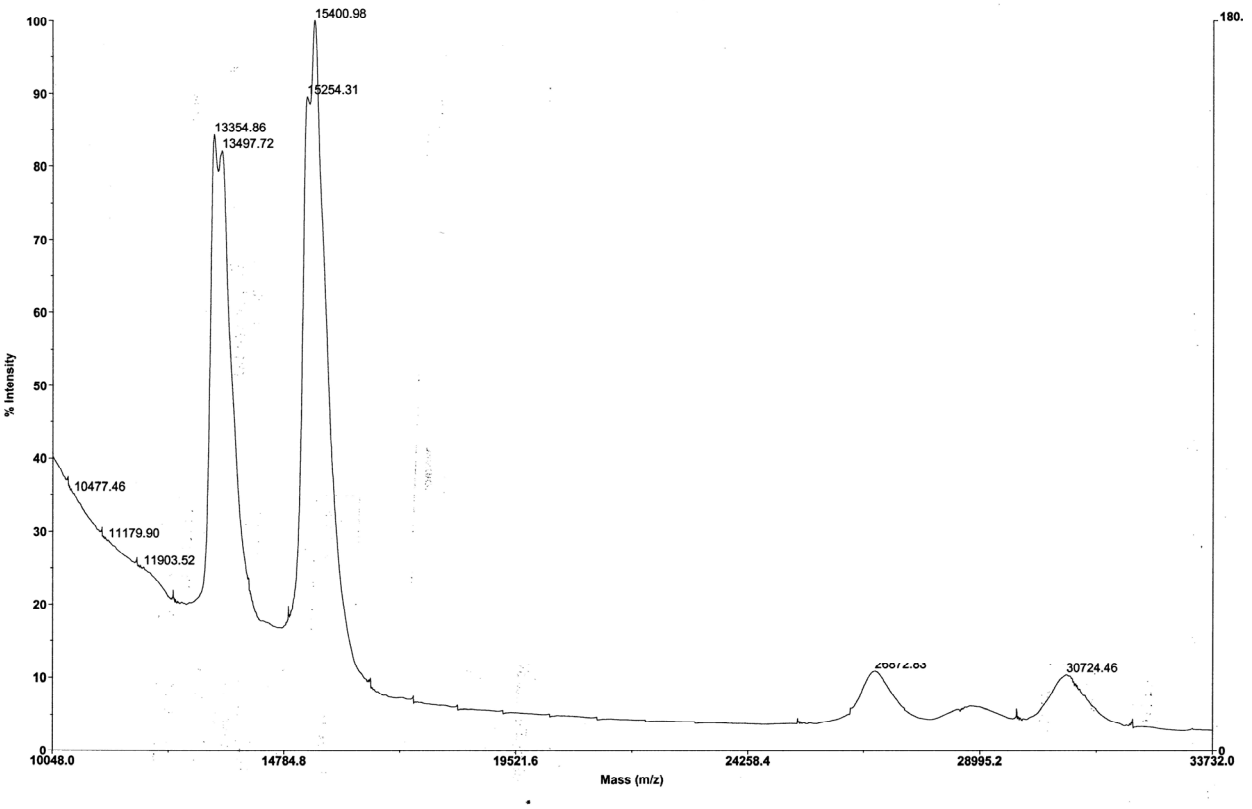

Figure III.3.3 Mass spectra of *Blue* Protein from *Desulfovibrio aminophilus*.

The molecular weight of *D. alaskensis Blue* protein determined by mass spectrometry (MALDI-TOF) analysis was 15.30 kDa (Figure III.3.4). In agreement with this result, the molecular weight of the protein determined by SDS-PAGE was 15.4±1.3 kDa (Figure III.3.2a).

A peak of approximately 260.2 kDa was found by gel-exclusion chromatography on a Superdex 200 column. Therefore, it is likely that the as-prepared protein is a multimer of approximately 16 identical subunits.

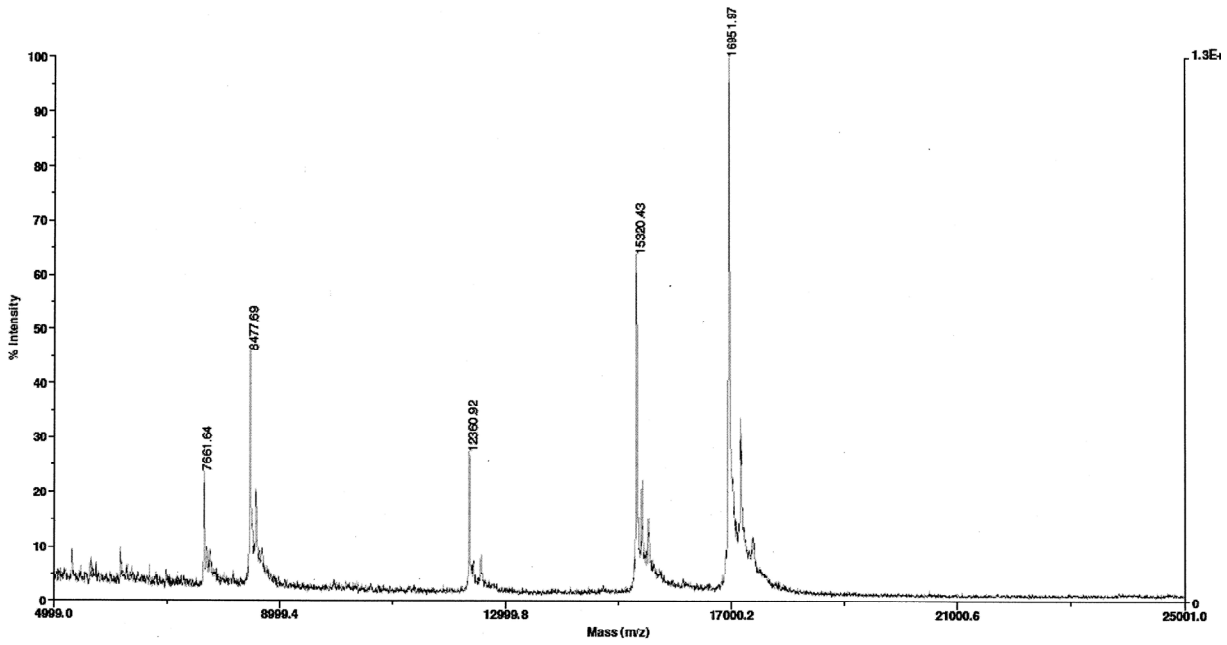

Figure III.3.4 MALDI spectra of *Desulfovibrio alaskensis Blue* Protein. Peaks at 16.95 and 12.36 kDa correspond to apomyoglobin and cytochrome *c* used for internal calibration.

III.3.4 Metal quantification

Table III.3.2 shows the metal content per monomer of *Blue* Protein from *D. aminophilus* and *D. alaskensis*. Values determined for *D.gigas* protein are including for comparison. Different preparations of *D. aminophilus Blue* protein yielded zero or very low Mo concentration.

Table III.3.2 Metal ions per monomer for *Desulfovibrio aminophilus, Desulfovibrio alaskensis,* and *Desulfovibrio gigas Blue* Proteins.

	Fe	Cu	Mo
D.aminophilus	1.3(6)	0.5(2)	
D.alaskensis	1.3		1.3
D.gigas	1.0	0.6	0.35

Determination of copper oxidation state by the modified Hanna, et al. method [8, 9] on the as-prepared sample, indicates that Cu is present as Cu^{1+} ions.

III.3.5 Labile sulphide quantification

Quantification of labile sulphide of *Blue* protein from *D. aminophilus* yielded 4.5±1.3 sulphur atoms *per* protein molecule, whereas that of the *Blue* protein from *D. alaskensis* varied from 4 to 8 sulphur atoms *per* protein molecule in the different determinations..

III.3.6 Protein and gene sequence

III.3.6.1 *Desulfovibrio aminophilus Blue* Protein

Figure III.3.5 shows a DNA fragment from the *D. aminophilus* genome containing the ORF coding for *Blue* Protein. A potential RBS was identified at -14 bp from ATG initiator codon (upperlined and light grey sequences in Figure III.3.5, respectively).

The deduced amino acid sequence matches with the peptides chemically sequenced from the pure *Blue* protein (arrows in Figure III.3.5 and Table III.3.3). The analysis of the amino acid sequence indicates high probability of a signal peptide cleavage site between amino acids 29 and 30 (▼, Figure III.3.5), which suggests that this protein is located on the periplasmic side of the cytoplasmic membrane. The N-terminal of the mature protein was in good agreement with the one chemically sequenced (data not shown).

Figure III.3.5 DNA and deduced amino acid sequence from *Desulfovibrio aminophilus Blue* Protein. Upperlined sequence: potential Ribosomal Binding Site (RBS), light grey sequence: ATG initiator codon, ▼: signal peptide cleavage site, arrows: peptides sequenced from *Blue* Protein. Amino acid sequence of peptide 10 was included at C-termini.

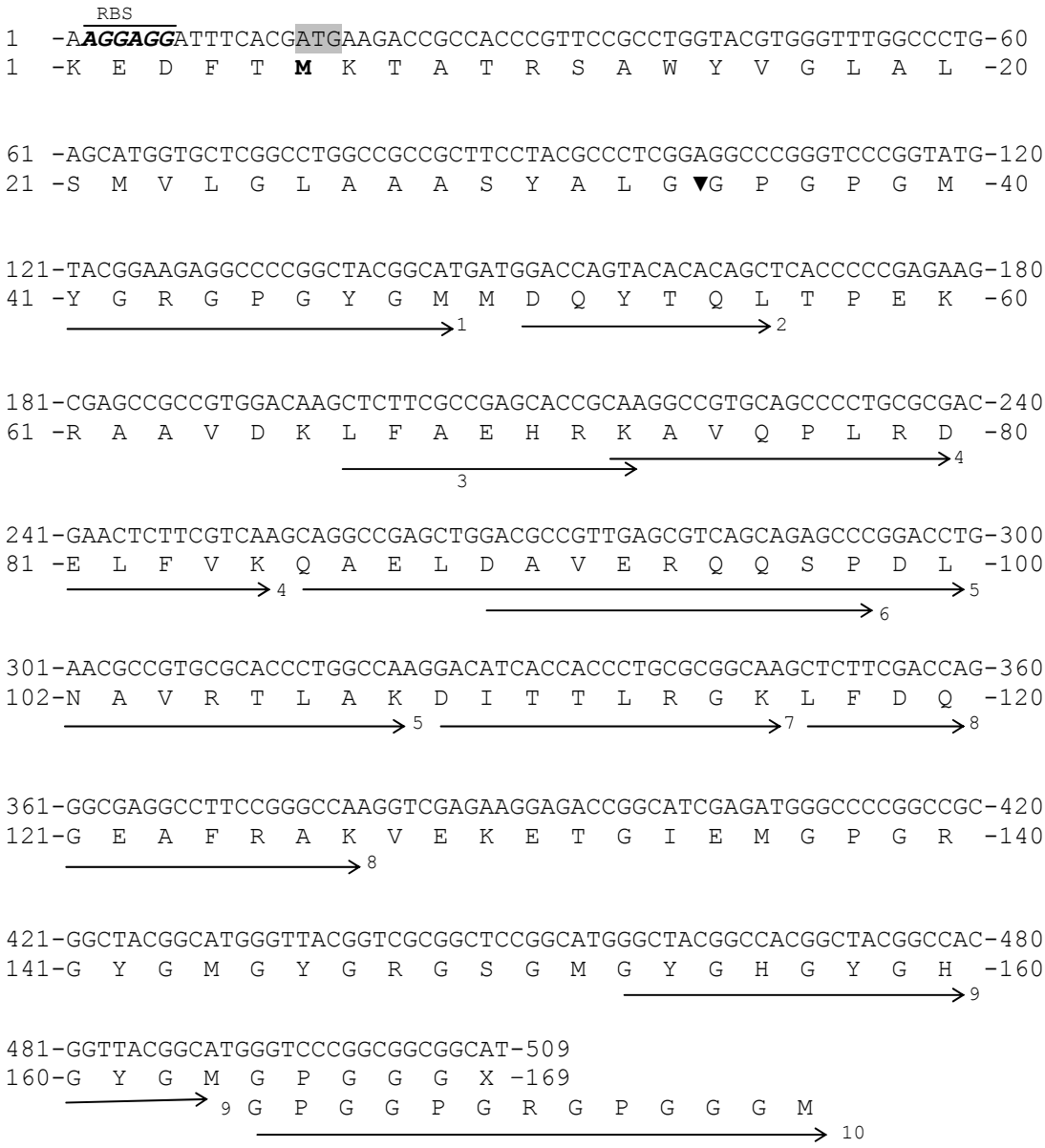

Table III.3.3 Amino acid sequence of peptides obtained from *Desulfovibrio aminophilus Blue* Protein. Numbers in the first column correspond to peptide sequences indicated in Figure III.3.5. Amino acid sequences aligned on the right column correspond to peptide sequence (upper) and amino acid deduced sequence from DNA (lower).

Peptide	Endoprotease or chemical reagent	First Aminoacid Position	Sequence and Alignment
1	Cyanide Bromide	36	YGRGPGYGM YGRGPGYGM
2	Asparagine N	46	DQYTQL DQYTQL
3	Lys-C	62	**D**FAEHRK LFAEHRK
4	Trypsin	68	KAVQPLRDELFVK KAVQPLRDELFVK
5	Lys-C	81	QAELDAVERQQSPDLNAVRTLAK QAELDAVERQQSPDLNAVRTLAK
6	Asparagine N	85	DAVE**XXT**SP DAVE**RQQ**SP
7	Lys-C	105	**L**ITTLRGK **D**ITTLRGK
8	Lys-C	112	LFDQGEAFRAK LFDQGEAFRAK
9	Cyanide Bromide	148	GYGHGYGHGYGM GYGHGYGHGYGM
10	Cyanide Bromide	160	GPGG**PG**RGPGGGM **M**GPGG**GM**

Although two peaks and two bands were observed by mass spectrometry (Figure III.3.3) and SDS-PAGE (Figure III.3.1), respectively, the N-terminal amino acid sequencing of the as-prepared protein seems to be the same sequence with some ambiguities. Interestingly, the molecular weight calculated for the first 122 amino acids of the mature protein (13.36 kDa) is in very good agreement with one of the two peaks observed by mass spectrometry (13.35 kDa, Figure III.3.3). Furthermore, the molecular weight calculated for the 142 amino acids, taking into account peptide 10, is in good agreement with the high molecular weight peak observed by mass spectrometry (Figure III.3.3). Consequently,

the two subunits observed could derive from the same gene by alternative splicing and differ only at their C termini.

To evaluate this hypothesis, the subunits were separated by reverse-phase chromatography and SDS-PAGE, and chemically sequenced. Figure III.3.6 shows the multiple sequence alignment of the N-terminal region of the samples obtained as described above and the one deduced from the DNA sequence. Owing to the ambiguity observed in many residues, the results obtained are not conclusive and more studies should be carried out to confirm the proposal.

Figure III.3.6 Multiple sequence alignment of isolated N-Terminal subunits with DNA deduced amino acid sequence. DNAdeduced: amino acid sequence deduced from the nucleotide sequence, RPalpha/beta: N-Terminal sequenced from alpha/beta subunit isolated by phase reverse chromatography, PAGEalpha/beta: N-Terminal sequenced from alpha/beta subunit isolated by SDS-PAGE.

```
                                  10                  20                      30
                                   |                   |                       |
DNAdeduced      --    G  P  G  P  GMY  G  RG  P  GY-G- M  M  D  QYT  Q  L  T    P  EK  R  AAVDKL
RPalpha         F(Q/G)G  P  G(P/H)GMY(M/G)RS(P/L)-YAG(L/M)T  P  QYT(Q/A)L(V/T)(P/D)EI(F/R)AAVQ-L
PAGEalpha       F  G  G  P  G  H  GMY  G  RG  P  GY------------------
RPbeta          F  Q  G(R/P)G(P/H)GMY  M  RS(P/L)-YAG(L/M)T(P/D)QYT  A  L  V  (P/D)KI  F  XAVQPL
PAGEbeta        G  Q  G  R  G  P  GGC  M  GS  L  -YA--------------------
```

III.3.6.2 *Desulfovibrio alaskensis Blue* Protein

The N-Terminal of the pure *Blue* protein from *D. alaskensis* was chemically sequenced. The amino acid sequence obtained was submitted to BLAST at the NCBI web site, and a significant identity (94%) was found with a Zinc resistance-associated protein from *D. desulfuricans* G20 (Figure III.3.7). Furthermore, known protein sequences from *D. alaskensis* were also aligned with their homologous proteins from *D. desulfuricans* G20 and high percentage of similarity was found (99.9% 16s rDNA, 94% cytochrome c_3 N-terminal, and 99% cytochrome c_{553} N-terminal identity). Owing this fact, the DNA fragment containing the ORF coding the *D. alaskensis Blue* protein was amplified with primers

designed from *D. desulfuricans* G20 DNA sequence. The PCR product obtained is shown in Figure III.3.8.

Figure III.3.7 Alignment of N-Terminal sequences of *Blue* Protein from *Desulfovibrio alaskensis* (PP) and Zinc resistance-associated protein from *Desulfovibrio desulfuricans* G20 (Dd)

```
                    10              20              30
                    |               |               |
PP      GPYGHGYGHR      GGYGGMGSCG      GAAVCPFGGS      (G/C)PGGQAA
Dd      GPYGHGYGHR      GGYGGMGAGG      GAAVCPFGGS        G  PGGQAA
```

Figure III.3.8 DNA sequence containing the ORF for *Blue* Protein. Underlined sequence: potential Ribosomal Binding Site (RBS), light grey sequence: ATG initiator codon of *D. alaskensis Blue* protein, ▼: signal peptide cleavage site, **M** and ***** (at positions 34 and 226, respectively): ORF of *D. alaskensis Blue* protein, **V** and ***** (at positions 256 and 294, respectively): ORF of hypothetical protein, **M** (at position 312): start codon of Ribunucleotido Reductase large subunit.

```
  1 - CGATATTGCTTCATGTGCGTGTATGGCACGCCTGTTGCTCTATCATGAGCAAATGCAAGC - 60
  1 - R  Y  C  F  M  C  V  Y  G  T  P  V  A  L  S  *  A  N  A  S  - 20

 61 - AACGCACCAGAAGGTGCACAAGGTAATCCGGAGGACATTATGAAGACCCGTTCCATTATC - 120
 21 - N  A  P  E  G  A  Q  G  N  P  E  D  I  M  K  T  R  S  I  I  - 40

121 - ACCATAGTAGCAGCCCTCGGTATTTTTGCTCTGGCAGCAGTGGCTTTTGCCGGTCCTTAC - 180
 41 - T  I  V  A  A  L  G  I  F  A  L  A  A  V  A  F  A  G  P  Y  - 60
181 - GGACACGGATACGGCCATCGCGGCGGATACGGTGGCATGGGCTCCGGCGGCGGGGCGGTC - 240
 61 - G  H  G  Y  G  H  R  G  G  Y  G  G  M  G  S  G  G  G  A  V  - 80

241 - GTGTGCCCCTTTGGCGGCAGCGGACCCGGCGGTCAGGCCGCATATGATTCGCTGACACCC - 300
100 - V  C  P  F  G  G  S  G  P  G  G  Q  A  A  Y  D  S  L  T  P  - 120

301 - GACAAGCAGGCTCTGTATGACAAGATTGTGGCCGAAGCCGACGGCAAGATGACCCCCCTG - 360
121 - D  K  Q  A  L  Y  D  K  I  V  A  E  A  D  G  K  M  T  P  L  - 140

361 - CGCGACAAGCTGTTTGCCAAGCAGGCAGAATTGAATGCCATGTACAACAATCCGGCCACA - 420
141 - R  D  K  L  F  A  K  Q  A  E  L  N  A  M  Y  N  N  P  A  T  - 160

421 - GACCCCGCGGCAGTGGGCAAGACTGCCGGTGAAGTGGCCCAGCTGCGCACTCAGCTGCGC - 480
161 - D  P  A  A  V  G  K  T  A  G  E  V  A  Q  L  R  T  Q  L  R  - 180

481 - AACCTGCACATTGAACTTTCCCAGCGCCTTGAAAAGGAAGTGGGGCTCAAGTCCGGCTTC - 540
181 - N  L  H  I  E  L  S  Q  R  L  E  K  E  V  G  L  K  S  G  F  - 200

541 - GGACGCGGTCACCGCGGCGGGTTTCATCGGGGCGGCGGCTACCATATGGGTGGCGGCATG - 600
201 - G  R  G  H  R  G  G  F  H  R  G  G  G  Y  H  M  G  G  G  M  - 220

601 - ATGGGCGGACACTACTAAACAGCACAACGGCGCTGCTTCCTTCACAGCGGCAGCCGCGGC - 660
221 - M  G  G  H  Y  *  T  A  Q  R  R  C  F  L  H  S  G  S  R  G  - 240
```

```
661 - ATACTGCGGGTACAGACCGGCCGGAGCAATTCCGGCCGGTTTTTTTGTGCGCGGTCAGCG - 720
241 - I  L  R  V  Q  T  G  R  S  N  S  G  R  F  F  C  A  R  S  A  - 260
                                                   V  R  G  Q  R

721 - GTGTGCCGCGGCGGCAGTGTACGGACACGCACCGTGTCAACAACTGCAGATTGTGATGCG - 780
261 - V  C  R  G  G  S  V  R  T  R  T  V  S  T  T  A  D  C  D  A  - 280
    -  C  A  A  A  A  V  Y  G  H  A  P  C  Q  Q  L  Q  I  V  M  R

781 - GCAGTGGCTTTTTCCGGCAGGGCATGCTAAGCTCCGTAGCAGGTAGTAAAAGTTGAGAAA - 840
281 - A  V  A  F  S  G  R  A  C  *  A  P  *  Q  V  V  K  V  E  K  - 300
    -  Q  W  L  F  P  A  G  H  A  K  L  R  S  R  *

841 - AACTATAACCAATTGATTTGATACGTTAAAGGGATGACATGAAACAGCCGGAAGACTTGC - 900
301 - N  Y  N  Q  L  I  *  Y  V  K  G  M  T  *  N  S  R  K  T  C  - 320
                                       M  K  Q  P  E  D  L  Q

901 - AGCCCGTTGTGCTCAACCAGAATGCAGAGGTCGTGCTTTCGAAGCGTTATTACCGCAAAG - 960
321 - S  P  L  C  S  T  R  M  Q  R  S  C  F  R  S  V  I  T  A  K  - 340
    -  P  V  V  L  N  Q  N  A  E  V  V  L  S  K  R  Y  Y  R  K  G

961 - GCCCTGACGGAGAACCGCTGGAAGATGCCACGGGGCTTTTCTGGCGTGTGGCGTCTGCCA -1020
341 - A  L  T  E  N  R  W  K  M  P  R  G  F  S  G  V  W  R  L  P  - 360
    -  P  D  G  E  P  L  E  D  A  T  G  L  F  W  R  V  A  S  A  I

1021 - TCGCGGCGGAGGAGGGTAAATACCCTGATTCGTCGTGCAGGGCGGACGAACTGGCCCGTG -1080
361 - S  R  R  R  R  V  N  T  L  I  R  R  A  G  R  T  N  W  P  V  - 380
    -  A  A  E  E  G  K  Y  P  D  S  S  C  R  A  D  E  L  A  R  E

1081 - AATTTTACGACCTGATGACATC - 1102
381 - N  F  T  T  *  *  H  X - 388
    -  F  Y  D  L  M  T  X
```

A potential ribosomal binding site was identified 10 bases upstream from the ATG start codon (underlined and grey highlighted sequences in Figure III.3.8, respectively). The ORF corresponding to the *Blue* Protein codify for a 171 amino acids proteins with a calculated molecular weight of 17.65 kDa. Analysis of amino acids sequence shows a high probability of a signal peptide cleavage site between amino acids 24 and 25 which suggests that, as the homologous protein isolated from *D. aminophilus,* this is a periplasmic protein. The N-Terminal sequence and the molecular weight calculated for mature protein (15.22 kDa) are in good agreement with the chemically sequenced N-Terminal and the mass spectrometry results obtained the mature protein, respectively.

III.3.7 EPR spectroscopy

D. aminophilus Blue protein is EPR silent in the as-prepared form and upon dithionite or ferricyanide addition. In contrast, the as prepared protein from *D. alaskensis* shows an isotropic signal with a g-value of 2.012 (Figure III.3.9), which is similar to the one observed in *D. gigas Blue* Protein [3]. Reduction of this sample by sodium dithionite does not significantly change either the intensity or the line-shape of the signal.

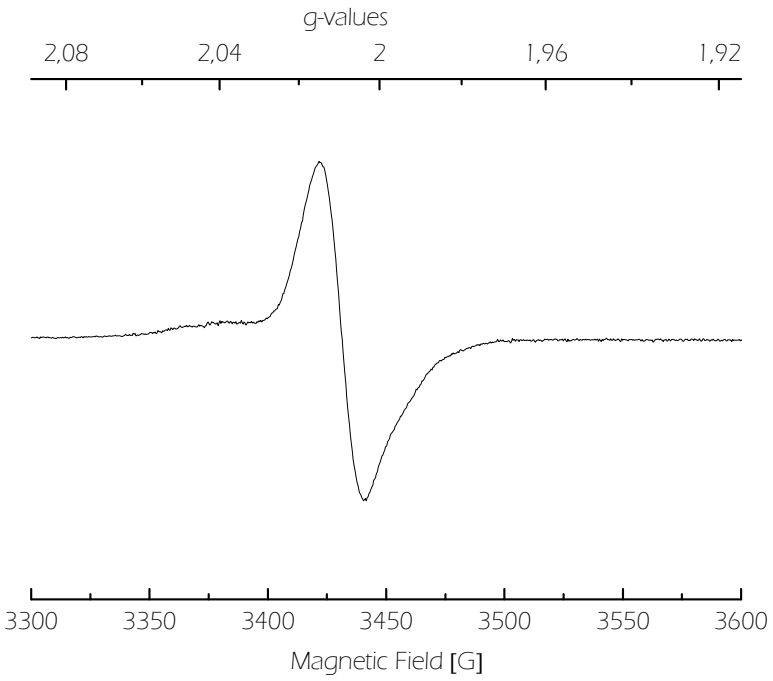

Figure III.3.9 X-Band EPR spectroscopy on as prepared *Blue* Protein from *Desulfovibrio alaskensis* g=2.012, A=19 G, Frequency: 9.65 GHz, Microwave power: 2 mW, Modulation amplitude: 1 G_{pp}, Temperature: 100 K.

III.3.8 X-ray Absorption Spectroscopy of Mo, Cu and Fe site of *Blue* proteins

III.3.8.1 *Desulfovibrio aminophilus* and *Desulfovibrio gigas Blue* protein

III.3.8.1.1 Fe K-Near edge and K-edge EXAFS

Figure III.3.10 compares the Fe K-edge near edge spectra of the *D. aminophilus* (a) and *D. gigas Blue* protein (b) with coordination models (c and d). The results indicate that the Fe is mostly in the form of iron-sulphur sites, with significant presence of $[Fe(OH)_6]^{2+}$ or related species for de *D. gigas* protein. According with these results, the Fe EXAFS spectra (Figure III.3.11) are also suggestive of a Fe-S cluster for the *Blue protein* from both

organisms. Nevertheless, the coordination around the Fe ion in the *D. aminophilus Blue* protein seems to be different from the one of *D. gigas Blue* protein.

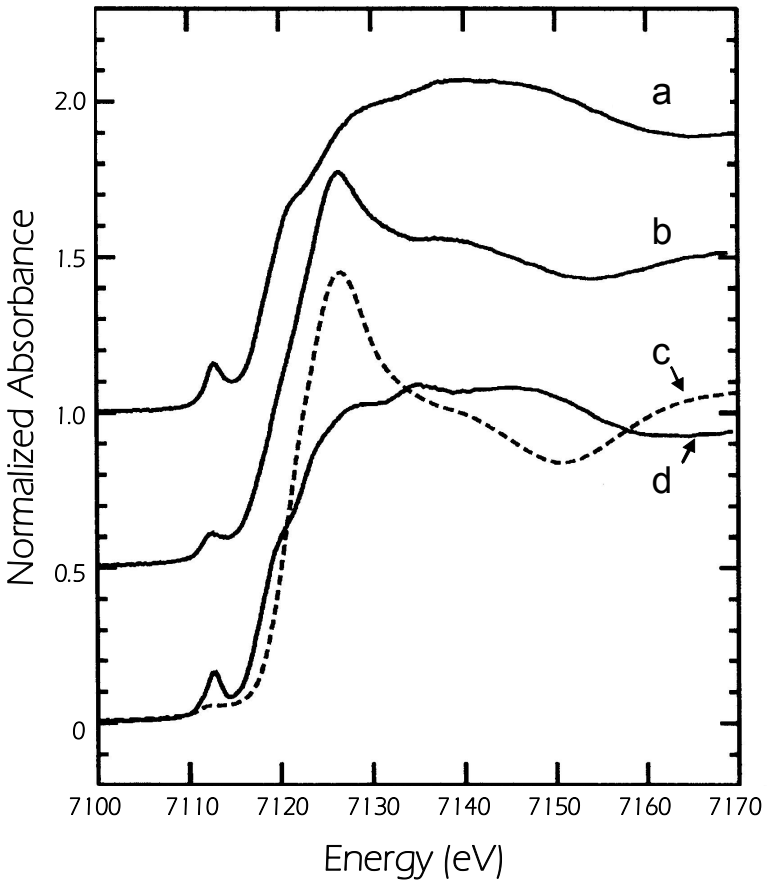

Figure III.3.10 Iron K-edge near edge spectra of as- prepared *Blue* Proteins. (a) *Da*, (b) *D. gigas Blue* protein, (c) $Fe^{II}O_6$, and (d) $Fe^{III}(SR)_4$.

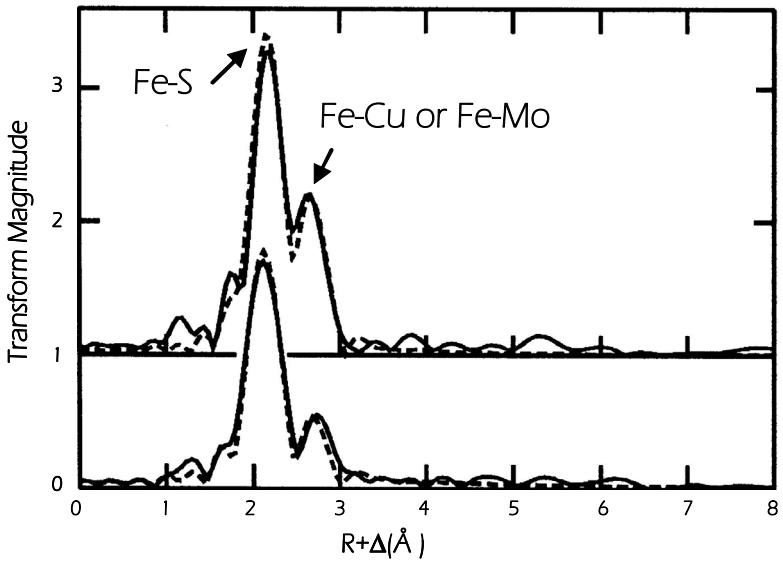

Figure III.3.11 Fe EXAFS Fourier transforms of as-prepared *Blue* proteins. Upper panel: *D. aminophilus Blue* protein, Lower panel: *D. gigas Blue* protein. The solid line indicates experimental data and broken lines show best fits.

III.3.8.1.2 Cu K-Near edge and K-edge EXAFS

The Cu K-edge near edge spectra is shown in Figure III.3.12. The spectra from both organisms suggest a cuprous site with four-coordination to thiolate type donors.

Figure III.3.13 shows the Cu EXAFS Fourier transforms for *D. gigas Blue* protein (upper panel) and *D. aminophilus Blue* protein (lower panel), together with the best fits from the curve-fitting analysis (broken lines). These results also indicate sulphur coordination and for the *D. gigas* protein (Figure III.3.13, lower panel) suggest an outer shell which might be Mo possibly similar to that found in the Orange protein from *D. gigas* [15, 16] but, again, different to that of the *D. aminophilus Blue* protein.

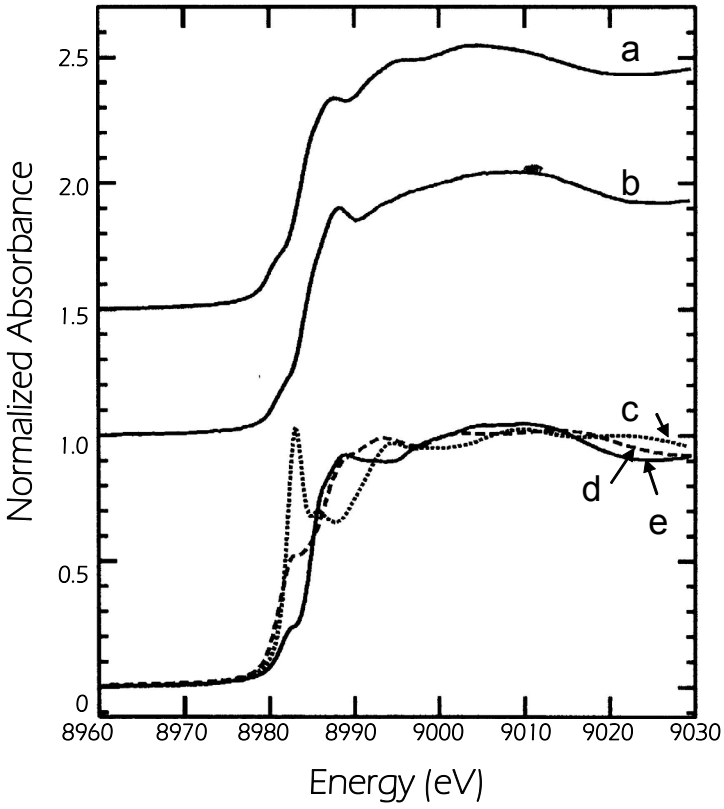

Figure III.3.12 Copper K-edge near edge spectra of as-prepared *Blue* Protein. (a) *D. aminophilus,* (b) *D. gigas Blue* protein, (c) $Cu^{I}(SR)_2$, (d) $Cu^{I}(SR)_3$, and (e) $Cu^{I}(SR)_4$.

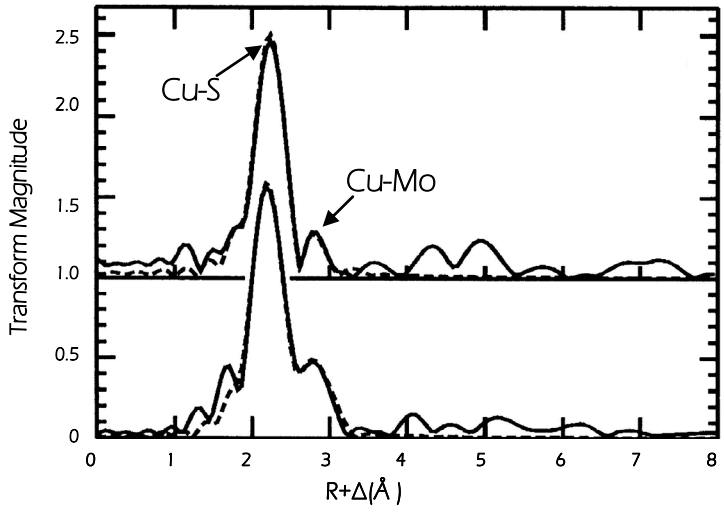

Figure III.3.13 Cu Fe EXAFS Fourier transforms of as prepared *Blue* proteins. Upper panel: *D. aminophilus Blue* protein, Lower panel: *D. gigas Blue* protein. The solid line indicates experimental data and broken lines show best fits.

III.3.8.1.3 Mo K-Near edge and K-edge EXAFS

Figure III.3.14 shows Mo K-edge near edge spectra of *D. gigas* and *D. aminophilus Blue* proteins. According with the very low concentration of Mo detected in *D. aminophilus Blue* protein, Mo-edge near edge spectrum (a) is very noisy when compared with *Dg Blue* protein spectrum (b). Similar to that observed for iron, the results suggest a molybdenum site with four-coordinated thiolate type donors.

Figure III.3.15 shows Mo EXAFS Fourier transforms of *D. aminophilus* (broken line) and *D. gigas* (solid line) *Blue* proteins. The double peak in the spectra clearly indicates a multinuclear cluster, with the first peak being mostly due to Mo-S bond and the second one to either Mo-Cu or Mo-Fe bonds.

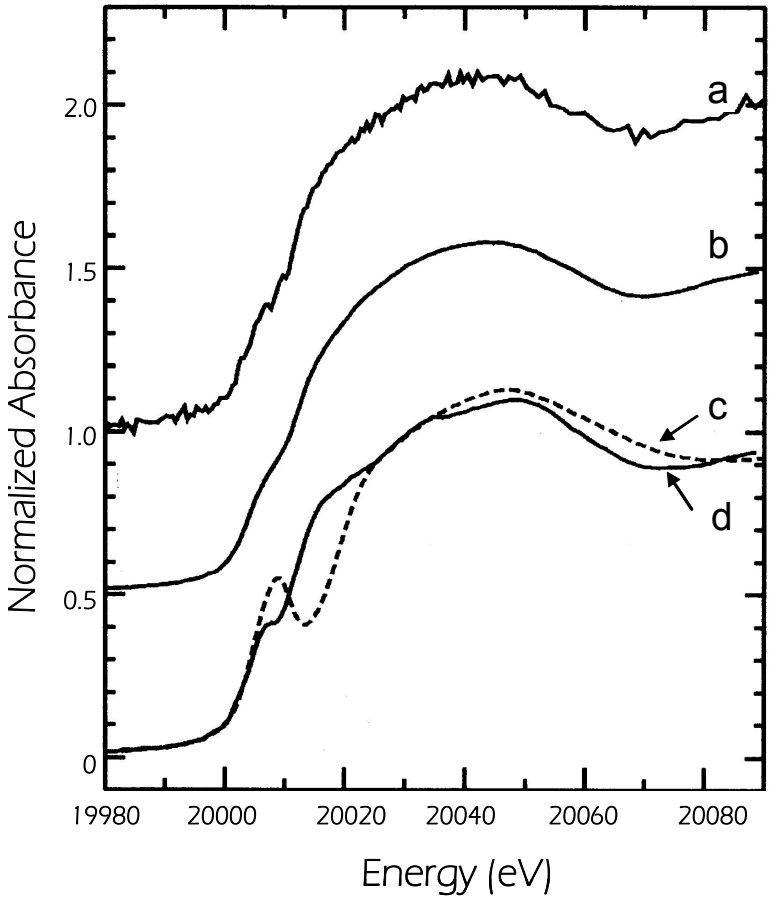

Figure III.3.14 Molybdenum K-edge near edge spectra of as-prepared *Blue* proteins. (a) *Da*, (b) *D. gigas Blue* protein, (c) $[MoO_4]^{2-}$, and (d) $[MoS_4]^{2-}$.

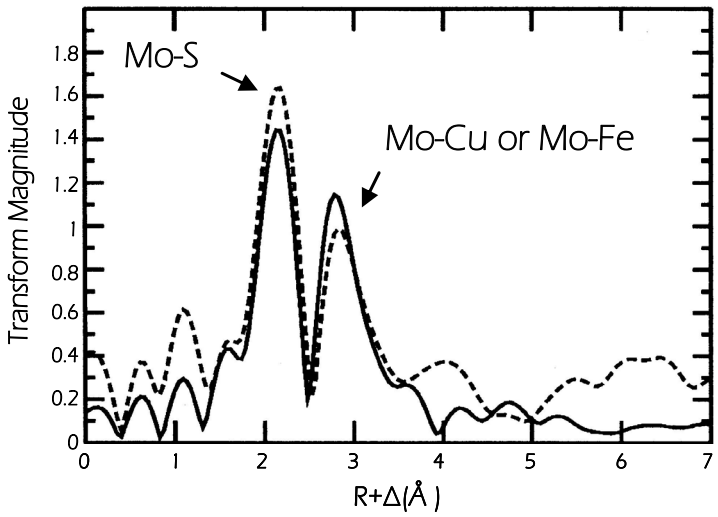

Figure III.3.15 Mo EXAFS Fourier transforms of as-prepared *Blue* proteins. Broken line: *D. aminophilus Blue* protein, and solid line: *D. gigas Blue* protein.

III.3.8.2 *D alaskensis Blue* protein

III.3.8.2.1 Mo and Fe K- near edge spectra

Figure III.3.16 shows the Mo K-edge of the *D. alaskensis Blue* protein spectrum together with the ones of Mo-Fe-S clusters, molybdate in aqueous solution, and $(NH_4)_2MoS_4$. The comparison of these spectra suggests that *D. alaskensis Blue* protein contains a FeMo cluster. Furthermore, the shoulder at approximately 2008 eV could indicate the presence of Mo=O ligation.

The Fe K-edge spectrum of the *D. alaskensis Blue* protein together with Mo-Fe-S and Fe-S clusters are shown in Figure III.3.17. The comparison of the shape of these spectra suggests that coordination around the Fe ion is more similar to that of the 2Fe-2S clusters than that of the Fe-Mo clusters.

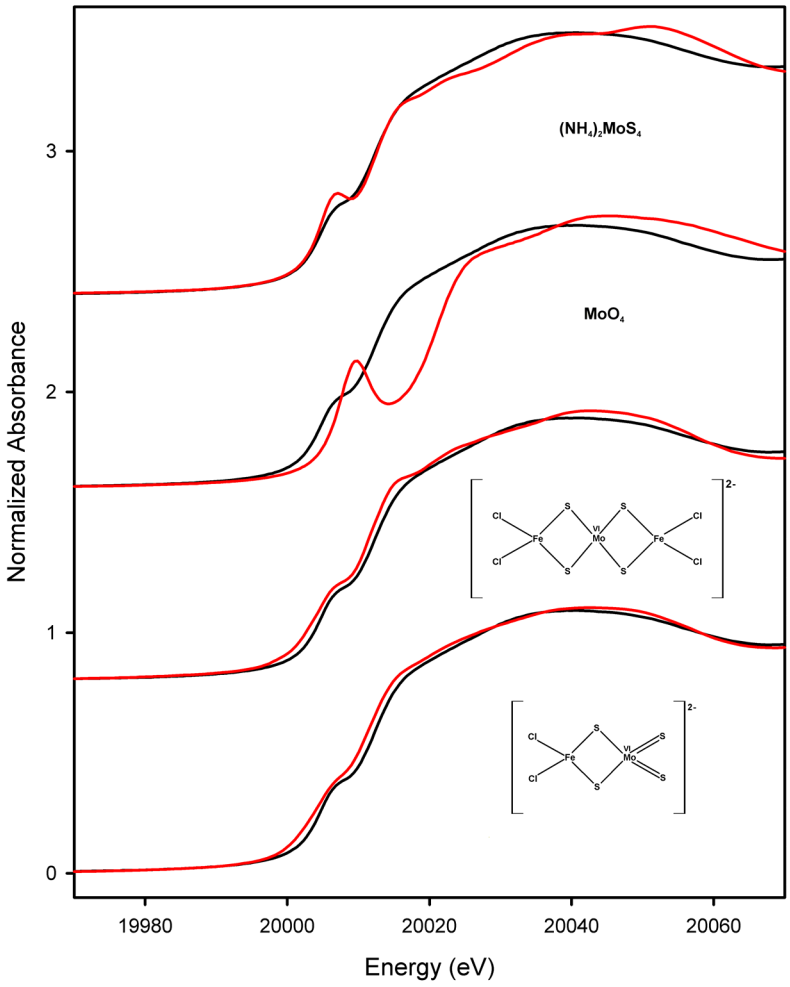

Figure III.3.16 Comparison of the Mo K near-edge spectrum of *Blue* protein from *D. alaskensis* (black lines) with molybdenum-iron-sulfur clusters, molybdate in aqueous solution and $(NH_4)_2MoS_4$ (red lines).

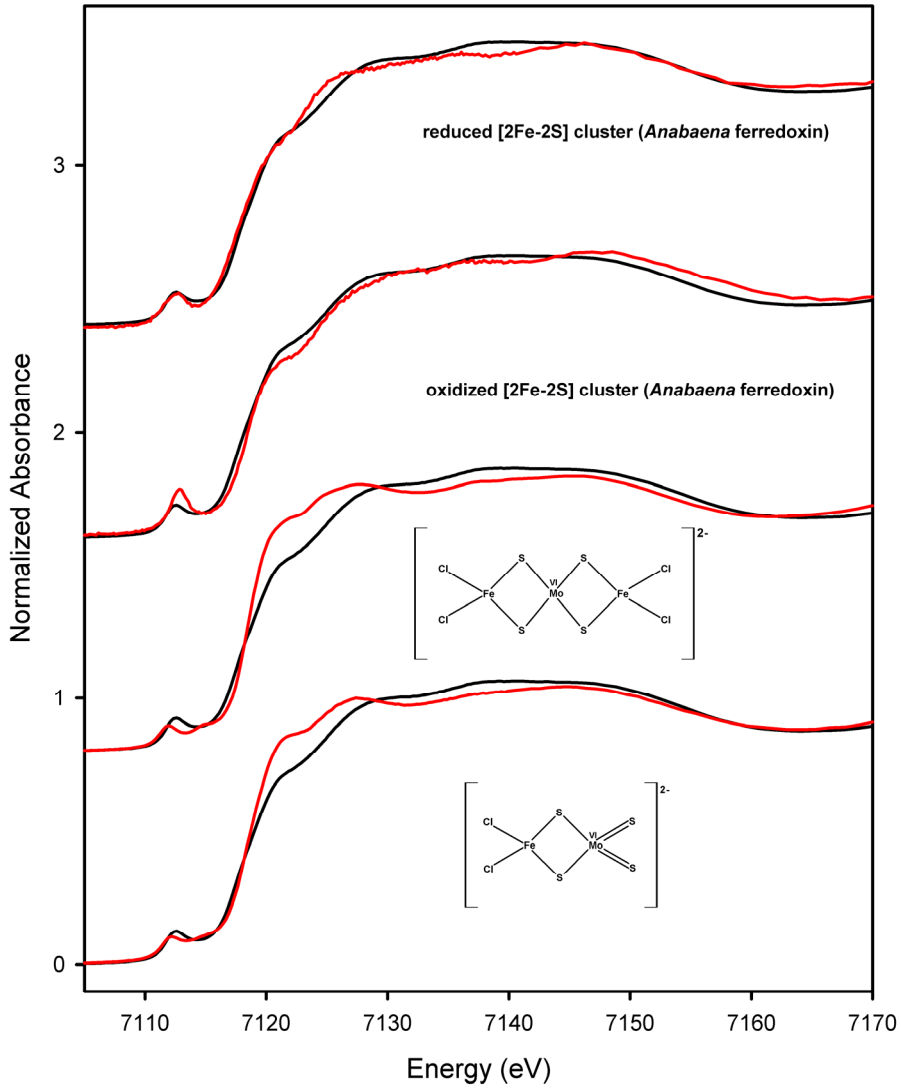

Figure III.3.17 Comparison of the Fe K-near-edge spectrum of *Blue* protein from *D. alaskensis* (black lines) with molybdenum-iron-sulphur and iron-sulphur clusters (red lines).

III.3.8.2.2 Fe and Mo K-edge EXAFS

Figure III.3.18 shows the Mo K-edge k^3-weighted EXAFS spectra (top panel) and the Fourier transforms (lower panel) of *Blue* protein from *D. alaskensis*. The best fit (dashed lines) of the experimental data (solid lines) comes from the analysis of several different coordination models of the Mo site (Table III.3.4). The following interactions were identified: Mo=O bond at 1.68 Å, Mo-O bond at 2.02 Å, a short Mo-S bond at 2.19 Å, a long Mo-S bond at 2.35 Å and a Mo-Fe bond at 2.71 Å. The slightly increased Debye-Waller factor of the single Mo=O contribution (σ^2=0.0032 Å^2) together with highly elevated Debye-Waller

factor of the single Mo-O contribution (σ^2=0.013 Å^2) suggested the occupancy of both ligands to be lower than one. This could be explained by partial reduction of the Fe-Mo cluster in the analyzed protein, i.e. conversion of the double-bonded oxo group to a hydroxyl ligand. It was tested it and obtained significantly better fit with 60% occupancy for the Mo=O group and 40% for the Mo-O ligand. Therefore, the final structural model of the Mo site in *Blue* protein consists of 0.6 O at 1.68 Å, 0.4 O at 2.02 Å, 1 S at 2.19 Å, 2 S at 2.35 Å and 1 Fe at 2.71 Å.

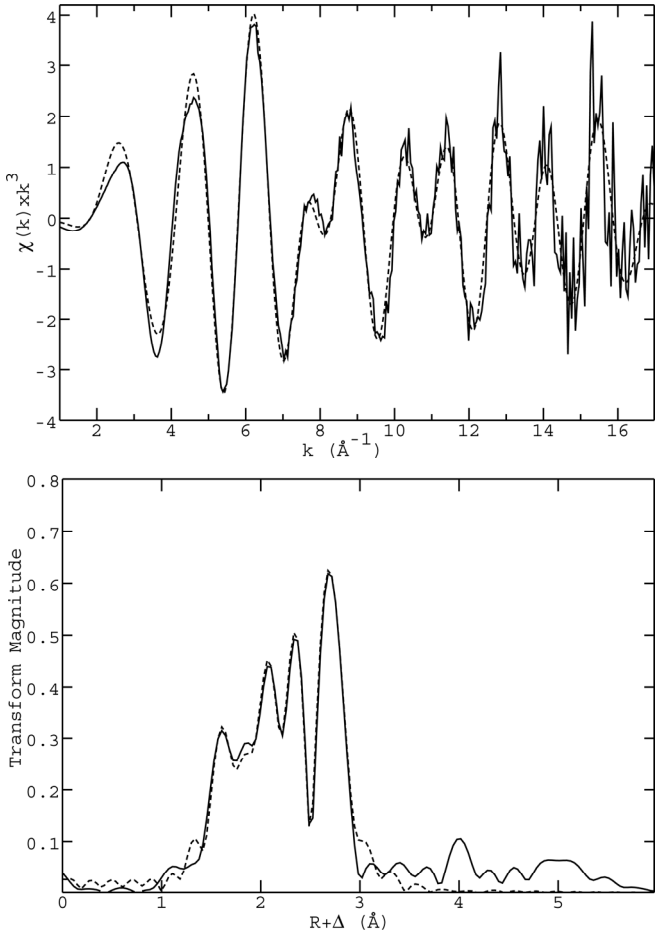

Figure III.3.18 Mo K-edge k^3-weighted EXAFS spectra (top) and the Fourier transforms (bottom) of *Blue* protein from *D. alaskensis*. Solid lines: experimental data, Dashed lines: fit using the best model given in Table III.3.4.

Table 1. EXAFS refinement parameters of different structural models of the Mo site in blue protein from *D. alaskensis*. The best fit is highlighted in red. The values in parentheses are the estimated standard deviations obtained from the diagonal elements of the covariance matrix. The value of F represents the goodness of the fit.

Mo = O			Mo – S			Mo – S			Mo – Fe			Mo – O			F
N	R	σ^2	N	R	σ^2	N	R	σ^2	N	R	σ^2	N	R	σ^2	
1	1.677 (3)	0.0033 (3)	1	2.181 (4)	0.0037 (3)	2	2.335 (3)	0.0055 (3)	1	2.708 (2)	0.0030 (2)				0.372
1	1.675 (3)	0.0032 (3)	2	2.197 (4)	0.0073 (4)	2	2.355 (3)	0.0054 (3)	1	2.707 (2)	0.0028 (1)				0.360
1	1.677 (3)	0.0032 (2)	2	2.194 (8)	0.0073 (5)	2	2.354 (5)	0.0055 (4)	1	2.709 (3)	0.0029 (1)	1	2.16 (5)	0.02 (2)	0.350
1	1.680 (3)	0.0032 (2)	1	2.186 (6)	0.0048 (5)	2	2.346 (4)	0.0060 (3)	1	2.712 (2)	0.0029 (1)	1	2.00 (2)	0.013 (3)	0.345
0.6	1.678 (2)	0.0012 (2)	1	2.188 (7)	0.0050 (6)	2	2.347 (4)	0.0060 (3)	1	2.713 (2)	0.0029 (1)	0.4	2.02 (3)	0.006 (3)	0.324
0.6	1.677 (3)	0.0012 (2)	2	2.201 (8)	0.0066 (8)	2	2.362 (5)	0.0056 (6)	1	2.712 (2)	0.0028 (1)	0.4	2.20 (4)	0.002 (2)	0.332

Figure III.3.19 shows the Fe K-edge k^3-weighted EXAFS spectra (top panel) and the Fourier transforms (lower panel) of *D. alaskensis Blue* protein. The magnitude of the Fourier transform of the EXAFS data exhibits two main peaks at ~2.2 Å and at ~2.6 Å. The first peak corresponds to iron-first shell ligand backscattering contributions, which, using the best model given in Table III.3.5, has been modelled as 3 S atoms at 2.25 Å and 1 N atom at 2.02 Å. Based on the Mo K-edge analysis the second peak has been attributed to the Fe-Mo contribution. However, the EXAFS curve fitting resulted in significantly longer Fe-Mo distance as compared with that obtained from the Mo K-edge analysis (2.79 Å vs. 2.71 Å) and the respective Debye-Waller factor was higher (0.006 Å2 vs. 0.003 Å2). These results prompted the investigation of the presence of an additional metal-metal contribution at similar distance, which potentially could interfere destructively with the Fe-Mo signal. The presence of the Fe-Fe bond concomitantly with the Fe-Mo bond was tested and resulted in better fit. In addition, the refined Fe-Mo distance was consistent with Mo K-edge analysis (Table III.3.5).

In summary, there is some evidence that the Fe-Mo cluster in *Blue* protein from *D. alaskensis* may consist of 1 Mo ion and more than 1 Fe ion.

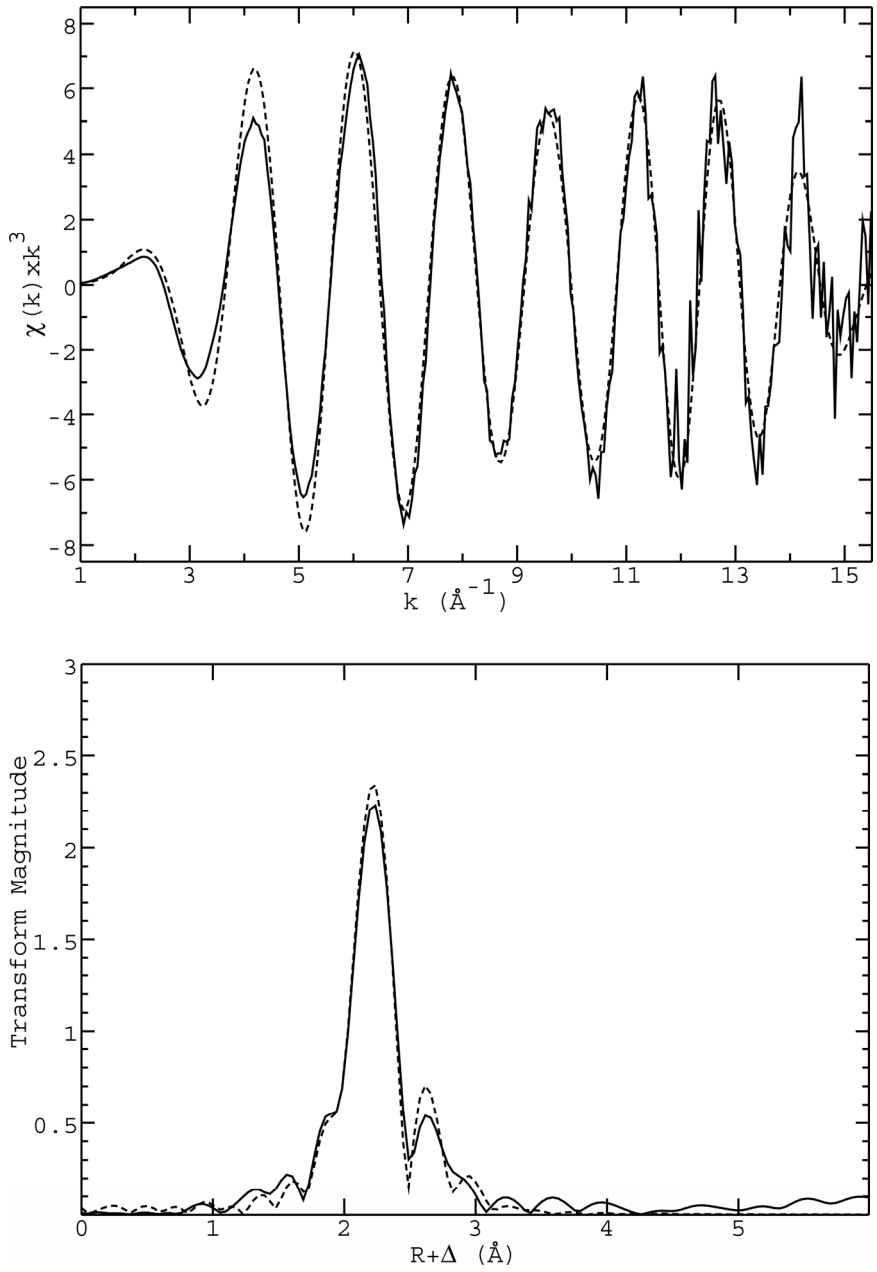

Figure III.3.19 Fe K-edge k^3-weighted EXAFS spectra (top) and their Fourier transforms (bottom) of *Blue* protein from *Desulfovibrio alaskensis*. Experimental data are shown by solid lines; calculated spectra based on the best model given in Table III.3.5 are represented by dashed curves.

Table III.3.5. EXAFS refinement parameters of different structural models of the Fe site in blue protein from *D. alaskensis*. The best fit is highlighted in red. The values in parentheses are the estimated standard deviations obtained from the diagonal elements of the covariance matrix. The value of F represents the goodness of the fit.

Fe – S			Fe – N			Fe – Mo			Fe – Fe			F
N	R	σ^2	N	R	σ^2	N	R	σ^2	N	R	σ^2	
3.3	2.248 (2)	0.0026 (2)										0.309
3	2.248 (2)	0.0022 (1)										0.313
3	2.253 (2)	0.0019 (1)	1	2.022 (8)	0.0010 (6)							0.287
2	2.266 (2)	0.0004 (11)	2	2.060 (5)	0.0014 (4)							0.269
3	2.252 (2)	0.0019 (1)	1	2.021 (7)	0.0013 (6)	1	2.790 (5)	0.0063 (4)				0.265
3	2.253 (2)	0.0019 (1)	1	2.023 (7)	0.0011 (6)				1	2.658 (5)	0.0061 (6)	0.278
3	2.250 (2)	0.0022 (1)	1	2.03 (1)	0.004 (1)	1	2.713*	0.0029*	1	2.694 (1)	0.0006 (1)	0.232
3	2.252 (2)	0.0022 (1)	1	2.03 (1)	0.003 (1)	1	2.72 (1)	0.0034 (5)	1	2.70 (1)	0.0013 (6)	0.232
4	2.245 (2)	0.0035 (1)				1	2.73 (1)	0.0028 (5)	1	2.70 (1)	0.0012 (6)	0.263

*to limit the number of refined parameters, the structural parameters of the respective Mo-Fe interaction were used and kept constant during refinement

III.4 DISCUSSION

III.4.1 Primary characterization of *Blue* Proteins from *Desulfovibrio* genus

Blue proteins containing Fe-Cu and Fe-Mo clusters have been isolated from the sulphate reducing bacteria *D. aminophilus* and *D. alaskensis*. The primary characterization of these proteins indicates that they could belong to the same family of proteins isolated from *D. africanus* [1], *D. salexigens* [2], and *D.gigas* [3].

A comparison of the UV-visible spectra of *Blue* proteins is shown in Figure III.4.1. The bands observed at 320 and 410 nm suggest the presence of iron-sulphur clusters, which is in agreement with the XAS results. The absorption peak at 615 nm observed in the electronic spectra of *D. aminophilus* and *D. gigas Blue* protein, is absent in the *D. alaskensis Blue* protein spectrum. This fact does not seem to be related with Cu deficiency since is present in UV-visible spectrum of the Mo-Fe protein isolated from *D. africanus* [1] (Figure III.4.2).

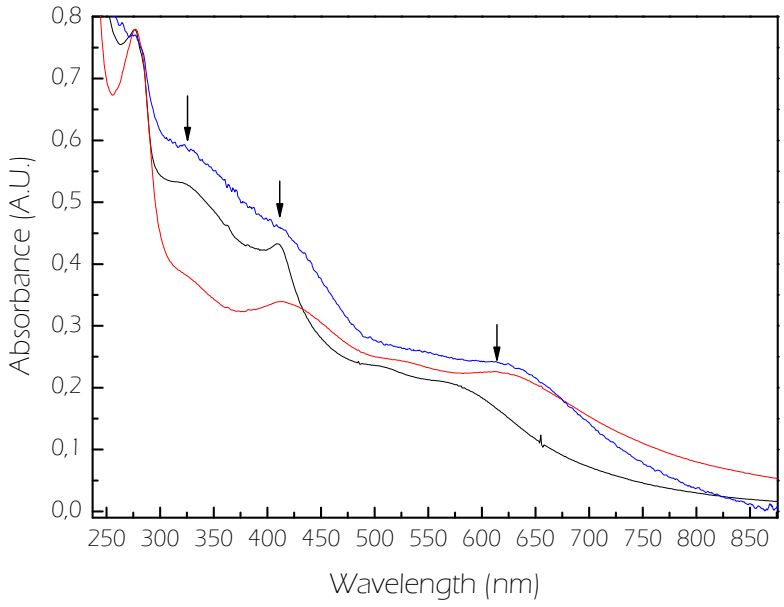

Figure III.4.1 Comparison of UV-visible spectrum of *Blue* proteins from *Desulfovibrio aminophilus* (red line), *Desulfovibrio alaskensis* (black line), and *Desulfovibrio gigas* (*Blue* line)

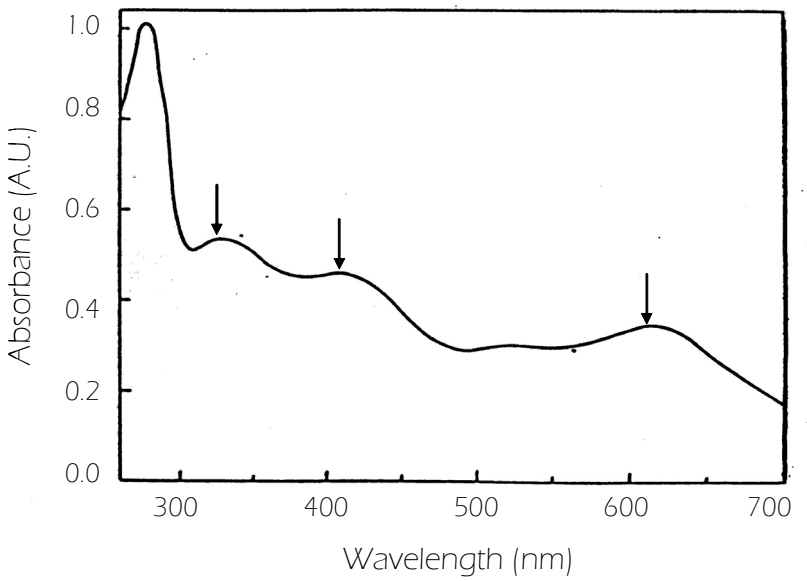

Figure III.4.2 UV-visible spectrum of Mo-Fe proteins from *Desulfovibrio africanus*. Reproduced from reference [1].

In agreement with the homologous proteins previously isolated [1-3], *Blue* proteins from *D. aminophilus* and *D. alaskensis* are multimers having 14-16 subunits. The mass spectrometry data (Figure III.3.4) and the electrophoretic pattern (Figure III.3.2) show that the protein isolated from *D. alaskensis* is composed by identical subunits. In contrast, the protein isolated from *D. aminophilus* shows two components in both electrophoretic pattern and MALDI-TOF spectra. As analyzed in section III.3.61, this protein could be composed by subunits which differ at C-termini. Additional work is necessary to confirm this hypothesis.

III.4.2 Amino acid sequence: conserved motifs and homology with other proteins

A BLAST search of *D. aminophilus, D. alaskensis* and *D gigas* amino acid sequence revealed homology with a Zinc resistance associated protein from *D. vulgaris* Hildenborough and *D. desulfuricans* G20 (Table III.4.1). Despite this fact, preliminary experiments show no increase of expression levels when *D. aminophilus* cells are grown until 45 μM of Zn (data not shown). Additional work should be necessary to elucidate a putative relation between the metal concentration and expression of *Blue* proteins.

Furthermore, the high identity percentage between proteins sequenced from *D. alaskensis* and *D. desulfuricans* G20 (section III.3.6.2) suggests that *D. desulfuricans* G20 should be reclassified.

Table III.4.1 Identity percentages of *Blue* proteins amino acid sequences including the homologous protein identified in *Desulfovibrio vulgaris* Hildenborough. *Dam: D. aminophilus, Dg: D. gigas, Dal: D. alaskensis, and DvH.: Desulfovibrio vulgaris* Hildenborough

	DvH	*Dal*	*Dg*
Dam	31.25	32.02	19.51
Dg	18.5	15.52	
Dal	36.32		

Figure III.4.3 shows amino acid sequence alignment of the *Blue* proteins purified from *Desulfovibrio* including the sequence of a homologous protein identified in *D. vulgaris* Hildenborough. Although low identity percentage is observed when amino acid sequences are compared (Table III.4.1), a segment between amino acids 65 to 85 shows to be conserved in the analyzed sequences (red box, Figure III.4.3). This sequence could be a signature of this family of proteins.

Figure III.4.3 Multiple amino acid sequence alignment of *Blue* proteins. (Dam): *D. aminophilus*, (Dal): *D. alaskensis*, (Dg): *D. gigas*, (DvH_DVU3384): *D. vulgaris* Hildenborough, locus tag DVU3384, (*): identity, (:): strongly similar, and (.) weekly similar.

```
                                        10        20        30        40
                         |         |    |         |         |         |
Dam             MKTATRSAWYVGLALSMVLGLAAAS-YALGGPGPGMYG-------------RGPGYGMMD
Dg              ----------------------------MNAPHERFRG----------------CSPLER
Dal             MKTRSIITIVAALGIFALAAVAFAGPYGHGYGHRGGYGGMGAGGGAAVCPFGGSGPGGQA
DvH_DVU3384     MNSK-----RIALGIIALATVVSLGTAANNAFARG-HG-----------NYHGQGQMMGQ
                                        .         *

                        50        60        70        80        90        100
                         |         |         |         |         |         |
Dam             QYTQLTPEKRAAVDKLFAEHRKAVQPLRDELFVKQAELDAVERQQSPDLNAVRTLAKDIT
Dg              LEQFLPPEVRESAKTLLMEHRKAIYPLQERAKGKKHELNALIATPNTSDDTINKLVDEIN
Dal             AYDSLTPDKQALYDKIVAEADGKMTPLRDKLFAKQAELNAMYNNPATDPAAVGKTAGEVA
DvH_DVU3384     AYEALTPEKQAKFDSLIDAFNTKVTPLRDKLWAKHTELNALSSNPNTKPEDIRKLTDEIT
                    *.*: :   ..:.      : **::.   *: **:*:     ..   : . . ::

                       110       120       130       140       150       160
                         |         |         |         |         |         |
Dam             TLRGKLFDQGEAFRAKVEKETGIEMGPG-RGYG--MGYGRGSGMG-----YGHGYGHGYG
Dg              GLHAQIFKANVAMRKEFFKVTGVPLPEK-------P--GRGPR-----------------
Dal             QLRTQLRNLHIELSQRLEKEVGLKSGFG-RGHR--GGFHRGGGYH-----MGGGMMGGHY
DvH_DVU3384     ALRTQYRTEAANLDASMQKEVGIKTHFATMGHRGMGGMGGGCGMMGGKGGMGSGMMQMHD
                 *: :       :   . * .*:                  *

                       170
                         |
Dam             -MGPGGG---
Dg              ----------
Dal             ----------
DvH_DVU3384     GEGPHRGQNM
```

III.4.3 Novel cofactors in proteins isolated from *Desulfovibrio* genus

Three different metals have been detected in *Blue* proteins from *Desulfovibrio* genus: Cu, Mo and Fe. Although all these proteins seem to belong to the same family, EXAFS studies point to a multinuclear cluster with some differences in the coordination around metal ions (Figure III.4.4).

In addition, some contradictions between XAFS studies and metals quantification remains to be elucidated. The ratio metal ion *per* protein molecule is not in agreement with the XAS studies for the *D. aminophilus* and the *D. alaskensis Blue* protein. Therefore, the studies on the metallic clusters of *Blue* proteins presented in this work are preliminary and more work need performed to a better understanding of the metal composition and structure of these centres.

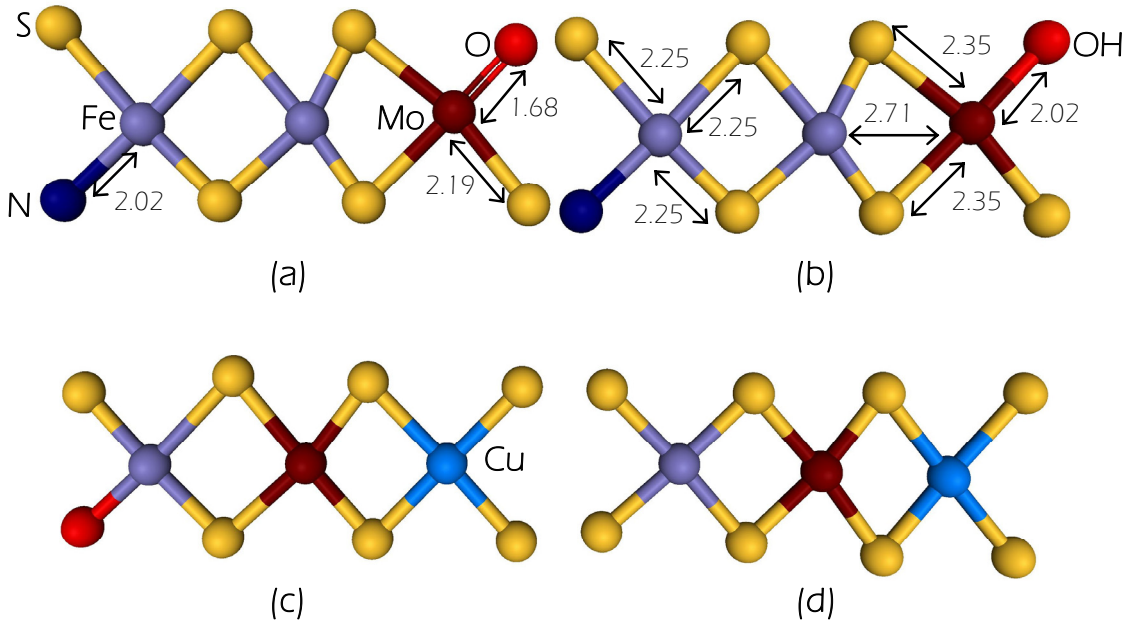

Figure III.4.4 Proposed metals centres in Blue proteins from *Desulfovibrio alaskensis* (a and b), *Desulfovibrio gigas* (c), and *Desulfovibrio aminophilus* (d).

II.5 REFERENCES

1. Hatchikian EC and Bruschi M, *Isolation and characterization of a molybdenum iron-sulfur protein from Desulfovibrio africanus*. Biochem Biophys Res Commun, **1979**. 86(3): p. 725-734.

2. Czechowski M, Fauque G, Galliano N, Dimon B, Moura I, Moura JJG, Xavier AV, Barata BAS, Lino AR, and LeGall J, *Purification and characterization of three proteins from a halophilic sulfate reducing bacterium Desulfovibrio salexigens*. J. of Ind.Microb., **1986**. 1: p. 139-147.

3. Andrade S, *Biochemical and spectroscopic characterization of Mo-containing enzymes from sulfate reducing bacteria*, in *Chemistry Department*. **2002**, New University of Lisbon: Lisbon- Portugal.

4. Widdel F and Pfennig N, *A new anaerobic, sporing, acetate-oxidizing, sulfate-reducing bacterium, Desulfotomaculum (emend.) acetoxidans*. Arch Microbiol, **1977**. 112(1): p. 119-122.

5. Laemmli UK, *Cleavage of structural proteins during the assembly of the head of bacteriophage T4*. Nature, **1970**. 227(5259): p. 680-685.

6. Schagger H and von Jagow G, *Tricine-sodium dodecyl sulfate-polyacrylamide gel electrophoresis for the separation of proteins in the range from 1 to 100 kDa*. Anal Biochem, **1987**. 166(2): p. 368-379.

7. Brondino CD, Passeggi MC, Caldeira J, Almendra MJ, Feio MJ, Moura JJ, and Moura I, *Incorporation of either molybdenum or tungsten into formate dehydrogenase from Desulfovibrio alaskensis NCIMB 13491; EPR assignment of the proximal iron-sulfur cluster to the pterin cofactor in formate dehydrogenases from sulfate-reducing bacteria*. J Biol Inorg Chem, **2004**. 9(2): p. 145-151.

8. Hanna PM, Tamilarasan R, and McMillin DR, *Cu(I) analysis of blue copper proteins*. Biochem J, **1988**. 256(3): p. 1001-1004.

9. Pauleta SR, *Electron transfer complexes between Paracoccus cytochrome c peroxidase and its electron donors"*. **2003**, Universidade Nova de Lisboa: Lisbon.

10. Fogo JJ and Popowsky M, *Spectrophotometric determination of hydrogen sulfide, methylene blue method*. Anal. Chem., **1949**. 21: p. 732-734.

11. Chamberlain JS, Gibbs RA, Rainer JE, Nguyen PN, and Thomas C, *Deletion screening of the Duchenne muscular dystrophy locus via multiplex DNA amplification*. Nucleic Acids Res., **1988**. 16(23): p. 11141-11156.

12. Henegariu O, Heerema NA, Dlouhy SR, Vance GH, and Vogt PH, *Multiplex PCR: critical parameters and step-by-step protocol*. Biotechniques, **1997**. 23(3): p. 504-511.

13. Wilson K, *Preparation of genomic DNA from bacteria*. in Current protocols in molecular biology., ed. FM Ausubel, et al. Vol. 1. 1994, New York, NY: John Wiley & Sons. 2.4.1-2.4.5.

14. Ochman H, Gerber AS, and Hartl DL, *Genetic Applications of an Inverse Polymerase Chain Reaction*. Genetics, 1988. 120(3): p. 621-623.

15. Bursakov SA, Gavel OY, Di Rocco G, Lampreia J, Calvete J, Pereira AS, Moura JJ, and Moura I, *Antagonists Mo and Cu in a heterometallic cluster present on a novel protein (orange protein) isolated from Desulfovibrio gigas*. J Inorg Biochem, 2004. 98(5): p. 833-840.

16. George GN, Pickering IJ, Yu EY, Prince RC, Bursakov SA, Gavel OY, Moura I, and J.J.G. M, *A Novel Protein-Bound Copper-Molybdenum Cluster. J. Am. Chem. Soc.*, 2000. 132: p. 8321-8322.

IV. CONCLUDING REMARKS

The present work describes distinct types of studies performed on two different types of proteins isolated from the *Desulfovibrio* genus. One of them belongs to the well-known family of the mononuclear Mo-containing enzymes, the Fdh from the sulphate reducer *Desulfovibrio desulfuricans* ATCC 27774. The second type comprises of two proteins belonging to a family of novel proteins that present heterometallic clusters and unknown function so far.

The sequencing of the gene cluster of Formate dehydrogenase isolated from *Desulfovibrio desulfuricans* ATCC 27774 gave important information about gene organization and conserved motifs in the different subunits. The presence of the UGA codon together with the SECIS element in the *fdhA* gene is in agreement with the SeCys residue coordinated to the Mo atom at the active site reported in the first characterization of the enzyme. The presence of a signal peptide containing the twin arginine motif in this subunit shows that, as for the W-Fdh from *D. gigas*, it is located on the periplasmic side of the cytoplasmic membrane being transported by a Sec-independent system. The conserved residues proposed to be involved in the oxidation of formate were also identified, which supports a common reaction mechanism for all these Fdhs. Concerning to the FdhC subunit, four histidine motifs as well as four histidine residues were found which is in agreement with the number of low spin hemes previously reported.

The improvement of the kinetic assays allowed performing careful studies of the kinetic properties of Fdh from *D. desulfuricans* ATCC 27774. The use of deuteroformate as substrate provided important advances on mechanistic aspects showing that the C-H break is the rate-limiting step in the formate oxidation. EPR studies of the Mo(V) species obtained by reducing the enzyme with formate or deuteroformate were important to elucidate the nature of some of the ligands coordinated to the Mo(V) ion. Furthermore, the development of a different signal when the formate reduced enzyme is incubated with

inhibitor (azide or cyanide) suggests changes in the coordination around the Mo atom in presence of any of these molecules. The accepted catalytic mechanism for Fdhs is proposed on the basis of an enzyme purified in presence of azide, but the results obtained here suggest that the inhibitor induces structural changes of the Mo site. It is evident that additional work is necessary to understand the enzyme changes induced by the inhibitor molecule.

The second part of this work is devoted to the characterization of two new proteins isolated from the sulphate reducing bacteria *D. aminophilus* and *D. alaskensis*. Biochemical analysis confirmed the multimeric character of these proteins and the amino acid sequence of both *D. aminophilus* and *D. alaskensis Blue* proteins confirm their periplasmic location in the cell. Although X-ray absorption spectroscopy studies are not absolutely conclusive yet, it is evident that the two analyzed *Blue* proteins contain multinuclear centres with no resemblance with other clusters containing a well-known function in biology. Several points of the results presented here show some controversies, e.g.: whether Mo is present or not of Mo in the cluster of *D. aminophilus Blue* protein and the different metal/protein ratios given by biochemical analysis and EXAFS data. As stated at the beginning of this manuscript, these data are preliminary and additional work should be carried out to elucidate all these discrepancies. In this sense, ongoing X-Ray data analysis of some of these proteins is hopefully awaited for a better understanding of the 3D structure of these clusters. Another important point that needs additional work is regarding the function. Preliminary studies showed an increasing of the expression level of the protein from *D. alaskensis* as the Mo concentration increase, which suggests a putative involvement of this protein in response to metal stress. These results are preliminary and not included in this work.

In the last years, structural and spectroscopic studies on several mononuclear Mo-containing proteins have provided valuable information on mechanistic aspects of these metalloproteins. However, it is evident that the exact natures of the molecular processes

occurring during catalysis are not well understood yet. Furthermore, the discovery of proteins containing new metallic cofactors not only open new research fields but also suggests that the role of Mo is not limited to the well-documented processes of the reactions catalyzed by mononuclear containing enzymes and nitrogenase. All these points and others not mentioned here are within the most important challenges for the coming years.